①

A DESIGN OF A TRAJECTORY ESTIMATOR

USING MULTIPLE DME RANGE MEASUREMENTS

THESIS

AFIT/GGC/EE/78-4   Robert N. Riggins
                          Lieutenant   USAF

D D C

JUN 16 1978

E

78 06 13 036

A DESIGN OF A TRAJECTORY ESTIMATOR

USING MULTIPLE DME RANGE MEASUREMENTS

THESIS

Presented to the Faculty of the School of Engineering

of the Air Force Institute of Technology

Air University

in Partial Fulfillment of the

Requirements for the Degree of

Master of Science

by

Robert N. Riggins, B.S.E.E.

Lieutenant   USAF

Graduate Electrical Engineering

March 1978

Preface

The content of this study was proposed by Major Richard M. Potter in support of current CIGTF research efforts at Holloman AFB. Both AFIT and ASD at Wright-Patterson AFB provided computer allocations for the design and testing stages.

I would like to give sincere thanks to both Major Potter and Peter S. Maybeck for aid and guidance through the complexities of the project. I would also like to express my appreciation to Captain Richard M. Reeves for computer assistance, and Captain Gary Reid for helpful suggestions, and Donna Hadley, Sheri Vogel, and Cindy Held for typing.

Most of all, I would like to acknowledge my indebtedness to my wife, Debbie, for providing assistance in all phases of the project and for displaying patience and understanding throughout the duration of the study.

<div align="right">Robert N. Riggins</div>

Table of Contents

List of Figures

vi

List of Tables

List of Symbols

Symbol	Defined or First Used	Symbol	Defined or First Used
ε_1	p. 6	$\hat{\underline{P}}^-(k+1)$	Eq (6)
ε_2	p. 6	$\hat{\underline{P}}^+(k)$	Eq (6)
ε_3	p. 6	$\underline{G}$	Eq (6)
r_{T_1}	p. 6	$\underline{Q}$	Eq (6)
r_{T_2}	p. 6	$\underline{K}(k+1)$	Eq (7)
r_{T_3}	p. 6	$\underline{H}(k+1)$	Eq (7)
r_{A_i}	p. 7	R	Eq (7)
r_{B_i}	p. 7	$\hat{\underline{X}}^+(k+1)$	Eq (8)
r_{C_i}	p. 7	$\Delta\varepsilon$	Eq (8)
ε	p. 11	$\hat{\underline{P}}^+(k+1)$	Eq (9)
b_i	p. 11	$\omega(t)$	p. 16
ν	p. 11	$\eta(t)$	p. 16
XYZ	p. 12	$\omega(s)$	p. 16
$\hat{\underline{X}}^-(k+1)$	Eq (5)	$\eta(s)$	p. 16
$\hat{\underline{X}}^+(k)$	Eq (5)	a	p. 16

Symbol	Defined or First Used	Symbol	Defined or First Used
$\underline{\Phi}$	Eq (5)	ϕ_g	p. 16
λ	p. 16	Δt	Eq (19)
P	p. 17	$\omega_{\phi g}$	p. 20
V	p. 17	ω_λ	p. 20
A	p. 17	$\underline{\hat{P}}_o^+$	p. 23
η	p. 17	$q_{\phi g}$	p. 24
$P_{\phi g}$	Figure 2	q_λ	p. 24
$V_{\phi g}$	Figure 2	Hgt	Eq (47)
$A_{\phi g}$	Figure 2	$\hat{\varepsilon}$	Eq (48)
P_λ	Figure 2	$\hat{X}_\upsilon$	Eq (48)
V_λ	Figure 2	$\hat{Y}_\upsilon$	Eq (48)
A_{λ}	Figure 2	$\hat{Z}_\upsilon$	Eq (48)
$\eta_{\phi g}$	Figure 2	X_s	Eq (48)
η_λ	Figure 2	Y_s	Eq (48)
$t_{(k)}$	p. 17	Z_s	Eq (48)
$t_{(k+1)}$	p. 17	$R(t)$	p. 32
$\underline{\omega}_{(k)}$	p. 17	$\underline{Q}_7$	p. 46

Symbol	Defined or First Used	Symbol	Defined or First Used
$\underline{Q}_9$	p. 47	σ_{RES}	p. 92
f	p. 52	X	p. 94
$\underline{d}_{EF}$	Eq (71)	T	p. 102
$\underline{e}_E$	Eq (72)	e	p. 104
$\hat{\underline{P}}_{(k)}^{+}(1,1)$	p. 62		
$\hat{\underline{P}}_{(k)}^{+}(4,4)$	p. 62		
$\hat{\underline{P}}_{(k)}^{+}(7,7)$	p. 62		
$\underline{d}_{EC}$	Eq (75)		
$\underline{e}_c$	Eq (76)		
$\sigma_{Long.}$	Table VII		
$\sigma_{Lat.}$	Table VII		
$\sigma_{Alt.}$	Table VII		
σ_{VE}	Table VII		
σ_{VN}	Table VII		
σ_{VV}	Table VII		
$\Delta t'$	p. 76		

x

Abstract

This report is directed toward the design of a real-time estimation algorithm, a Kalman filter, that estimates aircraft position and velocity using multiple DME range measurements. The estimator is designed and tested for feasibility as a reference system for examining Inertial Navigational System (INS) low frequency errors. Both a 9-state estimator including jerk states and a 7-state estimator without the jerk states are designed.

With the tuning parameters used in the estimator tests, the 7-state estimator provides better performance than the 9-state estimator. An approximate analysis of the 7-state estimator performance (by comparison to FASTMAP, a currently used and accepted filter, and CIRIS, the Completely Integrated Reference Instrumentation System), reveals that estimator errors in the high frequency range are greater than those of an INS, but errors in the DME-based estimator are consistent in strength and do not exhibit an unbounded growth as typical of INS errors. For the estimator in this study, the approximate values that encompass 50 percent of all the errors (as compared to CIRIS) for latitude, longitude, latitude velocity, and longitude velocity were

Latitude position	$\Longrightarrow$ $\pm$ 83	feet
Longitude position	$\Longrightarrow$ $\pm$183	feet
Latitude velocity	$\Longrightarrow$ $\pm$ 8.4	feet/sec
Longitude velocity	$\Longrightarrow$ $\pm$ 7.5	feet/sec

Improving estimator performance is suggested by proper tuning and by using an adaptive approach.

A DESIGN OF A TRAJECTORY ESTIMATOR

USING MULTIPLE DME RANGE

MEASUREMENTS

I. Introduction

An important component of the modern navigation system
acquisition process is the flight test program. The flight
test program is used to evaluate and verify the performance
of inertial navigational systems (INS) and includes the
proper selection of reference navigational systems. Current
flight test reference systems employ external measurements
such as radar, Distance Measuring Equipment (DME), corre-
lation techniques, and onboard reference INS. These meas-
urements are used to form reference trajectories which are
compared with the INS trajectory data to evaluate the INS.

Depending on the type of reference system used, such an
analysis can either be a post-flight evaluation or a real-
time evaluation. A real-time evaluation of the system keeps
the pilot (or operator) continuously aware of the system's
performance. In this way, an INS malfunction is quickly
detected, and perhaps a costly mission is aborted.

Trajectory errors of high frequency are relatively
uncommon in INS; that is, INS short-term oscillations are
minimal. In contrast, INS trajectory errors of low frequency

1

are of substantial importance. (The 84-minute Schuler period is always evident in the flight tests.) Although inertial navigational systems may be highly accurate for a short time after initialization (alignment), these systems are hindered by long-term drift errors that increase with time. A reference system for the INS should be more accurate than the INS in the low frequency error domain to provide an adequate method for checking INS performance for typical flight time. Since high frequency errors in the INS are usually insignificant, INS superiority to the reference in the high frequency range is not intolerable.

The need for a low-cost, real-time, and easily deployable reference system (with a relatively small low frequency error) has led to investigating the use of existing DME stations as a source of reference systems (Refs 3; 4; 5). DME stations are capable of giving noise-corrupted range measurements to aircraft by returning a signal received from the aircraft. A continuous input of local station ranges can conceivably be employed in a minicomputer algorithm or central processor to produce aircraft trajectory estimates. This multiple DME reference system would have small low frequency errors since DME errors are rather consistent in RMS magnitude and are not characterized by unbounded error growth as typical in inertial navigation systems. A reference system using DME stations could also exploit bearing data for a trajectory determination. However, bearing data, available when the DME stations are a part of VOR/DME or

2

TACAN, are generally much noisier than range data. In light of the noisy nature of this data, a trade-off exists between keeping the reference as simple as possible, and increasing complexity by the addition of more information. In consideration of the reference system in this study, trajectory information that could be extracted from bearing data is simply neglected in favor of avoiding a more complex design. Only DME range measurements are used.

Available local station ranges include measurements from stations within 150 nautical miles for aircraft attitudes above 18,000 feet (Ref 5:150). (Greater ranges can be obtained for higher altitudes.) Every point in the United States, except for portions of the Northwest, is covered by at least ten DME stations within a 150 nautical mile radius (Ref 5:150). Because over 750 DME stations already exist in the continental United States as a part of VORTAC, VOR/DME, and TACAN facilities (Ref 1:Chap. IX, p. 8), the transition to this type of reference system should be reasonably quick and inexpensive.

This study is directed toward the design of a real-time estimation algorithm, a Kalman filter, that estimates position and velocity of an aircraft using multiple DME range measurements. In addition to position and velocity, the algorithm also estimates a bias associated with each station measurement. In order for the estimator to be a feasible reference compared with currently used references (see Chapter II), accuracy goals are set to encompass half of the longitude and half of

the latitude position errors within ±100 feet and half of
the velocity errors within ±8 feet per second. Such accu-
racy in the reference should verify long-term INS errors;
(typical INS can have one nautical mile/hour drift rates).
Although the Kalman filter is designed and analyzed in
FORTRAN on the 60-bit CDC 6600 at Wright-Patterson Air Force
Base, an extension of this study includes the writing of the
algorithm into assembly language. Bearing in mind the word-
length problem (numerical precision and numerical stability)
associated with converting from 60 bits to 16 bits (or so),
a minicomputer or a general purpose machine already onboard
can then be used in-flight to process the incoming range
data with the algorithm.

II. Background

History

In December 1976, the Central Inertial Guidance Test
Facility (CIGTF) conducted flight tests of the FASTMAP (Fast
Multi-DME Airborne Position) system. The FASTMAP tests
involved the use of multi-DME range measurements to compute
aircraft position and velocity. FASTMAP system operations,
once initiated, were automatic; the DME airborne interrogator
automatically sequenced frequencies of stations in the vicin-
ity of the flight. A frequency corresponds to the identifi-
cation number of a particular station. The channel number
of each DME station, system time, signal power level, atmo-
spheric temperature and pressure, and each noise-corrupted
measurement were stored in a raw data package. Trajectory
data from CIGTF's Completely Integrated Reference Instru-
mentation System (CIRIS) were also stored for the same flights.
The position and velocity computations were accomplished post-
flight and compared to CIRIS. Position and velocity accuracy
obtained from the FASTMAP system were 109.4 feet CEP (Circular
Error Probable) and 9.2 feet per second CEP respectively
(Ref 3:21).

Use of Multiple DME for a Position Determination

An actual DME measurement involves determining the time
required for a radar signal to travel from the aircraft to

5

the DME station and back to the aircraft. Knowledge of the signal propagation velocity (C) and time lapse (Δt) can be used for a rough distance measurement. The common formula $D = C\Delta t$ is employed for the range calculation. Each station has a nominal 50 microsecond delay which must be subtracted from Δt automatically or by an operator in the aircraft (Ref 5:151).

Although many range measurements should be available to the system, the type of equations to be employed in the position determination can be illustrated best by the use of three DME range measurements in the following simplified example. Without the presence of system errors, three (or more) DME range measurements can be used to determine an aircraft's position by triangulation methods. This requirement of triangulation no longer applies when a dynamic model is introduced, as in the Kalman filter. In other words, with a dynamic model, flight trajectory information is attainable from DME measurements taken one measurement at a time. Nevertheless, the equation required for each of the three range measurement determinations in the example is essentially the same equation used for the dynamic model.

In Figure 1, a diagram for the acquisition of three DME stations is shown. ε_1, ε_2, and ε_3 are the actual DME measurements, r_T is the position vector, and the coordinate frame xyz is arbitrary. Three equations can be solved for r_{T_1}, r_{T_2}, and r_{T_3} in terms of ε_1, ε_2, and ε_3 and station

6
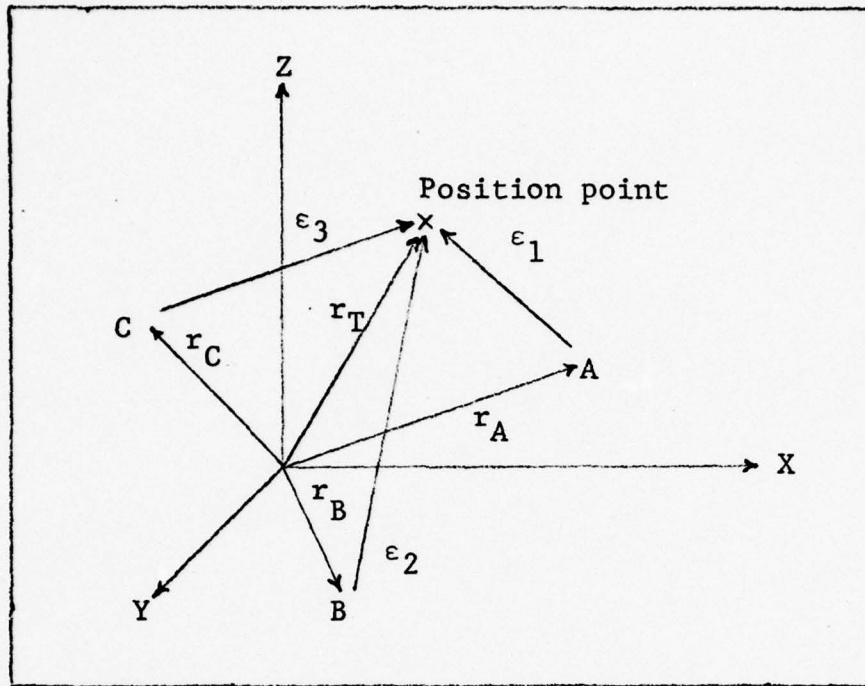
Figure 1. Position Via Three DME Stations

position coordinates, r_{A_i}, r_{B_i}, r_{C_i}:

$$\epsilon_1^{\ 2} = (r_{T_1} - r_{A_1})^2 + (r_{T_2} - r_{A_2})^2 + (r_{T_3} - r_{A_3})^2 \tag{1}$$

$$\epsilon_2^{\ 2} = (r_{T_1} - r_{B_1})^2 + (r_{T_2} - r_{B_2})^2 + (r_{T_3} - r_{B_3})^2 \tag{2}$$

$$\epsilon_3^{\ 2} = (r_{T_1} - r_{C_1})^2 + (r_{T_2} - r_{C_2})^2 + (r_{T_3} - r_{C_3})^2 \tag{3}$$

The subscripts A, B, and C represent the three different DME
stations, and the subscript T represents the aircraft
position; i = 1, 2, or 3 denotes the particular component.

7

In practice it is impossible to acquire three stations at once. Therefore, the algorithm for this study must have the capability to calculate positions from a single measurement a finite time apart from another measurement. Also, unlike the simplified example, the algorithm design needs initial positions and velocities to start the estimating procedure. Though the approaches are quite different, a range measurement equation similar to the ones used in the example is employed in the algorithm as the measurement equation.

DME Error Model

In the preceding example, measurement errors were assumed absent. However, associated with each DME range measurement is an uncertainty due to several different types of errors. These errors can be separated and analyzed to form an overall DME measurement model. The following DME error model is credited to the investigation of DME errors by R. W. Latham and R. S. Townes in 1975 (Ref 6:332-342) and others (Refs 2; 7).

The error in each DME measurement consists of errors in the airborne equipment, the propagation path, and the ground station. Latham has devised an error model, based on previous models, that separates each of these error types into a bias error and a wideband noise error. Bias errors consist of constant errors which cause the range measurement to be always more or less than the true value. In contrast, noise

errors randomly oscillate about the bias and can change from measurement to measurement. The four major error contributions have been found by past experience to be: bias errors in the ground station (394 feet RMS), bias errors in the airborne equipment (164 feet RMS), noise in the airborne equipment (50 feet RMS), and noise in the ground station (26 feet RMS) (Ref 6:332).

DME ground stations are intended to transmit a radio signal exactly 50 microseconds after receiving a signal from the aircraft. The 50 microsecond delay comes from natural delays in the electronic equipment, a delay line, and a finely adjustable electronic delay. Any deviation from the 50 microsecond delay will cause an error in the range measurement. Inaccuracies inherent in the ground equipment are responsible for such deviations.

Airborne equipment errors are caused mainly by power level uncertainties. Latham has shown that as the power level increases, the bias errors change. Because of this functional dependence of bias on signal strength, the amount of free space attenuation also affects the error.

The development of a DME error model now allows the use of Kalman filtering to calculate the best estimate of the position and velocity states. Bias errors are for the most part removed by repeated experiments (see Chapter IV), and the mean value of noise errors is assumed to be zero.

Whereas the example in this chapter presents a static and noiseless situation, a Kalman filter must take into

9

account the dynamic quality of an aircraft in flight and an error model such as the one described above. The Kalman filter in this study is constructed to give estimates of the trajectory states. These estimates are essentially statistically weighted averages of the solution to a set of dynamic equations and of DME range measurement information. The algorithm, or Kalman filter, is henceforth referred to as an "estimator."

III. Estimator Design

Theory

Now that a noise model and measurement equation have been developed in the previous chapter, the estimator can be designed to meet the prescribed accuracy goals. Before actually building the estimator, the dynamics equations, measurement equation, and statistical characterization of noises and uncertainty need to be specified. The estimator uses information from both the dynamic equations and DME measurements to obtain best estimates of the aircraft position and velocity states.

An alternative to estimating trajectory states is to estimate error states, such as INS states minus estimator states. A reference system using this approach can conceivably be used for evaluating INS output. However, the reference designed in this study estimates total trajectory states, and comparison to INS states is accomplished outside of the estimator algorithm.

For the most part, the usual methods for extended Kalman filter (EKF) design are employed to keep the design straight-forward. Nevertheless, several ad hoc procedures are necessary for this estimator problem. For example, the measurement computations require an evaluation of the range equation:

$$\varepsilon = \left[(r_{T_1} - r_{A_1})^2 + (r_{T_2} - r_{A_2})^2 + (r_{T_3} - r_{A_3})^2\right]^{\frac{1}{2}} + b_i + \nu$$

$$(4)$$

where b_i is the DME measurement bias associated with station i and ν is zero-mean white noise. Use of Equation (4) requires keeping track of which station is being acquired, both for the appropriate station coordinates and the bias evaluation. Since

11

the bias is unique for each station, a procedure is necessary to keep the bias and bias variance for each station separate.

Both a 9 - state estimator and a 7 - state estimator are designed. The synthesis of the 9 - state estimator includes as states the first three derivatives of the position states: velocity, acceleration, and rate of change in acceleration (jerk). The 7 - state estimator includes the first two derivatives of the position states: velocity and acceleration. First, the estimator that includes jerk is designed. The 9 - state estimator is then easily transformed to the 7 - state estimator by modelling the noise as entering at the next lower derivative level. (See page 21). Both estimators are tested for performance and the final choice between these are made in Chapter IV.

In every estimator problem, a suitable coordinate frame and appropriate units must be chosen. Two different approaches are investigated. One possible coordinate frame for the estimator states is an XYZ eartesian frame centered at the earth's center with the Z - axis through the north pole, the Y - axis through the Greenwich Meridian and equator, and the X - axis forming a right - handed coordinate system. Position inputs would be in terms of latitude, longitude, and height from the local geodetic frame of reference, but they would be converted to the XYZ frame by the estimator using an oblate earth model. At the conclusion of each estimation process, the updated states in XYZ coordinates would be converted back to the familiar latitude, longitude, and height for output.

Another possible approach is to skip the input/output conversion required above and perform the estimation process directly in the local geodetic frame using latitude and longitude in the estimator equations. For this study, working directly in the local geodetic frame proves to be most useful because only one conversion from the local geodetic frame to the XYZ frame is used. The estimator performs entirely in the local geodetic frame, but one conversion is needed to utilize the DME information in the distance relationship. (See page 25) Table I illustrates the units of each quantity used in the estimator. The last column contains actual converted output units; a blank in this

Table I. Units of Estimator States

QUANTITY	ESTIMATOR UNITS	OUTPUT UNITS
Angular Position	radians	radians
Angular Velocity	radians/second	knots or feet
Angular Acceleration	radians/second^2	--
Angular Jerk	radians/second^3	--
Bias	radians	feet
Position Covariance	radians^2	feet^2 or radians^2
Velocity Covariance	(radians/second)^2	--
Acceleration Covariance	(radians/second^2)^2	--
Jerk Covariance	(radians/second^3)^2	--

column signifies there is no output for the listed quantity.

The estimator synthesis necessitates the use of five basic filter equations:

$$\hat{\underline{X}}^-_{(k+1)} = \underline{\Phi}\ \hat{\underline{X}}^+_{(k)} \tag{5}$$

$$\hat{\underline{P}}^-_{(k+1)} = \underline{\Phi}\ \hat{\underline{P}}^+_{(k)}\underline{\Phi}^T + \underline{G}\ \underline{Q}\ \underline{G}^T \tag{6}$$

$$\underline{K}_{(k+1)} = \hat{\underline{P}}_{(k+1)}\ \underline{H}^T_{(k+1)} \left[\underline{H}_{(k+1)}\ \hat{\underline{P}}^-_{(k+1)}\ \underline{H}^T_{(k+1)} + R \right]^{-1} \tag{7}$$

$$\hat{\underline{X}}^+_{(k+1)} = \hat{\underline{X}}^-_{(k+1)} + \underline{K}_{(k\_1)}\ \Delta\varepsilon \tag{8}$$

13

$$\hat{\underline{P}}_{(k+1)} = \hat{\underline{P}}^-_{(k+1)} - \underline{K}_{(k+1)} \ \underline{H}_{(k+1)} \ \hat{\underline{P}}^-_{(k+1)} \tag{9}$$

Superscripts (-) and (+) denote before and after a measurement respectively. $\underline{\Phi}$ in Equations (5) and (6) is the state transition matrix relating the states at time instant (k+1) to the states at time instant (k). (See page 22). The matrix $\underline{Q}$ in Equation (6) represents the strengths of the white noises that are added to the last (or highest) derivative states. (See page 20). R in Equation (7) is a scalar denoting the uncertainty in the DME measurements. (See page 31). The residual, $\Delta\varepsilon$ in Equation (8), is the difference between an actual DME measurement and what the estimator predicts it to be. (See page 27). The $\underline{H}_{(k+1)}$ matrix in Equations (7) and (9) is the partial of Equation (4) with respect to the estimator states, evaluated at $\hat{\underline{X}}_{(k+1)}$. (See page 27).

First, Equations (5) and (6) are used to propagate the states and state covariances up to, but not including, the next measurement as $\hat{\underline{X}}_{(k+1)}$ and $\hat{\underline{P}}_{(k+1)}$, respectively. Second, the Kalman gain matrix, $\underline{K}_{(k+1)}$, is calculated from the known state covariance propagation. It should be noted that, unlike the linear Kalman filter, the EKF covariance matrix cannot be precomputed because $\underline{H}_{(k+1)}$ is a matrix of partial derivatives evaluated at $\hat{\underline{X}}_{(k+1)}$, and thus requires knowledge of the measurement history. Finally, after the incorporation of each measurement, the estimator updates the states to $\hat{\underline{X}}^+_{(k+1)}$ and the state covariances to $\underline{P}^+_{(k+1)}$ via the Kalman gain.

System Dynamics

System. The system in this study is an aircraft flying at

14

some known altitude and known initial position and velocity.
The propagation equations, Equations (5) and (6), require a
knowledge of the dynamics of this system. In other words,
all system states - position, velocity, and so forth - are
propagated through space obeying a set of dynamic equations
that relates the system to its environment.

Approximations. To avoid a set of dynamic equations that
is too complex for real-time applications, the equations are
simplified or approximated whenever feasible. One simplification
stems from the fact that the aircraft flies at a known
altitude. The availability of an autopilot with an accurate
altimeter enables the estimator to omit the vertical states.
Latham has shown that typical altimetor errors degrade the
position CEP by less than 5%. (Ref 5:152). The vertical direction
is identified with the up direction in the local geodetic
frame. Since the vertical state is absent, the estimator assumes
no uncertainty in that direction, and only latitude and longitude
states are estimated.

In the 9 - state estimator, an assumption that the system
maintains roughly constant rate of change in acceleration
is another approximation. Just how "rough" depends on both
pilot control and natural disturbances. The time between
measurements (.05 to .5 seconds) is short enough to justify
that such disturbances cannot significantly alter the rate of
change in acceleration. For the 7 - state estimator, the above
approximation is moved to the next lower derivative level.
Since the 7 - state estimator does not model jerk, the
acceleration is assumed essentially constant between measurements.

15

Another simplification for the 9 - state estimator is
that each jerk state, denoted by $\eta(t)$, is modelled as the
output of a first-order lag driven by a white Gaussian noise
(totally random noise), $\omega(t)$. Diagram (a) depicts the relation-
ship between $\omega(t)$ and $\eta(t)$ in general Laplace form:

$$\xrightarrow{\omega(s)} \boxed{\dfrac{1}{s + a}} \xrightarrow{\eta(s)} \qquad (a)$$
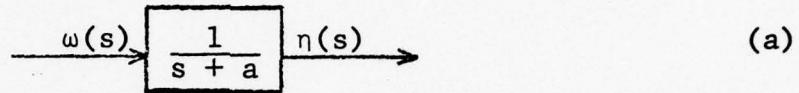
This effectively claims that disturbances in jerk are
exponentially time-correlated. Again, each acceleration state
in the 7 - state estimator is treated in the same manner
as the jerk states in the 9 - state estimator.

All three of these simplifications are employed in the
estimator design. The justification of such simplifications
is found via estimator performance.

Estimator States. Before the set of equations that relate
the states at time instant (k+1) to the states at time
instant (k) can be designed, the various states of the estimator
are propagated from time instant (k) to (k+1) with coordinates
of latitude and longitude in units of radians. Trajectory
states for the 7 - state estimator are chosen as position,
velocity, and acceleration in both latitude and longitude
(i.e. north and east) directions. The 9 - state estimator has
the jerk state added in both directions. Another state (of
both estimators) is the DME bias which is also propagated and
updated in each measurement interval. If latitude and
longitude are denoted by ϕ_g (subscripted "g" means geodetic)
and λ, respectively, and position, velocity, acceleration, and

jerk are denoted by P, V, A, and η, respectively, the states
of the two estimators can be summarized as in Figure 2.

$$P_{\phi_g} \quad V_{\phi_g} \quad A_{\phi_g} \quad P_\lambda \quad V_\lambda \quad A_\lambda \quad b_i \quad \bigg| \quad \eta_{\phi_g} \quad \eta_\phi$$

with 7 - State Estimator bracketed over the first group and 9 - State Estimator bracketed under the first group.
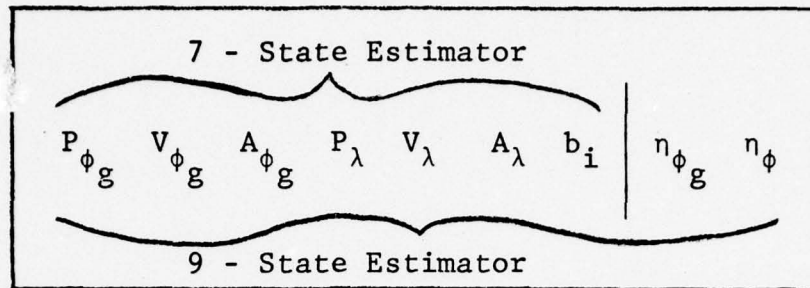
Figure 2.   Estimator States

Dynamic Equations. If the states in Figure 2 are represented
in an array, $\underline{X}$, the differential equations relating the states
to each other can be written as

$$\frac{d\underline{X}(t)}{dt} = \underline{g}\ (\underline{X}(t),\ \underline{\omega}(t)) \tag{10}$$

A discrete equation relating the values of $\underline{X}_{(k+1)}$ to $\underline{X}_{(k)}$
can be written as

$$\underline{X}_{(k+1)} = \underline{f}\ (\underline{X}_{(k)},\ \underline{\omega}_{(k)}) \tag{11}$$

Estimator states at time instant (k+1), or $t_{(k+1)}$, are
a function of the states at time instant (k), or $t_{(k)}$,
and a white noise vector $\underline{\omega}_{(k)}$. $\underline{\omega}_{(k)}$ represents the deviations
from a constant rate of change in acceleration in the 9 - state
estimator and represents the deviations from a constant
acceleration in the case of the 7 - state estimator.

The realtionship between $\omega(s)$ and $\eta(s)$ in each direction
for the 9 - state estimator is given by diagram (a). The
value of "a" in this diagram is set to zero for a pure integrator.
(It should be noted that only the case of "a" equal to zero is

17

investigated in this report, but other values of "a" are suggested for future study). With "a" equal to zero, the continuous stochastic process that models the change in jerk rate as white noise is

$$\frac{d\eta(t)}{dt} = \omega(t) \tag{12}$$

where η is jerk and $\omega(t)$ is zero-mean white noise. The discrete model for the expected values of P,V,A, and η is obtained by taking the expected value of Equation (12):

$$\frac{d\bar{\eta}(t)}{dt} = 0 \tag{13}$$

Given the best estimates of the states at $t_{(k)}$ ($\hat{P}_{(k)}$, $\hat{V}_{(k)}$, $\hat{A}_{(k)}$, and $\hat{\eta}_{(k)}$), Equation (13) can be integrated from $t_{(k)}$ to t:

$$\bar{\eta}(t) = \hat{\eta}_{(k)} \tag{14}$$

Integrating Equation (14) from $t_{(k)}$ to t yields

$$\bar{A}(t) = \hat{A}_{(k)} + \hat{\eta}_{(k)}(t - t_{(k)}) \tag{15}$$

Expected velocity is then obtained by integrating Equations (15):

$$\bar{V}(t) = \hat{V}_{(k)} + \hat{A}_{(k)}(t - t_{(k)}) + \tfrac{1}{2}\hat{\eta}_{(k)}(t - t_{(k)})^2 \tag{16}$$

An integration of Equation (16) provides an expression for expected position:

$$\bar{P}(t) = \hat{P}_{(k)} + \hat{V}_{(k)}(t - t_{(k)} + \tfrac{1}{2}\hat{A}_{(k)}(t - t_{(k)}) + \tfrac{1}{6}\hat{\eta}_{(k)}(t - t_{(k)})^3 \tag{17}$$

18

Evaluating Equations (14), (15), (16), and (17) at time instant (k+1) uields

$$\overline{\eta}_{(k+1)} = \hat{\eta}_{(k)} \tag{18}$$

$$\overline{A}_{(k+1)} = \hat{A}_{(k)} + \hat{\eta}_{(k)}(\Delta t) \tag{19}$$

$$\overline{V}_{(k+1)} = \hat{V}_{(k)} + \hat{A}_{(k)} \Delta t + \tfrac{1}{2} \hat{\eta}_{(k)} \Delta t^2 \tag{20}$$

$$\overline{P}_{(k+1)} = \hat{P}_{(k)} + \hat{V}_{(k)}\Delta t + \tfrac{1}{2} \hat{A}_{(k)}\Delta t^2 + \tfrac{1}{6} \hat{\eta}_{(k)} \Delta t \tag{21}$$

where

$$\Delta t = t_{(k+1)} - t_{(k)} \tag{22}$$

Equations (18) through (21) are the mathematically exact integrations of Equations (13) from $t_{(k)}$ to $t_{(k+1)}$, and provide expected values of P,V,A, and η at $t_{(k+1)}$ given their best estimates at $t_{(k)}$. Essentially, the mean state, values are propagated from $t_{(k)}$ to t_{k+1}.

Equations (18) through (21) can be expressed as the propagation equations between measurements for the 9 - state estimator when the expected state values at $t_{(k+1)}$ are recognized as the estimator's best estimate of the states at $t_{(k\_1)}$. In summary, the dynamic, or propagation, equations of the 9 - state estimator are

$$\hat{P}^-_{\phi_g(k+1)} = \hat{P}^+_{\phi_g(k)} + \hat{V}^+_{\phi_g(k)} \Delta t + \tfrac{1}{2} \hat{A}^+_{\phi_g(k)}\Delta t^2 + \tfrac{1}{6} \hat{\eta}^+_{\phi_g(k)}\Delta t^3 \tag{23}$$

$$\hat{V}^-_{\phi_g}(k+1) = \hat{V}^+_{\phi_g}(k) + \hat{A}^+_{\phi_g}(k) \, \Delta t + \tfrac{1}{2}\hat{\eta}^+_{\phi_g}(k) \, \Delta t^2 \tag{24}$$

$$\hat{A}^-_{\phi_g}(k+1) = \hat{A}^+_{\phi_g}(k) + \hat{\eta}^+_{\phi_g}(k) \, \Delta t \tag{25}$$

$$\hat{P}^-_{\lambda}(k+1) = \hat{P}^+_{\lambda}(k) + \hat{V}_{\lambda}(k)\Delta t + \tfrac{1}{2}\hat{A}^+_{\lambda}(k)\Delta t^2 + \tfrac{1}{6}\hat{\eta}^+_{\lambda}(k)\Delta t^3 \tag{26}$$

$$\hat{V}^-_{\lambda}(k+1) = \hat{V}^+_{\lambda}(k) + \hat{A}^+_{\lambda}(k)\Delta t + \tfrac{1}{2}\hat{\eta}^+_{\lambda}(k)\Delta t^2 \tag{27}$$

$$\hat{A}^-_{\lambda}(k+1) = \hat{A}^+_{\lambda}(k) + \hat{\eta}^+_{\lambda}(k) \, \Delta t \tag{28}$$

$$\hat{\eta}^-_{\phi_g}(k+1) = \hat{\eta}_{\phi_g}(k) \tag{28}$$

$$\hat{\eta}^-_{\lambda}(k+1) = \hat{\eta}^+_{\lambda}(k) \tag{30}$$

To model the uncertainty in the propagation equations, a first-order approximation of Equation (12) yields

$$\eta_{(k+1)} = \eta_{(k)} + \Delta t \, \omega_{(k)} \tag{31}$$

which can be expressed in latitude and longitude directions:

$$\eta^-_{\phi_g}(k+1) = \eta^+_{\phi_g}(k) + \Delta t \, \omega_{\phi_g}(k) \tag{32}$$

$$\eta^-_{\lambda}(k+1) = \eta^+_{\lambda}(k) + \Delta t \, \omega_{\lambda}(k) \tag{33}$$

A similar approach is used for the 7 - state estimator except the noises are added to the acceleration states. The propagation equiations for the 7 - state estimator are as follows:

$$\hat{P}^-_{\phi_g}(k+1) = \hat{P}^+_{\phi_g}(k) + \hat{V}^+_{\phi_g}(k) \; \Delta t + \tfrac{1}{2} \hat{A}^+_{\phi_g}(k) \; \Delta t^2 \tag{34}$$

$$\hat{V}^-_{\phi_g}(k+1) = \hat{V}^+_{\phi_g}(k) + \hat{A}^+_{\phi_g}(k) \; \Delta t \tag{35}$$

$$\hat{A}^-_{\phi_g}(k+1) = \hat{A}^+_{\phi_g}(k) \tag{36}$$

$$\hat{P}^-_{\lambda}(k+1) = \hat{P}^+_{\lambda}(k) + \hat{V}^+_{\lambda}(k) \; \Delta t + \tfrac{1}{2} \hat{A}^+_{\lambda}(k) \; \Delta t^2 \tag{37}$$

$$\hat{V}^-_{\lambda}(k+1) = \hat{V}^+_{\lambda}(k) + \hat{A}^+_{\lambda}(k) \; \Delta t \tag{38}$$

$$\hat{A}^-_{\lambda}(k+1) = \hat{A}^+_{\lambda}(k) \tag{39}$$

Entering the noise at the acceleration level and, again, using a first-order approximation provides expressions for the uncertainty in the propagation equations:

$$A^-_{\phi_g}(k+1) = A^+_{\phi_g}(k) + \Delta t \omega_{\phi_g}(k) \tag{40}$$

$$A^-_{\lambda}(k+1) = A^+_{\lambda}(k) + \Delta t \; \omega_{\lambda}(k) \tag{41}$$

An additional state is augmented to the estimator states (of both estimators) due to the presence of the DME range measurement bias. Measurement bias is modelled as an integrator with no white noise input and a random initial condition. Integrating a random initial condition produces what is known as a random constant or bias, $b_i(t)$.

Initial
Condition

$$\boxed{\int \cdot dt} \longrightarrow b_i(t) \qquad \text{(b)}$$

The bias differential equation from diagram (b) is

$$\frac{db_i(t)}{dt} = 0 \qquad (42)$$

Integrating Equation (42) from $t_{(k)}$ to $t_{(k+1)}$ yields

$$b_{i(k+1)} = b_{i(k)} \qquad (43)$$

The subscript (i) denotes a bias associated with station (i).
In changing from station to station, the initial condition in
diagram (b) must be reset to correspond to the correct station.
The method of separating the bias according to station is
covered in the section on "Bias Calculation" in this chapter.

A Gaussian random variable model is used for the initial
condition with zero mean and a variance consistent with
typical bias errors given in Chapter II. In this study,
bias variance is set at 10^{-12} rad^2, or 432 ft^2. The use of
different bias variances are not attempted in this report
but are suggested for further study.

Covariance Propagation

The state propagation of the previous section provides
the estimator with a state transition matrix, $\underline{\Phi}$. $\underline{\Phi}$ is the
matrix representation of the dynamic equations, and, for the
9 - state estimation, $\underline{\Phi}$ is denoted by the following 9 x 9
matrix:

22

$$
\underline{\Phi} = \begin{bmatrix}
1 & \Delta t & \Delta t^2/2 & 0 & 0 & 0 & \Delta t^3/6 & 0 & 0 \\
0 & 1 & \Delta t & 0 & 0 & 0 & \Delta t^2/2 & 0 & 0 \\
0 & 0 & 1 & 0 & 0 & 0 & \Delta t & 0 & 0 \\
0 & 0 & 0 & 1 & \Delta t & \Delta t^2/2 & 0 & \Delta t^3/6 & 0 \\
0 & 0 & 0 & 0 & 1 & \Delta t & 0 & \Delta t^2/2 & 0 \\
0 & 0 & 0 & 0 & 0 & 1 & 0 & \Delta t & 0 \\
0 & 0 & 0 & 0 & 0 & 0 & 1 & 0 & 0 \\
0 & 0 & 0 & 0 & 0 & 0 & 0 & 1 & 0 \\
0 & 0 & 0 & 0 & 0 & 0 & 0 & 0 & 1
\end{bmatrix}
\tag{44}
$$

$\underline{\Phi}$ for the 7 - state estimator is obtained in the same manner. The white noise coefficients from Equations (32) and (33) are represented in a separate matrix, $\underline{G}$:

$$
\underline{G}^T = \begin{bmatrix}
0 & 0 & 0 & 0 & 0 & 0 & \Delta t & 0 & 0 \\
0 & 0 & 0 & 0 & 0 & 0 & 0 & \Delta t & 0
\end{bmatrix}
\tag{45}
$$

The covariance is propagated between measurements as

$$
\hat{\underline{P}}^-_{(k+1)} = \underline{\Phi} \, \hat{\underline{P}}^+_{(k)} \, \underline{\Phi}^T + \underline{G} \, \underline{Q} \, \underline{G}^T
\tag{6}
$$

The diagonal terms of the 9 x 9 covariance matrix, $\hat{\underline{P}}^-_{(k+1)}$, give variances for state errors before each measurement. The off-diagonal terms yield an estimate of the correlation between each state. Near perfect initial conditions (position and velocity) are assumed for this estimator so $\hat{\underline{P}}^+_0$ is initiated with small starting values.

The matrix $\underline{Q}$ in Equation (6) is a 2 x 2 matrix denoting the strengths of the white noises ω_{ϕ_g} and ω_λ:

23

$$Q = \begin{bmatrix} q_{\phi g} & 0 \\ 0 & q_\lambda \end{bmatrix} \tag{46}$$

The values of the Q elements in equation (46) are fixed to reflect disturbances in jerk for the 7 - state estimator and disturbances in jerk rate for the 9 - state estimator.

The state propagation, Equation (5), and state covariance propagation, Equation (6), are used to propagate the states and covariances between each measurement. Now the estimator is ready to use incoming measurements to update the states and covariances at each measurement instant. Before the update equations are employed, the estimator must be able to predict the value of each measurement. Then a differencing of the prediction and the actual measurement (i.e. the residual) can be used as a means to update the states and covariances.

Measurement Prediction

Introduction. Once the state values have been propagated up to the end of the measurement interval, the estimator predicts a value of the next measurement. The prediction is the "best guess" at what the measurement should be and is based on all prior knowledge of the states up to, but not including the next measurement. DME station coordinates and the current estimate of aircraft coordinates are assigned to a common Cartesian coordinate frame. The distance (or measurement) equation, Equation (4), is then employed to yield a value for the measurement prediction.

Essentially, the measurement prediction is divided into three parts: DME station information, transformation of latitude, longitude, and height to a Cartesian coordinate frame, and finally the prediction of the measurement value itself.

DME Station Information. Incorporation of the channel information is accomplished with a subroutine, containing all the latitudes, longitudes, and heights of all the DME stations the aircraft might use on a particular flight. A simple "table-lookup" routine is used for associating the correct channel number to the respective station coordinates. This station information is obtained from DoD Flight Information Publication (IFR-Supplement, issued every eight weeks). Latitude and longitude are in units of degrees in the supplement and must be converted to radians for the estimator. The latitudes and longitudes in the supplement correspond to those on all Air Force maps (geodetic latitude). DME station information is inserted into the subroutine prior to each flight. The estimator then extracts this information from the subroutine in real-time.

Coordinate Transformation. In order to calculate a predicted range value, the latitudes, longitudes, and heights of the DME station and aircraft must be transformed to a common Cartesian coordinate frame. Range can then be computed using the geometric distance equation, Equation (4), for computing distances between two points in three dimensional space. As mentioned before, an appropriate Cartesian frame for the estimator is an XYZ frame centered at the earth's

center with the Z-axis through the north pole, the Y-axis through the Greenwich Meridian and equator, and the X-axis forming a right-handed coordinate system. Formulas that express X, Y, and Z Cartesian coordinates as functions of geodetic latitude, longitude, and height can be written as

$$X = f_1 \ (P_{\phi_g}, \ P_\lambda, \ Hgt)$$

$$Y = f_2 \ (P_{\phi_g}, \ P_\lambda, \ Hgt) \tag{47}$$

$$Z = f_3 \ (P_{\phi_g}, \ P_\lambda, \ Hgt)$$

where Hgt is height. Appendix A presents this set of equations in detail. These equations are used to obtain X,Y, and Z coordinates for both station and aircraft locations.

Measurement Prediction. A knowledge of the station and aircraft coordinates now allows the range estimate to be calculated from the measurement equation, Equation (4), using the zero mean value of the white noise, ν.

$$\hat{\varepsilon} = \left[(\hat{X}_u - X_s)^2 + (\hat{Y}_u - Y_s)^2 + (\hat{Z}_u - Z_s)^2 \right]^{\frac{1}{2}} + \hat{b}_{i(k+1)} \tag{48}$$

$\hat{\varepsilon}$ represents the predicted range value; X_s, Y_s, and Z_s are the station coordinates, and $\hat{X}_u$, $\hat{Y}_u$, and $\hat{Z}_u$ are the estimated aircraft coordinates. An estimated bias, $b_{i(k+1)}$ is added directly to the measurement prediction equation.

A comparison of the predicted measurement, $\hat{\varepsilon}$, with the actual incoming DME measurement provides the estimator with a residual for updating the states and covariances for each measurement. Before proceeding into the updating process,

26

The cutoff point has both a lower and an upper limit. The residual cutoff point is made small enough to ignore bad measurements, but it must also be set large enough to allow for aircraft trajectory changes. (Trajectory changes such as 180° turns will tend to temporarily increase residual size (See Chapter V)).

The updating process is, in essence, a method for changing the propagated states by amounts proportional to the residual. Obtaining an exact proportion, or Kalman gain, constitutes a central issue of Kalman filtering, and requires a linearized measurement equation to generate the desired $\underline{H}$ matrix for Equations (7) and (9). Since Equation (4) is nonlinear, some method for approximating this equation as linear constitutes the next step in the estimation process.

Linearized Measurement Equation

The residual computation of the last section employs the exact non-linear measurement equation, but, to permit matrix operations in the update equations, the measurement equation must be linearized. This linearization allows the measurement equation to be represented by a linear measurement matrix, or $\underline{H}$ matrix. The $\underline{H}$ matrix forms the crux for the update Equations (7), (8) and (9).

To calcualte the $\underline{H}$ matrix, the complete expression for ε,

$$\varepsilon = \left[(X_u - X_s)^2 + (Y_u - Y_s)^2 + (Z_u - Z_s)^2\right]^{\frac{1}{2}} + b_i + \nu \qquad (50)$$

can be expressed as a first - order Taylor series linearized about the best estimates of the states. As long as the estimator remains close to the true state values, $\underline{H}$ will adequately

represent the non-linear measurement equation. A first-order Taylor series of Equation (50) yields ε as a linear function of X_u, Y_u, Z_u, X_s, Y_s, Z_s, b_i and ν:

$$\varepsilon(X_u, Y_u, Z_u, X_s, Y_s, Z_s, b_i, \nu) \cong \hat{\varepsilon}(\hat{X}_u, \hat{Y}_u, \hat{Z}_u, X_s, Y_s, Z_s, \hat{b}_i)$$

$$+ \left.\frac{\partial \varepsilon}{\partial X_u}\right|_{\hat{X}_u, \hat{Y}_u, \hat{Z}_u} (X_u - \hat{X}_u) + \left.\frac{\partial \varepsilon}{\partial Y_u}\right|_{\hat{X}_u, \hat{Y}_u, \hat{Z}_u} (Y_u - \hat{Y}_u)$$

$$+ \left.\frac{\partial \varepsilon}{\partial Z_u}\right|_{\hat{X}_u, \hat{Y}_u, \hat{Z}_u} (Z_u - \hat{Z}_u) + \left.\frac{\partial \varepsilon}{\partial b_i}\right|_{\hat{b}_i} (b_i - \hat{b}_i) + \nu \qquad (51)$$

Errors in station coordinates, X_s, Y_s, and Z_s, are assumed to be negligible.

Equation (51) can be written equivalently as a function of P_{ϕ_y}, P_λ, height, b_i, and ν using Equation (47):

$$\varepsilon(P_{\phi_g}, P_\lambda, \text{Hgt}, b_i, X_s, Y_s, Z_s) \cong \hat{\varepsilon}(\hat{P}_{\phi_g}, \hat{P}_\lambda, \text{Hgt}, \hat{b}_i, X_s, Y_s, Z_s)$$

$$+ \left.\frac{\partial \varepsilon}{\partial P_{\phi_g}}\right|_{\underline{\hat{X}}^-_{(k+1)}} (P_{\phi_g} - \hat{P}_{\phi_g}) + \left.\frac{\partial \varepsilon}{\partial P_\lambda}\right|_{\underline{\hat{X}}^-_{(k+1)}} (P_\lambda - \hat{P}_\lambda)$$

$$+ \left.\frac{\partial \varepsilon}{\partial b_i}\right|_{\underline{\hat{X}}^-_{(k+1)}} (b_i - \hat{b}_i) + \nu \qquad (52)$$

where errors in height are assumed negligible and $\hat{\underline{X}}_{(k+1)}$

is the best estimate of the states.

An investigation of Eq (52) shows that the equation is in the form

$$\varepsilon - \hat{\varepsilon} = \Delta\varepsilon \stackrel{\sim}{=} [\underline{H}] \; [\underline{X} - \hat{\underline{X}}] + \nu$$

where $\underline{H}$ is given by

$$\underline{H} = \left.\frac{\partial\varepsilon}{\partial P_{\phi_g}}\right|_{\hat{\underline{X}}_{(k+1)}}, \; 0, \; 0, \; \left.\frac{\partial\varepsilon}{\partial P\lambda}\right|_{\hat{\underline{X}}_{(k+1)}}, \; 0, \; 0, \; 0, \; 0, \; \left.\frac{\partial\varepsilon}{\partial b_i}\right|_{\hat{\underline{X}}^-_{(k+1)}} \tag{53}$$

The units of the $\underline{H}$ terms are feet/radian since the residual, $\Delta\varepsilon$, is in feet and the states are in radians.

The actual evaluation of the partials of Equation (53) involves the substitution of Equation (47) into the measurement prediction Equation (50). The details of this operation are presented in Appendix B.

The bias is added directly in Equation (50), and consequently an incremental change in bias produces the same incremental change in range. In this light, it is evident that $\partial\varepsilon/\partial b_i = 1$ when ε and the bias are in common units. However, since ε is in units of feet and bias in units of radians, $\partial\varepsilon/\partial b_i$ is in units of feet/radian. Because longitude lines converge as the latitude angle increases, the number of feet per radian cannot be calculated using the conversion factor of 60 nautical miles per degree. Both latitude and longitude components are involved in the

direction of the range, thus making each degree contain less
than 60 nautical miles in the calculation of $\partial\varepsilon/\partial b_i$.

The orthogonality of the directions from which
latitude and longitude are measured yields a simple
method for obtaining the value of the bias partial. Figure 3
shows that $\partial\varepsilon/\partial b_i$ contains components of $\partial\varepsilon/\partial P_{\phi_g}$ and $\partial\varepsilon/\partial P_\lambda$.
Applying the Pythagorean theorem provides an expression for
$\partial\varepsilon/\partial b_i$:

$$\frac{\partial\varepsilon}{\partial b_i} = \left[\frac{\partial\varepsilon}{\partial P_{\phi_g}}^2 + \frac{\partial\varepsilon}{\partial P_\lambda}^2 \right]^{\frac{1}{2}} \tag{54}$$

The dependency of $\partial\varepsilon/\partial b_i$: on $\partial\varepsilon/P_{\phi_g}$ and $\partial\varepsilon/P_\lambda$ leaves
the estimator only the latter two partials to determine.
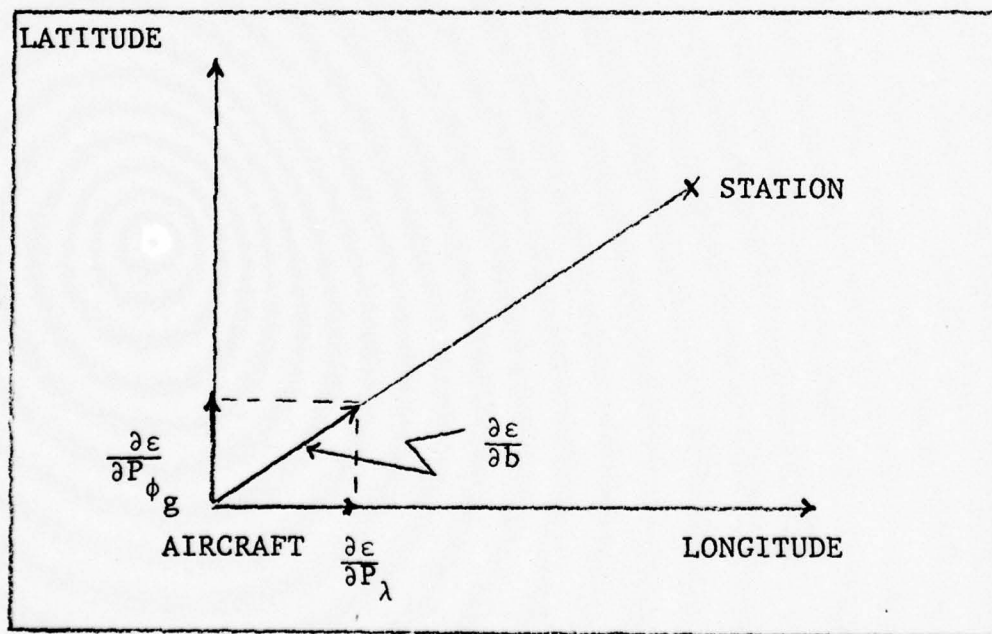
Figure 3. Dependence of $\partial\varepsilon/\partial b_i$ on $\frac{\partial\varepsilon}{\partial P_{\phi_g}}$ and $\partial\varepsilon/\partial P_\lambda$ in
$\underline{H}$ Matrix.

The equations needed to evaluate $\partial \varepsilon / \partial P_{\phi_g}$ and $\partial \varepsilon / \partial P_\lambda$ always depend on the current best state estimates-a property of any extended Kalman filter. Essentially, for each new measurement a new set of nominal conditions is used to solve the first-order Taylor series. The $\underline{H}$ matrix will therefore change its values from one measurement to the next. For each measurement, the algorithm recalculates an $\underline{H}$ and utilizes it in the state and state covariance update process.

Kalman Gain and Update Equations

The update process consists of the implemention of Equations (7), (8), and (9). The update portion is accomplishable only after the states and state covariances are propagated and after the residuals and linearized measurement equation are obtained. The algorithm divides the update process into three separate steps: the Kalman gain, the state update, and the covariance update.

The proportion by which the propagated estimates are changed after the incorporation of each measurement is called the Kalman gain. Equation (7) is repeated here for convenience:

$$\underline{K}_{(k+1)} = \hat{\underline{P}}^-_{(k+1)} \underline{H}_{(k+1)} \left[\underline{H}_{(k+1)} \hat{\underline{P}}^-_{(k+1)} \underline{H}^T_{(k+1)} + R \right]^{-1} \tag{7}$$

The Kalman gain, $\underline{K}_{(k+1)}$, essentially determines how much "faith" the estimator has in the measurements with respect to the state propagations. Since $\underline{H}_{(k+1)}$ changes from measurement to measurement, $\underline{K}_{(k+1)}$ also changes.

The value of R represents the uncertainty of incoming DME measurements; a low R value reflects accurate measurements.

The DME error model presented in Chapter II gives a "ball-park" range for R. Proper R values are best obtained by a process called filter tuning. However, in this report, R is set at 1000 feet^2. So allow for changes in R, R can be made a function of time, represented by R(t). It may be advantageous to have a changing R to allow for time-varying noise characteristics in the real world system (such as due to changing ranges from DME stations).

Sometimes the Kalman gain is referred to as a weighting matrix because, in a sense, the algorithm "weighs" the residuals with the Kalman gain. The weighted residuals are then added to the best prior state estimates to achieve a new updated estimate of the states. This is accomplished by Equation (8):

$$\hat{\underline{X}}^+_{(k+1)} = \hat{\underline{X}}^-_{(k+1)} + \underline{K}_{(k+1)} \, \Delta\varepsilon \tag{8}$$

where $\hat{\underline{X}}^+_{(k+1)}$ represents the updated estimates and $\Delta\varepsilon$ is the residual.

The propagated state covariance is updated in the same fashion using Equation (9):

$$\hat{\underline{P}}^+_{(k+1)} = \hat{\underline{P}}^-_{(k+1)} - \underline{K}_{(k+1)} \, \underline{H}_{(k+1)} \, \hat{\underline{P}}^-_{(k+1)} \tag{9}$$

As in the state case, a new updated estimate of the state covariance matrix is formed.

Bias Calculation

The bias calculation is an example of an _ad_ _hoc_ procedure to be incorporated in the estimator. The bias is composed

of random constant errors in both the airborne equipment and the DME stations. Because different stations are acquired, the bias will change from measurement to measurement. However, the bias must remain unique to each corresponding station. Some type of separation and bias variance reinitialization method is needed to maintain properly corresponding station biases.

This need for the algorithm to separate bias according to station has led to the following method. The bias is stored in an n x 1 array, where n is equal to or greater than the number of stations acquired during the flight. Bias values obtained from the state update equations are stored in different elements of the array for different channels. If a channel is acquired more than once (which is necessary for a good bias estimation), then only the bias array element corresponding to that station is called on as the best prior estimate of the bias state. Using mmm as an index and BI as the bias array, the estimator stores the bias as

BI (mmm)

BI (1) → mmm = 1 for Channel A
BI (2) → mmm = 2 for Channel B
BI (3) → mmm = 3 for Channel C
          etc.

A, B, and C denote arbitrary channels. BI is dimensioned at least the maximum amount of stations acquired in the flight. The estimator returns to the appropriate mmm value if that corresponding station is called on again, or if, in the case of a new station, mmm is incremented by one.

33

For example, after the estimator accepts 40 measurements and Channel B is called on again for a range measurement, the BI array element associated with mmm = 2 is updated and stored again in BI (2).

The separation technique must also include a method for reinitializing bias variance for each time a new DME station is acquired. Each time a new station (not previously used) is acquired, bias variance is reinitialized to the maximum value. If a station has been previously acuqired, the bias variance is reset to the latest value corresponding to that station. This effectively claims that a particular station's bias uncertainty is greatest for the first acquisition of that station. As that station is used again and again, bias uncertainty will generally decrease. (See Figure 15 in Chapter IV). The actual program in Appendix C shows the detailed procedure for treating the bias separation.

Truth Model Data

Data from an aircraft trajectory is necessary to test and analyze the estimator design. Measurements from a simulated flight or measurements recorded from an actual flight can be used to test the estimator. In the case of a flight simulation, the measurements to DME stations must be corrupted with a noise generator (random number generator). However, recorded measurements taken from an actual flight provide the best way to test the estimator.

Raw DME measurement data, CIRIS output data, and FASTMAP filter data for a test flight were stored on tapes.

Channel information, DME measurements, and system time (IRIG time) from the FASTMAP filter tape are used as the input for the estimator. The use of FASTMAP tape allows easier comparison of FASTMAP results with the real-time design estimator. (See Chapter IV). Essentially, the range data on the FASTMAP tape serves as a replacement for simulated system data.

The geometry of the station locations relative to the aircraft is important to the accuracy of the estimated aircraft position. A more spread out distribution of stations is preferred over a situation where all the available stations are in one direction. (See Figure 4 and Figure 5).
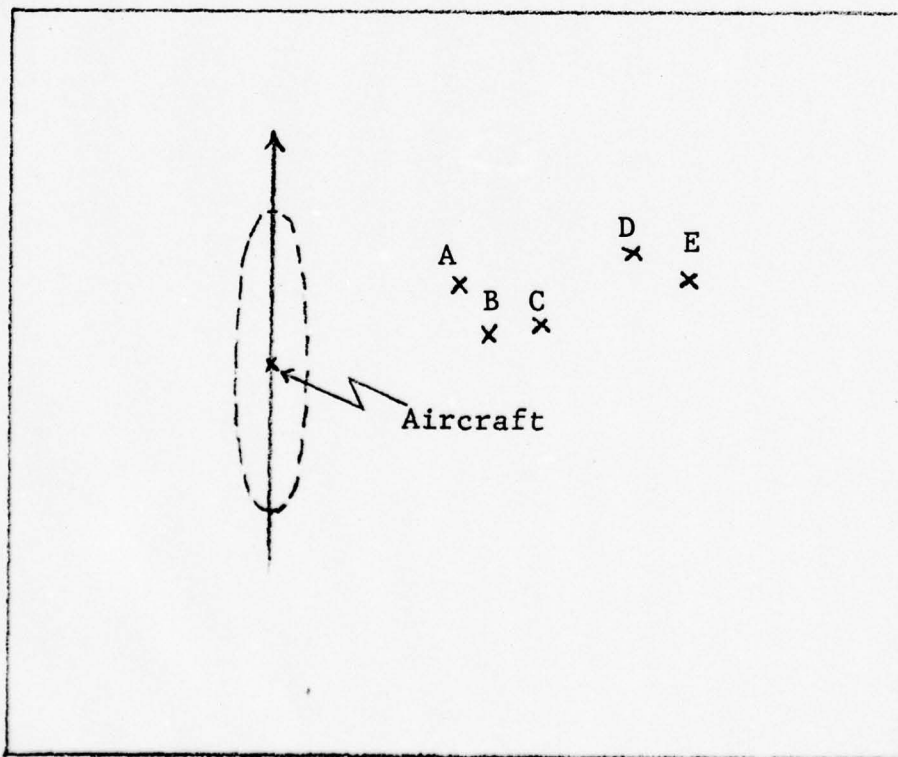
Figure 4. Relative Station and Aircraft Locations: Stations in Same General Direction.

In Figure 4, the stations are nearly colinear, and normal
to the aircraft trajectory. Therefore position accuracy
along the trajectory is much worse than position accuracy
normal to the trajectory. This results in a locus of constant
likelihood in the shape of a highly eccentric ellipse; constant
likelihood lines are represented by the dotted lines.
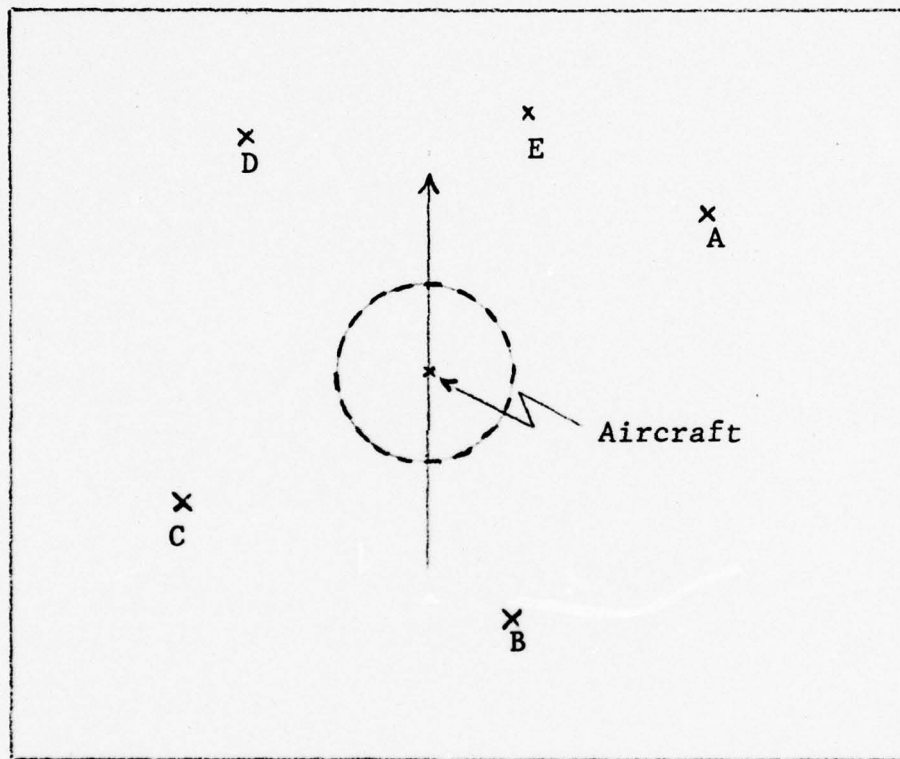
Figure 5. Relative Station and Aircraft Locations:
Stations Radially Distributed.

When the distribution of stations is spread out as in
Figure 5, errors are more radially distributed. As the
flight progresses and the number of station acquisitions
increases, the probability of better station distributions
increases. The first 30 minutes of the FASTMAP filter data
shows the use of 20 different DME stations. Figure 6
illustrates the distribution of these 20 stations relative

36
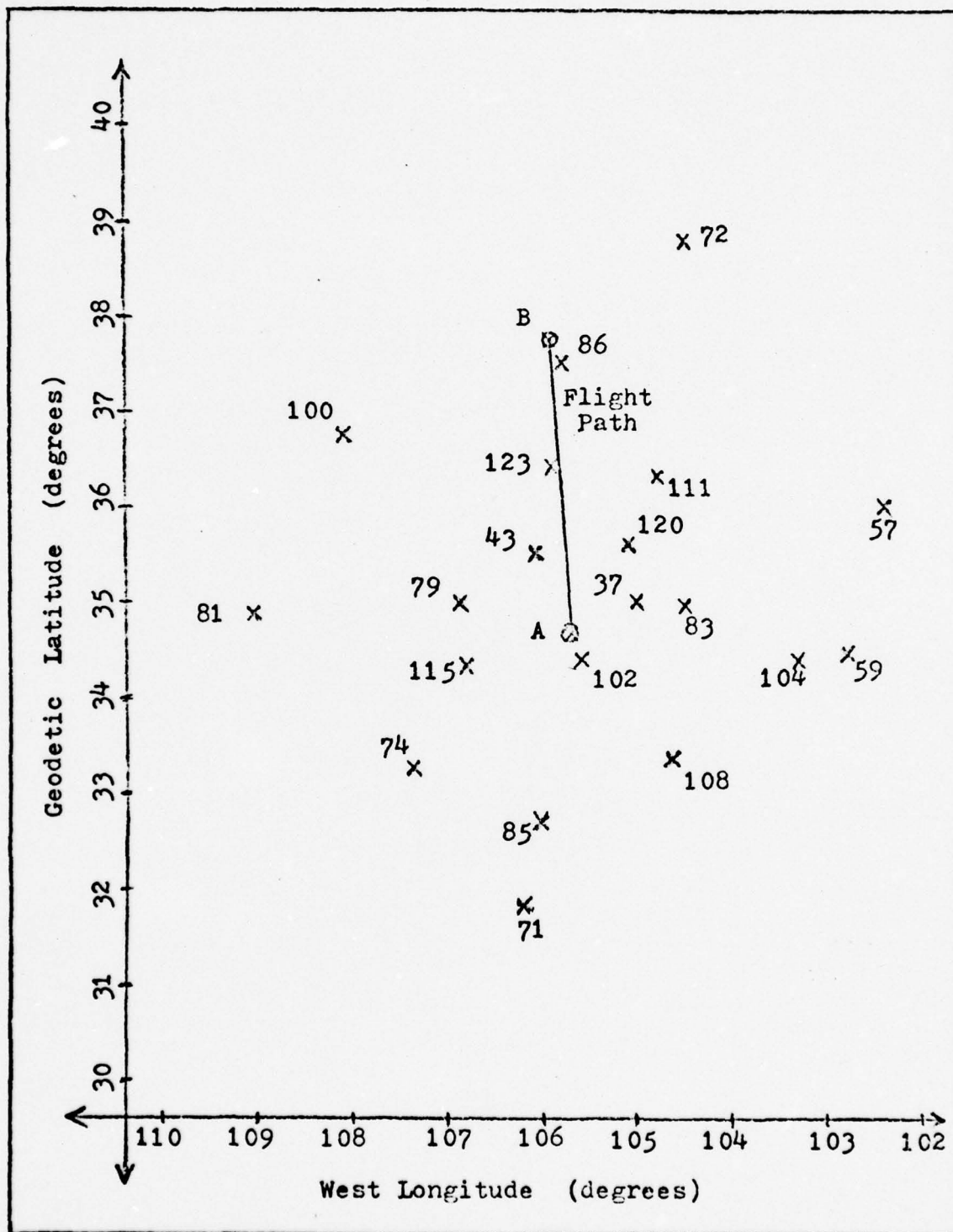
Figure 6. Example of Relative Station Locations

to the aircraft. The number labels in the figure correspond to the channels of the DME stations. "A" is the start of the flight and "B" is the aircraft location after 30 minutes of flight.

The Overall Estimator

The estimator is designed to produce the best estimate of the states by first propagating the states from time instant (k) to (k+1). The state update is accomplished with a new measurement at (k+1). (k) is then incremented by one and the procedure is repeated. The next propagation begins with the last interval's updated estimates, and a new measurement updates the estimates again. In transferring from one time interval to the next, the estimator renames the states, $\underline{\hat{X}}^+_{(k+1)}$, and covariances, $\underline{\hat{P}}^+_{(k+1)}$, with $\underline{\hat{X}}^+_{(k)}$ and $\underline{\hat{P}}^+_{(k)}$ respectively (in other words, the process iterates on (k)). This process is represented by

$$\underline{\hat{X}}^+_{(k)} \Leftarrow \underline{\hat{X}}^+_{(k+1)}$$

$$\underline{\hat{P}}^+_{(k)} \Leftarrow \underline{\hat{P}}^+_{(k+1)}$$

The overall estimator flow chart for the 7 - state estimator is shown in Figure 7.

38

START

Initialize $\hat{\underline{P}}^+(0)$, $\hat{P}^+_{\phi_g}(0)$, $\hat{A}_{\phi_g}(0)$, $\hat{P}^+_\lambda(0)$, $\hat{V}^+_\lambda(0)$, $\hat{A}^+_\lambda(0)$, $\hat{b}^+_i(0)$. Specify R and Q. $\Delta t = 0$.

$$\hat{P}^-_{\phi_g}(k+1) = P^+_{\phi_g}(k) + V_{\phi_g}(k)\Delta t + \tfrac{1}{2}\hat{A}^+_{\phi_g}(k)\Delta t^2$$

$$\hat{V}^-_{\phi_g}(k+1) = \hat{V}^+_{\phi_g}(k) + \hat{A}^+_{\phi_g}(k)\,\Delta t$$

$$\hat{A}^-_{\sigma_g}(k+1) = \hat{A}^+_{\phi_g}(k) + \omega_{\phi_g}(k)\,\Delta t$$

$$\hat{P}^-_\lambda(k+1) = \hat{P}^+_\lambda(k) + \hat{V}^+_\lambda(k)\Delta t + \tfrac{1}{2}\hat{A}^+_\lambda(k)\Delta t^2$$

$$\hat{V}^-_\lambda(k+1) = \hat{V}^+_\lambda(k) + \hat{A}^+_\lambda(k)\Delta t$$

$$\hat{A}^-_\lambda(k+1) = \hat{A}^+_\lambda(k) + \omega_\lambda(k)\,\Delta t$$

$$\hat{b}^-_i(k+1) = \hat{b}_i(k)^+$$

Obtain $\underline{\Phi}$ and $\underline{G}$ matrices from above

$$\underline{G}^T = \begin{matrix} 0 & 0 & \Delta T & 0 & 0 & 0 \\ 0 & 0 & 0 & 0 & \Delta t & 0 \end{matrix}$$

$\underline{\Phi}$ is matrix version of Eqs above

$$\hat{\underline{X}}^-(k+1) \Leftarrow \hat{\underline{X}}^+(k)$$
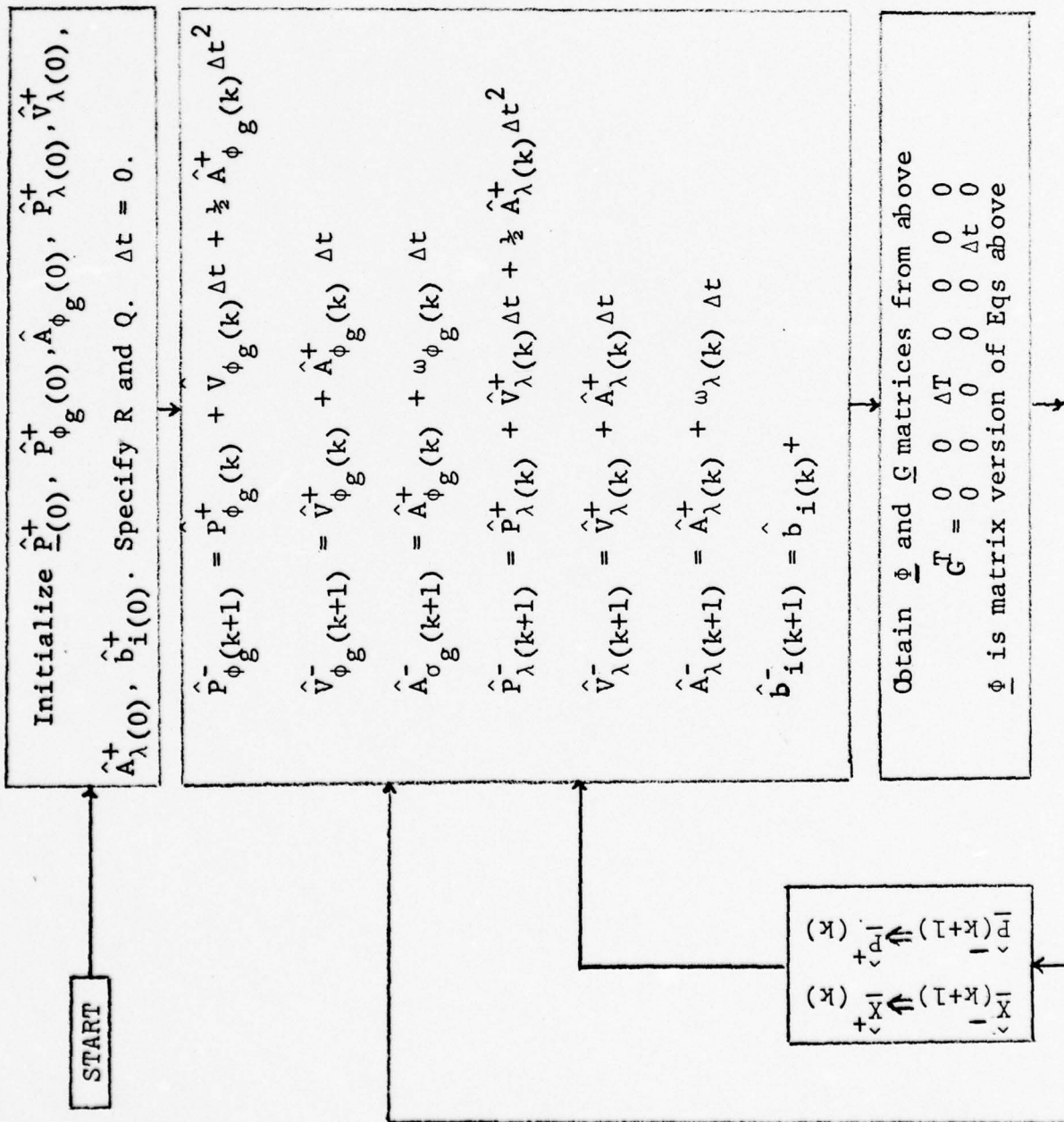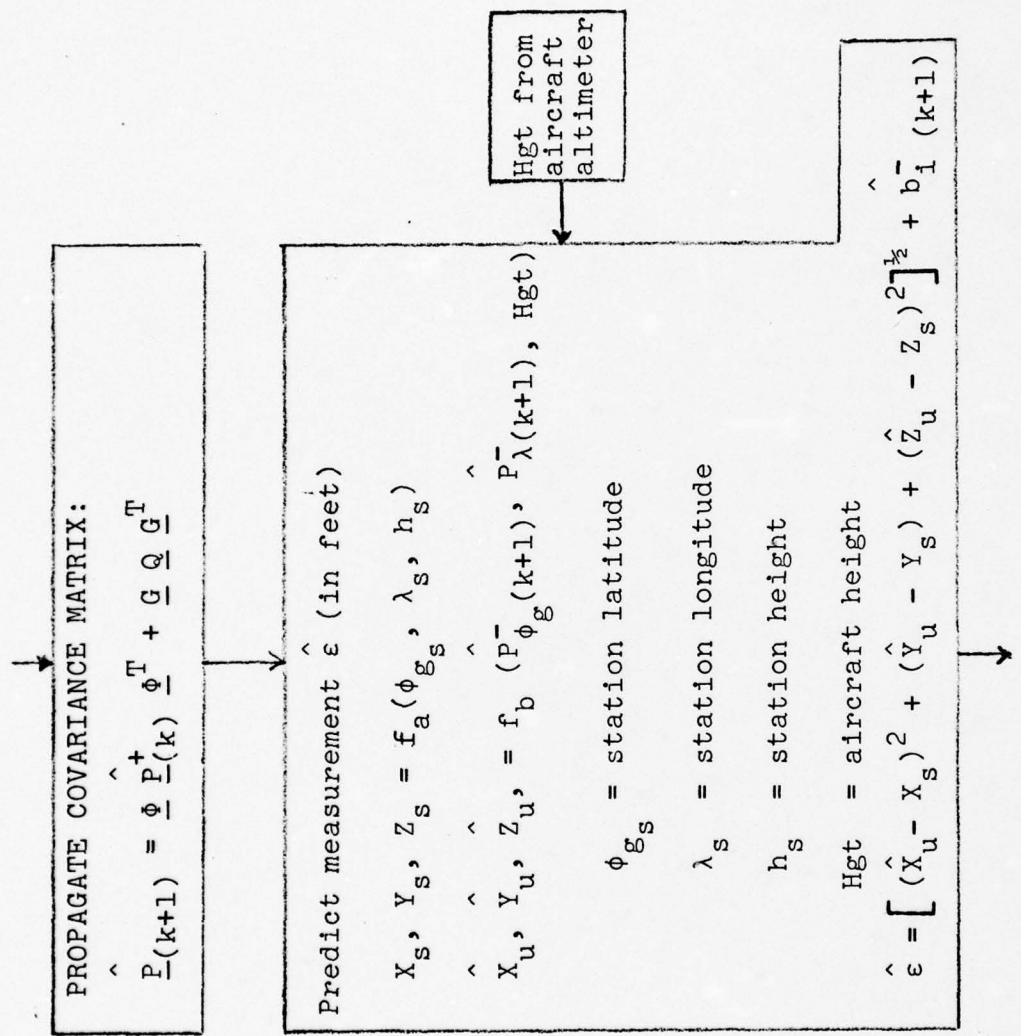
$$\hat{\underline{P}}^-(k+1) \Leftarrow \hat{\underline{P}}^+(k)$$

PROPAGATE COVARIANCE MATRIX:

$$\hat{\underline{P}}(k+1) = \underline{\Phi}\,\hat{\underline{P}}^{+}(k)\,\underline{\Phi}^{T} + \underline{G}\,\underline{Q}\,\underline{G}^{T}$$

Predict measurement $\hat{\varepsilon}$ (in feet)

$$\hat{X}_s,\ \hat{Y}_s,\ \hat{Z}_s = f_a(\hat{\phi}_{g_s},\ \hat{\lambda}_s,\ \hat{h}_s)$$

$$\hat{X}_u,\ \hat{Y}_u,\ \hat{Z}_u, = f_b(\bar{P}^-_{\phi_g}(k+1),\ \bar{P}^-_{\lambda}(k+1),\ \text{Hgt})$$

ϕ_{g_s} = station latitude

λ_s = station longitude

h_s = station height

Hgt = aircraft height

$$\hat{\varepsilon} = \left[(\hat{X}_u - \hat{X}_s)^2 + (\hat{Y}_u - \hat{Y}_s) + (\hat{Z}_u - \hat{Z}_s)^2 \right]^{\frac{1}{2}} + \bar{b}_i^-(k+1)$$

Hgt from aircraft altimeter

40

Take actual measurement ε:
Δt between measurements

Residual = $\Delta\varepsilon = \varepsilon - \hat{\varepsilon}$ (in feet)
is residual too large?

yes

no

Obtain linearized measurement equation
about best estimate of latitude
and longitude positions

Obtain $\underline{H}(k+1)$

Kalman gain and update

$$\underline{K}(k+1) = \hat{\underline{P}}^-(k+1) \ \underline{H}^T(k+1) \ [\underline{H}(k+1) \ \hat{\underline{P}}^-(k+1) \ \underline{H}^T(k+1) \ + R$$

$$\hat{\underline{X}}^+(k+1) = \hat{\underline{X}}(k+1) + \underline{K}(k+1) \ \Delta\varepsilon$$

$$\hat{\underline{P}}^+(k+1) = \hat{\underline{P}}^-(k+1) - \underline{K}(k+1) \ \underline{H}(k+1) \ \hat{\underline{P}}^-(k+1)$$

Separate bias according to station

Print

$$\hat{\underline{X}}^+(k+1) \quad \text{and} \quad \hat{\underline{P}}^+(k+1)$$

$$\underline{X}^+(k+1) \rightarrow \underline{X}^-(k)$$

$$\underline{P}^+(k+1) \rightarrow \underline{P}^+(k)$$
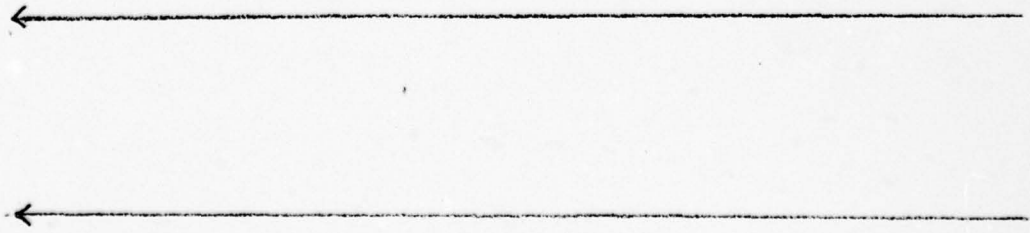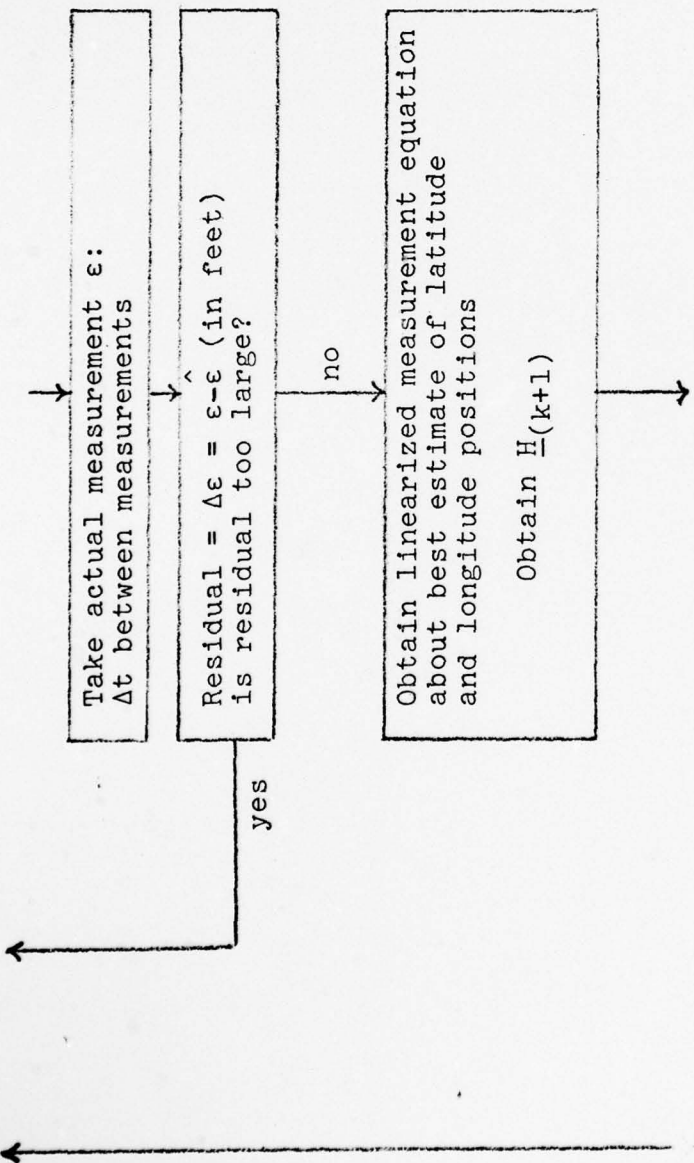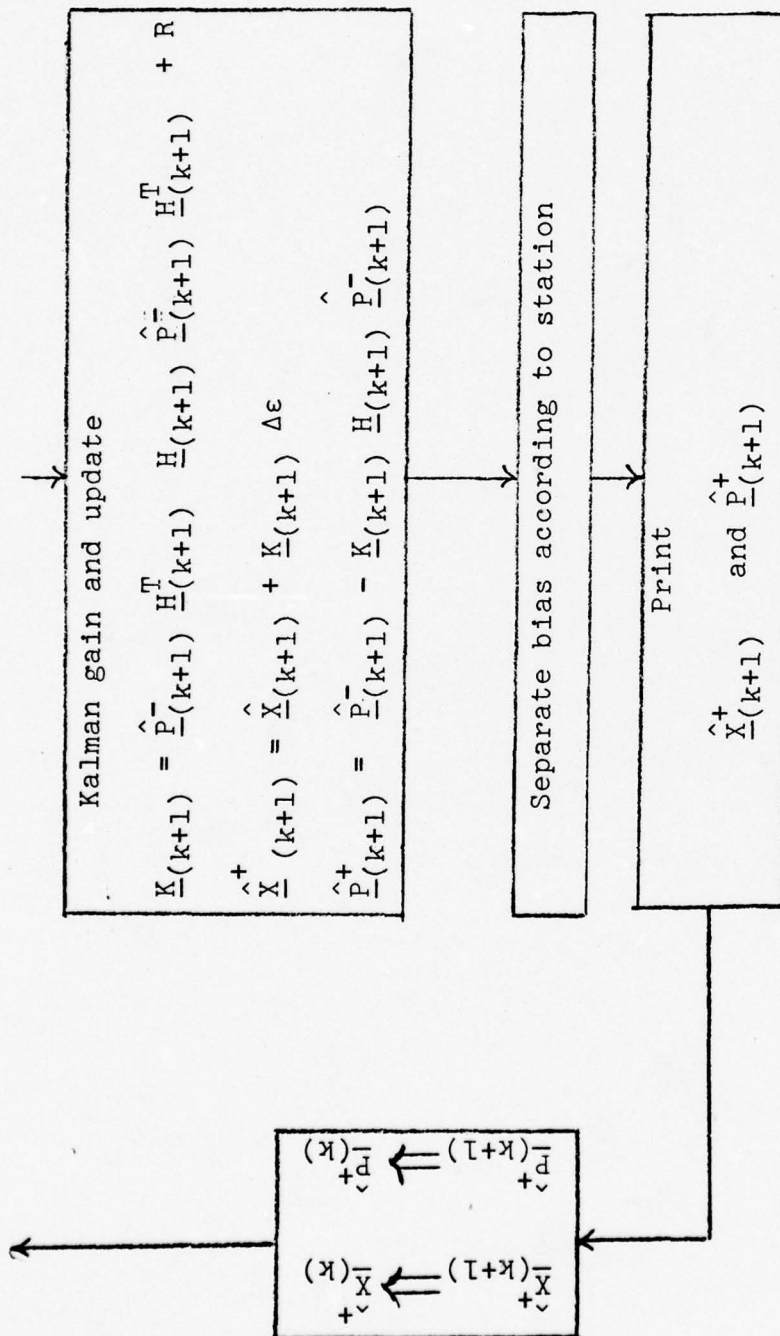
Figure 7. 7 – State Estimator Flow Chart.

42

IV. <u>Estimator Performance Compared to the FASTMAP Filter</u>

Initial Conditions

The estimator algorithm employing the design of the previous chapter is tested by using range and channel data from the FASTMAP tape. Trajectory data also recorded on the FASTMAP tape are the trajectory estimates from the post-flight FASTMAP filter. A direct comparison between the estimator and the FASTMAP filter trajectories provides a useful evaluation of estimator performance. Initial position and velocity for the estimator are obtained from the initial position and velocity of the FASTMAP filter. The test flight available from the FASTMAP test begins at latitude .606342425 NORTH (radians) and longitude 1.845317956 WEST (radians). A constant height of 31524 feet is maintained by the aircraft autopilot. The aircraft is headed in a northerly direction at approximately 300 nautical miles per hour. Two hundred miles north of the initialization of the FASTMAP test, the aircraft makes a 180° heading change and returns to the initial latitude and longitude. Initial conditions are as follows:

$$\hat{P}_{\phi_g}^{+}(o) = .606342425 \text{ radian} = 34.7409 \text{ degrees} \tag{55}$$

$$\hat{V}_{\phi_g}^{+}(o) = 2.2666 \times 10^{-5} \text{ rad/sec} = 279.06 \text{ nm/hr North} \tag{56}$$

$$\hat{A}_{\phi_g}^{+}(o) = 0.0 \text{ rad/sec}^2 = 0 \text{ ft/sec}^2 \tag{57}$$

$$\hat{P}_{\lambda}^{+}(o) = 1.845317956 \text{ radian} = 105.7289 \text{ degrees} \tag{58}$$

$$\hat{V}_{\lambda(o)}^{+} = 9.2103 \times 10^{-6} \text{ rad/sec} = 90.72 \text{ nm/hr West} \qquad (59)$$

$$\hat{A}_{\lambda(o)}^{+} = 0.0 \text{ rad/sec}^2 = 0 \text{ ft/sec}^2 \qquad (60)$$

$$\hat{b}_{i(o)}^{+} = 0.0 \text{ radian} = 0 \text{ feet} \qquad (61)$$

The 9-state estimator initializes the jerk states at zero:

$$\hat{\eta}_{\phi_g(o)} = 0.0 \text{ rad/sec}^3 = 0 \text{ ft/sec}^3 \qquad (62)$$

$$\hat{\eta}_{\lambda(o)} = 0.0 \text{ rad/sec}^3 = 0 \text{ ft/sec}^3 \qquad (63)$$

Initial covariance values depend on the uncertainty of
the initial values of the FASTMAP filter. Low uncertainty
for these initial conditions is assumed; therefore, the
diagonal terms of the initial covariance matrix, or $\hat{\underline{P}}_o^{+}$,
are set at small values. In other words, initial covariance
is made somewhat smaller than the anticipated steady state
covariances for the estimator. Position variances are
chosen as 10^{-14} radians squared, or 4.3 feet squared, which is
less than the anticipated steady state estimator covariances
(on the order of 10^4 feet squared, consistent with the
estimator goals). Velocity and acceleration initial variances
are assigned in the same manner. The correlations (off-
diagonal terms) between the states are initially assumed to be
zero. After the estimator begins, both the diagonal terms and
off-diagonal terms will increase except for the bias variance.
The bias variance, $\hat{\underline{P}}_o^{+}(9,9)$ in Equation (64), is initially
set at 10^{-12} radians squared or 432 feet squared, a value more
or less consistent with DME range bias errors as outlined in

44

in Chapter II. After the estimator begins, bias variance in the estimator is expected to decrease due to incorporating measurement information.

The $\hat{\underline{P}}_o^+$ matrix for the 9-state estimator is

$$\hat{\underline{P}}_o^+ = \begin{bmatrix} 10^{-14}(\text{rad})^2 & & & & & & & & \\ & 10^{-14}(\text{rad/sec})^2 & & & & & & & \\ & & 10^{15}(\text{rad/sec}^2)^2 & & & & & & \\ & & & 10^{14}(\text{rad})^2 & & & & & \\ & & & & 10^{-14}(\text{rad/sec})^2 & & & & \\ & & & & & 10^{-15}(\text{rad/sec}^2)^2 & & & \\ & & & & & & 10^{-17}(\text{rad/sec}^3)^2 & & \\ & & & & & & & 10^{-17}(\text{rad/sec}^3)^2 & \\ & & & & & & & & 10^{-12}(\text{rad})^2 \end{bmatrix} \quad (64)$$

The $\underline{P}_o^+$ matrix for the 7-state estimator is

$$\hat{\underline{P}}_o^+ = \begin{bmatrix} 10^{-14}(\text{rad})^2 & & & & & & \\ & 10^{-14}(\text{rad/sec})^2 & & & & & \\ & & 10^{-15}(\text{rad/sec}^2)^2 & & & & \\ & & & 10^{-14}(\text{rad})^2 & & & \\ & & & & 10^{-14}(\text{rad/sec})^2 & & \\ & & & & & 10^{-15}(\text{rad/sec}^2)^2 & \\ & & & & & & 10^{-12}(\text{rad})^2 \end{bmatrix} \quad (65)$$

45

The values of the Q elements of Equation (6) are fixed to reflect disturbances in jerk for the 7-state estimator and disturbances in jerk rate for the 9-state estimator. During the testing of the estimator (Chapters IV and V), such disturbances are assumed to be small; thus low values for the Q elements are used. The units of Q are obtained from the equation

$$E \{\underline{\omega}(t) \, \underline{\omega}^T(t + \tau)\} = Q(t) \, \delta(\tau) \tag{66}$$

For the 7-state estimator, $\underline{\omega}$ is added directly to acceleration through an intergrator and has units of rad/sec^3. The units of Q_7 (the Q matrix for the 7-state estimator) are obtained from a units breakdown of Equation (66):

$$(\text{rad/sec}^3)(\text{rad/sec}^3) = Q(t)1/\text{sec} \tag{67}$$

or Q_7 is in units of radians 2/seconds^5. A similar approach is employed for the 9-state estimator to yield the units of Q_9 as rad^2/sec^7. For this study (but not shown here), several different values of Q were initially attempted, and the best Q values seemed to be those smaller than 1 ft^2/sec^5 for Q_7 and 1 ft^2/sec^7 for Q_9. Nevertheless, it should be emphasized that fine tuning is not attempted in this study, and, therefore, only "ball park" figures for Q are suggested. A conversion from ft^2 to rad^2 yields

$$\text{diag} \{Q_7\} < 1(\text{ft}^2/\text{sec}^5)(1/6076 \text{ nm/ft})^2(1/60 \text{ deg/nm})^2$$
$$(1/57 \text{ rad/deg})^2 = 2.3 \times 10^{-15} \text{ rad}^2/\text{sec}^5$$

46

diag $\{Q_9\} < 2.3 \times 10^{-15}$ rad^2/sec^7 (68)

The Q diagonal values for both estimators are chosen as 10^{-17} rad^2/sec^5 or 10^{-17} rad^2/sec^7 and are stored in the 2 x 2 matrix as follows:

$$Q_7 = Q_9 = \begin{bmatrix} 10^{-17} & 0 \\ 0 & 10^{-17} \end{bmatrix}$$ (69)

Note that these Q values are design parameters and can be changed.

Comparison of 7- and 9-state Estimators

Both the 7-state and the 9-state estimator positions and velocities are compared to the FASTMAP filter positions and velocities using the specified initial conditions. Since the actual test flight initially begins straight, level, and with zero acceleration, proper estimation results should indicate this. The actual results of testing the estimators show that the 9-state estimator velocity wildly oscillates about the FASTMAP velocity. On the other hand, the 7-state estimator has the opposite effect; in other words, its velocity curve is even smoother than the FASTMAP velocity curve. (Note that R in either case is kept constant at 1000 ft^2 so that effects of measurement uncertainty are the same.) This phenomenon eventually leads to the exclusion of the 9-state estimator from the design in favor of the 7-state estimator. However, better performance may be attainable for the 9-state estimator through tuning. In fact, in this light no

conclusive thoughts can be drawn from this comparison except that utilizing the current values of Q and R, the 7-state estimator outperforms the 9-state estimator.

Estimator positions are essentially the same for both the 7- and 9-state estimators. For example, at the conclusion of the first record of data (42 DME measurements correspond to one record of data and the entire flight is represented by over 500 records on the FASTMAP flight data tape), updated position state values of both estimators compare well as shown in Table II. For easy comparison in Table II, FASTMAP filter position is subtracted from the positions of the two estimators. As shown in the table, the differences in both cases are almost the same, thereby proving good position agreement with the 7- and 9-state estimators.

Table II. Comparison of 7- and 9-State Estimator Positions

Reference Type / Direction	FASTMAP Position (Radians)	7-State Estimator Position (Radians)	9-State Estimator Position (Radians)	7-S EST. Minus FASTMAP (Feet)	9-S EST Minus FASTMAP (Feet)
Latitude	.606483606	.606482181	.606482155	-29.6	-30.0
Longitude	1.845375889	1.845366924	1.845366823	149.0	150.0

When velocities of the 9-state estimator and FASTMAP are compared, an interesting result is obtained. The estimator velocity states oscillate about the FASTMAP filter's velocity. The magnitude of the oscillations are quite unacceptable ranging from -15 to +15 nautical miles per hour from the

48

average in a 2 1/2 second period. To illustrate these
oscillations, longitude velocities of the estimator and
the filter are compared in the fifth record of data. (Using
the fifth data record of the tape should insure that effects
of perfect initial agreement are gone since estimator initial
conditions were taken from the FASTMAP filter's initial
conditions. Otherwise, using longitude velocity in the fifth
record is an arbitrary choice.) Table III tabulates the
time - average longitude velocity in the fifth record given
by

$$\sum_{i=1}^{42} \frac{\hat{v}_{\lambda(i)}^{+}}{42} \tag{70}$$

and the high and low longitude velocities in the same interval
for both the 9-state estimator and the FASTMAP filter.

Table III. 9-State Estimator and FASTMAP Filter Longitude
Velocity in Fifth Record

Quanity Reference	Time-Avg. Long. Velocity (nm/hr)	High Long. Velocity (nm/hr)	Low Long. Velocity (nm/hr)
9-State Estimator	85.74	125.83	71.65
FASTMAP Filter	84.74	104.27	71.68

The table shows that velocity drops for this particular
period of time to equal lows for both the 9-state estimator
and the FASTMAP filter, but the high velocities differ by over
16 nautical miles per hour. Since FASTMAP tests velocity

errors are ± 9.2 feet/second CEP, or ± 5.45 nautical miles/ hour CEP, such deviations in the estimator velocity states as illustrated in Table III cannot be accepted. Therefore, the performance of the estimator with jerk states reveals that the 9-state estimator must be rejected (that is, with the current values of R and Q).

Table IV shows a comparison between the 7-state estimator and the FASTMAP filter. As in the previous test, the comparison is accomplished using longitude velocities in the fifth record. The point to be drawn from Table IV is that the estimator velocity varies even less than the FASTMAP filter velocity. This result is far more advantageous than the 9-state estimator test results because the 7-state estimator velocity better reflects the fact that the flight is relatively straight, level, and has near zero acceleration. Again, it must be emphasized that these observations are also a function of tuning. A suggestion for tuning and testing the estimator utilizing different trajectories in a Monte Carlo analysis is reserved for the recommendations.

Table IV. 7-State Estimator and FASTMAP Filter Longitude Velocity in Fifth Record

| Quanity Reference	Time-Avg. Long. Velocity (nm/hr)	High Long. Velocity (nm/hr)	Low Long. Velocity (nm/hr)
7-State Estimator	84.52	106.08	84.25
FASTMAP Filter	84.74	109.27	71.68
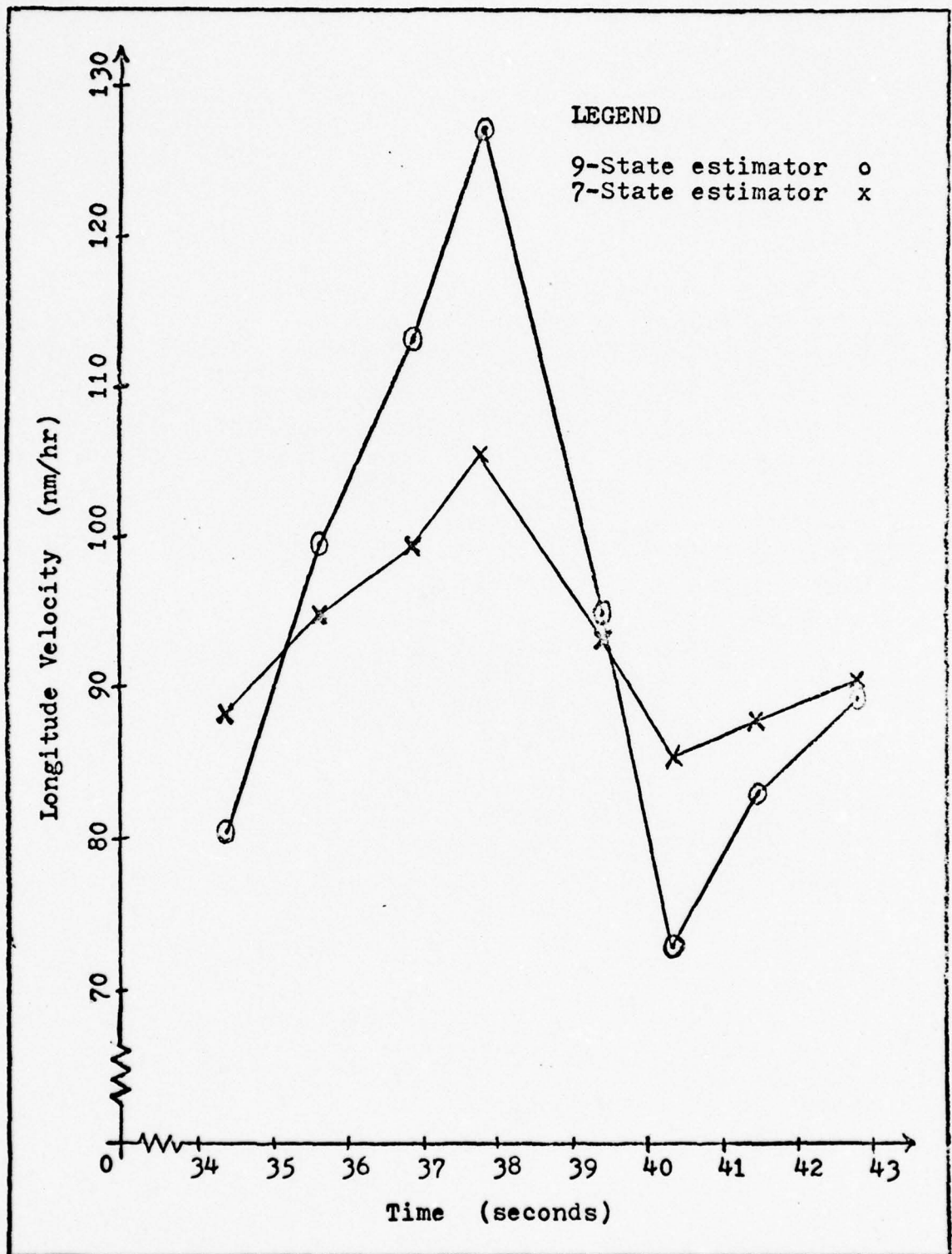
Figure 8. Comparison of 9- and 7-State Estimator Velocities

51

Figure 8 shows the plot of longitude velocity for the 7-state estimator versus the 9-state estimator for the fifth data record. The large magnitude of velocity deviations in the 9-state estimator relative to the 7-state estimator are apparent. Due to these velocity deviations in the 9-state estimator, only the 7-state estimator is considered for further testing. In other words, the jerk states are no longer modelled, and only the 7-state propagation equations, Equations (34) to (39), hold henceforth.

To recap the findings of the above test, it is concluded that, with the current values of $\underline{R}$ and $\underline{Q}$, dropping the jerk states produces better estimator performance. A white noise is an adequate model of jerk, but Brownian motion is not. A suitable representation of the aircraft dynamics is

White Noise $\xrightarrow{}$ $\boxed{\dfrac{1}{s+f}}$ Acceleration $\xrightarrow{}$ $\boxed{\dfrac{1}{s}}$ Velocity $\xrightarrow{}$ $\boxed{\dfrac{1}{s}}$ Position $\xrightarrow{}$
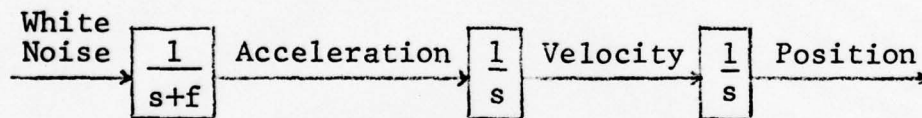
Suggestions for investigating other models are also reserved for the recommendations.

Comparison of Estimator and FASTMAP Filter Positions and Velocities

Figure 9 compares FASTMAP and estimator trajectories for the first 33 seconds of the test flight. Due to the identical initial conditions both begin in nearly perfect agreement for the first three seconds. After the estimator starts depending on its own propagation and update equations, the estimator and the FASTMAP filter diverge for this time period to a
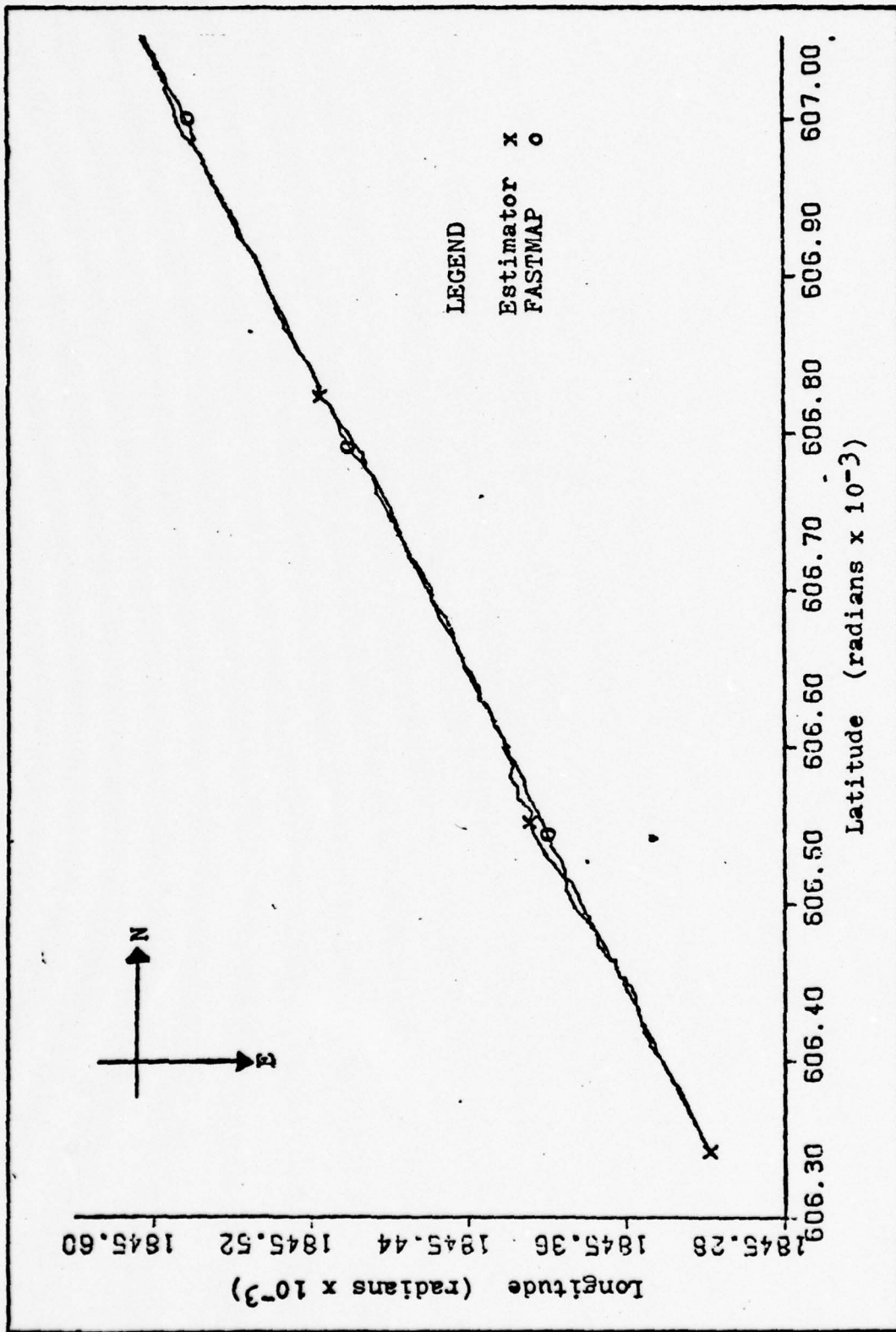
Figure 9. FASTMAP and Estimator Trajectories for First 33 Seconds

maximum separation of 180 feet at t equal to 14.5 seconds. (This information is obtained from output data).

An important note to emphasize is that the FASTMAP filter position does not represent true position. In other words, the difference vector $\underline{d}_{EF}$

$$\underline{d}_{EF} = \hat{\underline{X}}_{estimator} - \hat{\underline{X}}_{FASTMAP} \tag{71}$$

is not meant to be interpreted directly as an error $\underline{e}_E$:

$$\underline{e}_E = \hat{\underline{X}}_{estimator} - \hat{\underline{X}}_{true} \tag{72}$$

Rather, the estimator performance is just <u>compared</u> to the FASTMAP filter. Table V illustrates the differences in feet between the filter and the estimator indicated position. The differences in the last column are computed using the Pythagorean theorem:

$$\text{Difference} = \left(\begin{matrix}\text{Lat. Difference}\\ \text{in feet}\end{matrix}\right)^2 + \left(\begin{matrix}\text{Long. Difference}\\ \text{in feet}\end{matrix}\right)^2 \tag{73}$$

Table V. Comparison of FASTMAP Filter and Estimator Position

Time (sec)	No. of Measurements Since Initiation of Test Flight	Distance Between Estimator and Filter
3.43	20	33.25
6.12	40	135.34
10.22	60	80.03
14.41	80	178.00
18.91	100	80.08
22.97	120	57.60
26.97	140	61.31
31.34	160	74.99
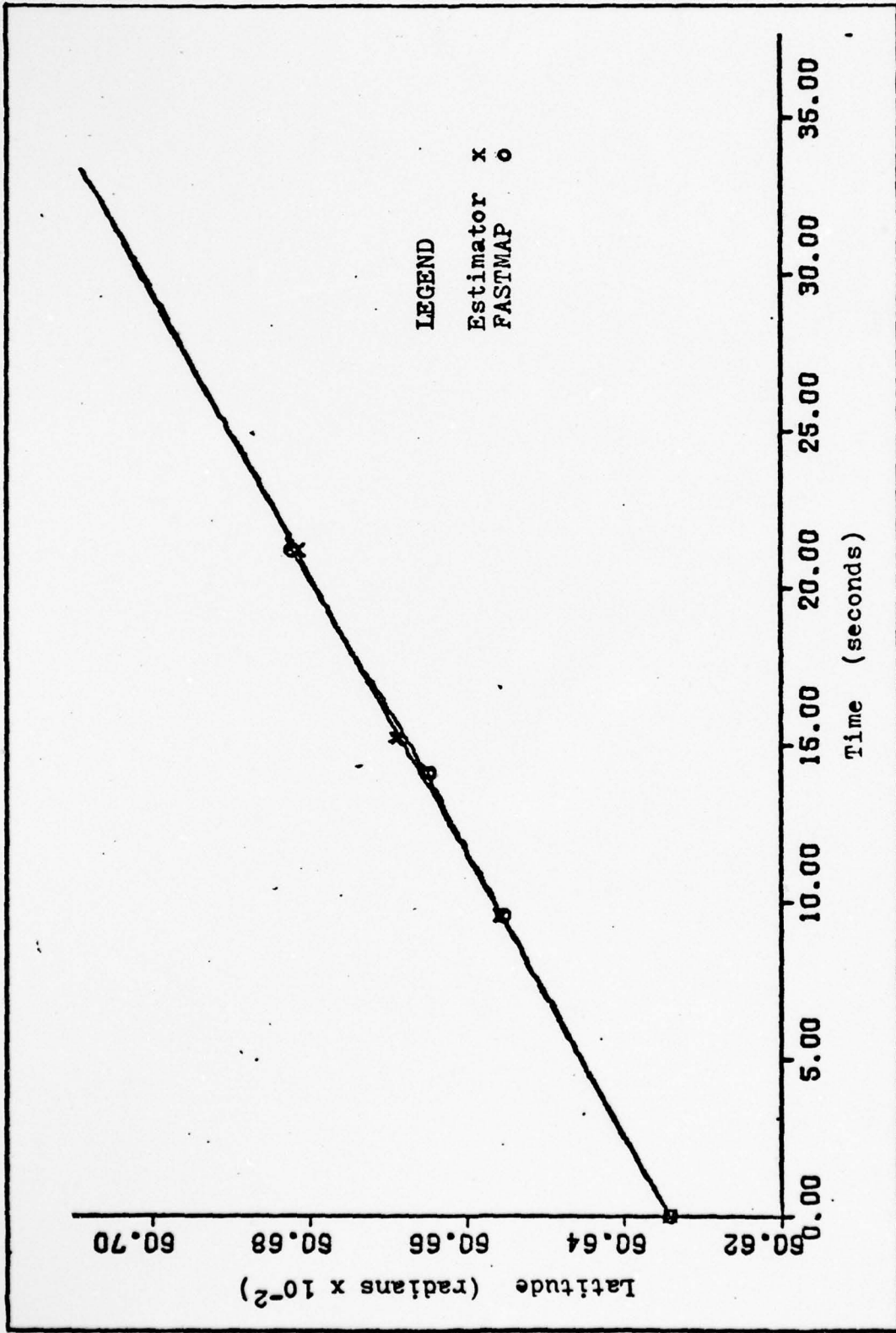
Figure 10. FASTMAP and Estimator Latitude for First 33 Seconds

55

Figure 11. FASTMAP and Estimator Longitude for First 33 Seconds

56
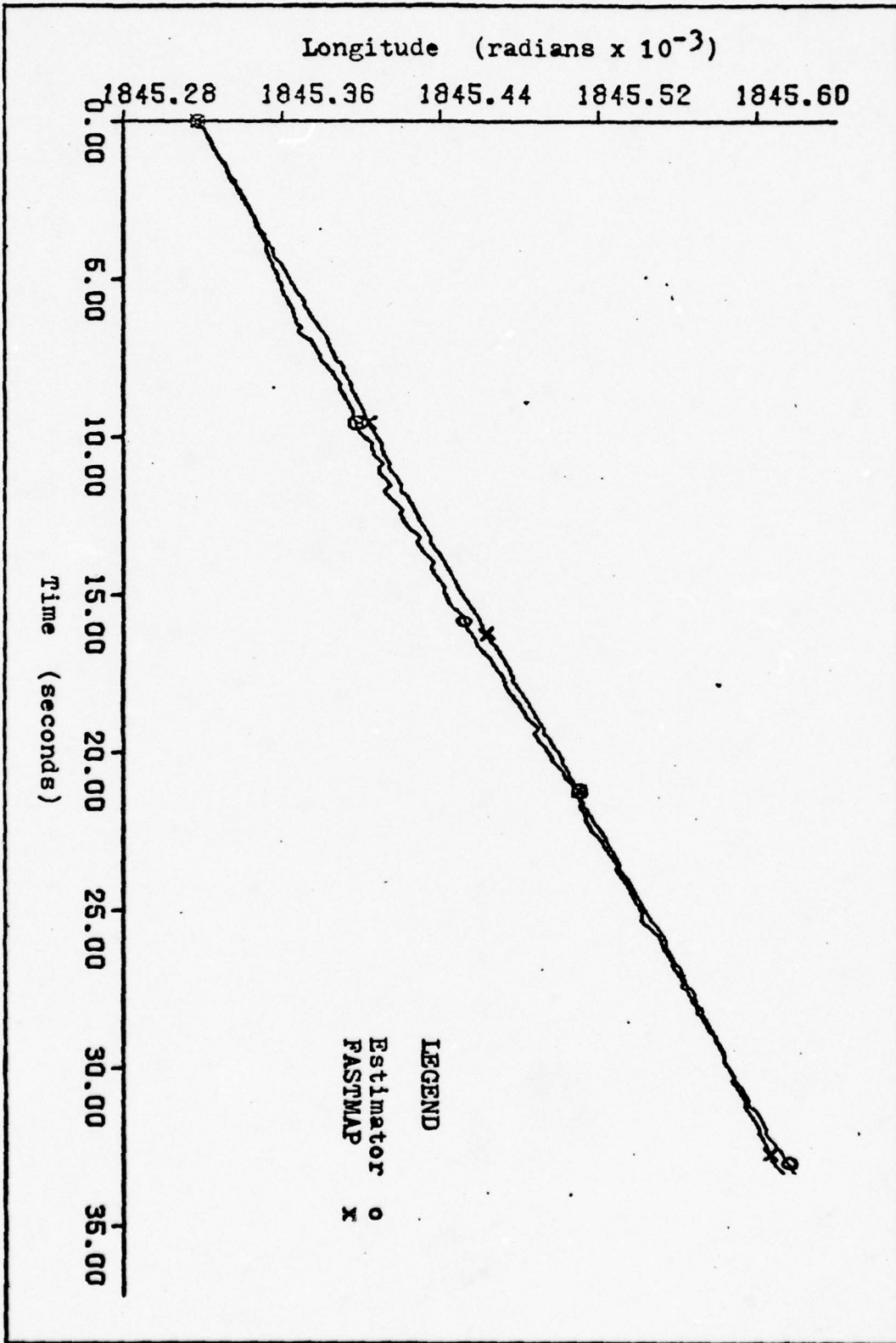
Figures 10 and 11 show the filter and estimator latitude versus time, and FASTMAP and estimator longitude versus time, respectively. The larger deviations occur in longitude, while latitude differences between the estimator and FASTMAP remain small.

An explanation for the larger longitude differences is obtained from a study of the geometry of the stations relative to the initial aircraft position. If all the stations lie in the same general direction relative to the aircraft, then accuracy in that direction can well be expected to be better than in the other orthogonal direction. During the time that Figures 10-11 cover, stations with channel numbers 57, 37, 59, and 43 are acquired. The geometry of these four stations relative to the aircraft is shown in Figure 12.
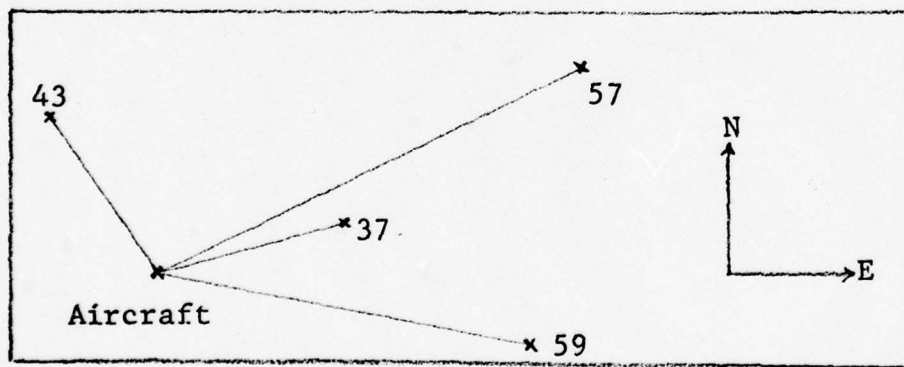

Figure 12.   Relative Station Geometry For
First 33 Seconds of Flight

From Figure 12, it is noted that the four stations supply ranges in a more East - West direction than in a North - South direction. This effectively causes the estimator to achieve more benefit from the measurement information in the longitude

direction than in the latitude direction. Since better measurement information is available in the East - West direction, the $\underline{H}$ matrix has a value of the partial of longitude with respect to range greater than that of the latitude partial which in turn produces a larger Kalman gain for the longitude (East - West) direction. Thus, the latitude states depend on the system dynamic equations more heavily than the longitude states. Because of the constant velocity (zero acceleration) model that is initially assumed and the lower latitude Kalman gains, the latitude state estimates show a constant velocity trend as depicted in Figure 10. Since FASTMAP also indicates an almost constant velocity trajectory for the first 30 seconds of flight, FASTMAP and the estimator closely agree in lattitude position estimates. Estimator longitude states on the other hand rely more on the measurement history rather than on the constant velocity model because of the higher Kalman gains.

The main point to be drawn from Figures 10 and 11 and the preceding note is that the accuracy of the position estimates in both directions depends on the geometry of the stations with respect to the aircraft. As the flight proceeds, different stations are acquired, and, therefore, the geometry constantly changes. (Also, the forward motion of the aircraft causes the geometry to change continuously.) Changing geometry in turn causes repeated transitions from a model dependence of the states to a measurement dependence and back, depending on the Kalman gain value ($\underline{K}_{(k+1)}$).

FASTMAP and the estimator latitude velocities are compared in Figure 13. Approximately one second after the test flight initialization, the velocities begin to differ. However, these differences are not biased in any one direction, but rather switch signs throughout the 30 second interval.

Due to the gap between FASTMAP and the estimator longitude position in Figure 11, longitude velocities are anticipated to be quite different. As Figure 14 indicates, longitude velocities are indeed different. In fact, the widest margin has a velocity difference of almost 25 nm/hr. (See Figure 14.) This may seem to be wholly unacceptable, but three points are to be noted. First the estimator is not tuned; in other words, R is still 1000 ft^2 and the Q elements are 1×10^{-17} rad^2/sec^5. Second, FASTMAP is only a reference and not an absolute truth model. Finally, the figure shows that the two filters begin at different initial conditions.

The justification for beginning the estimation process at a slightly different initial velocity is to illustrate the corrective nature of the estimator. Initial FASTMAP longitude velocity is 95.73 nm/hr in a westerly direction, and initial estimator longitude velocity is set at 93 nautical miles per hour in the same direction. In the first '12 to 13 seconds the two velocities diverge. After that time, the velocity difference decreases until t is equal to 19 seconds, where the difference remains near zero. The estimator essentially is shown by Figure 14 to be able to
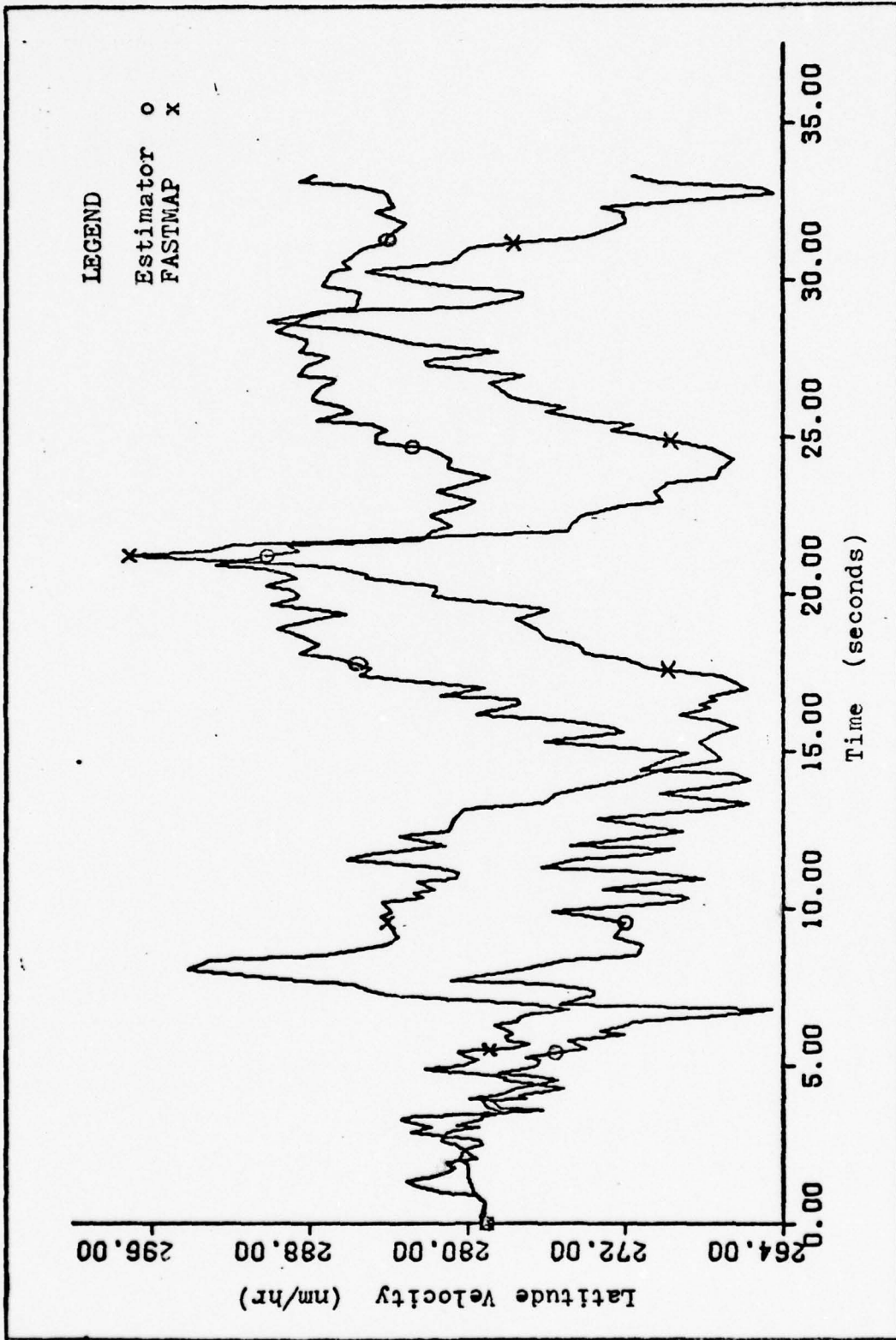
Figure 13. FASTMAP and Estimator Latitude Velocities for First 33 Seconds

60
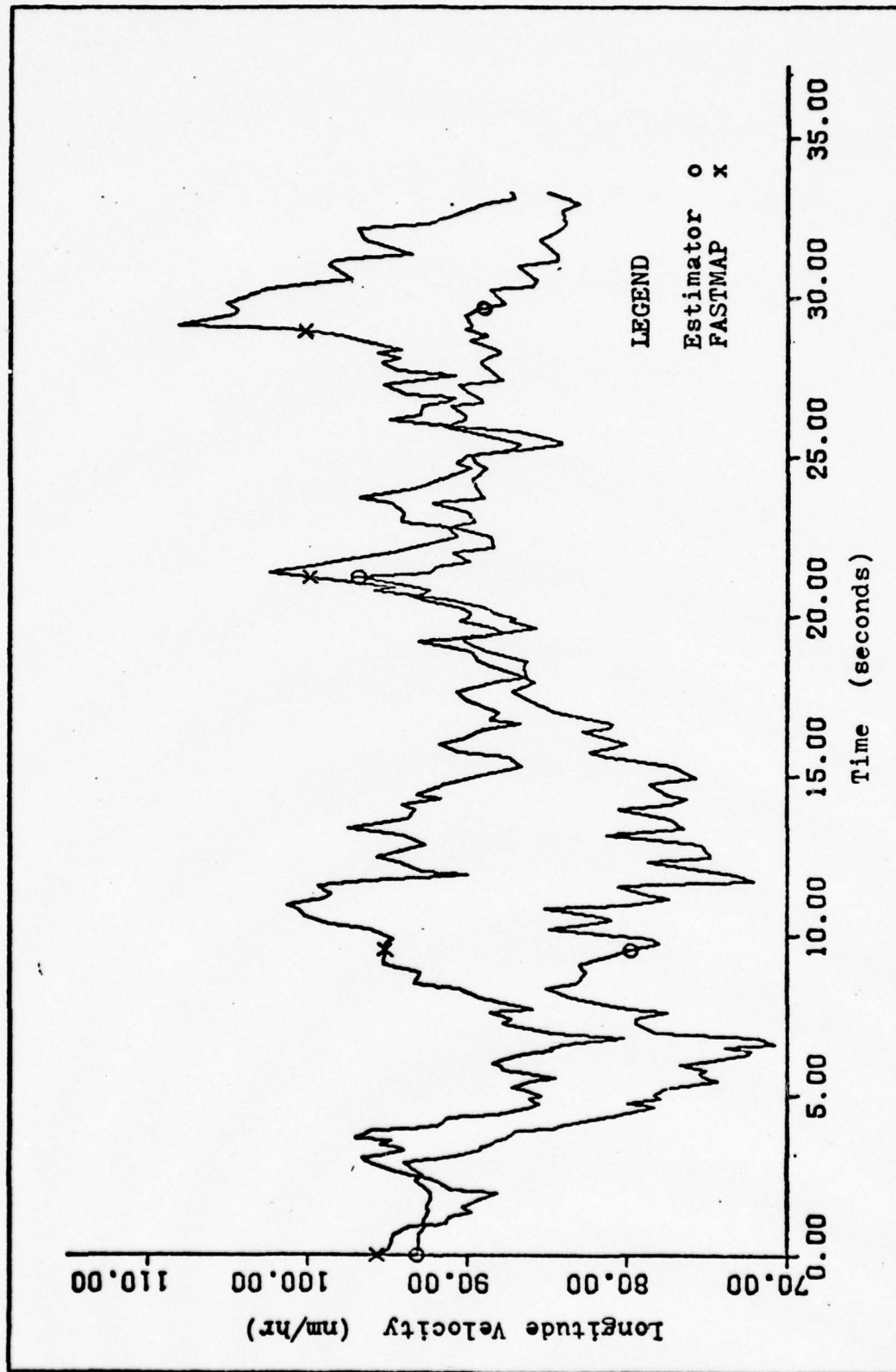
Figure 14. FASTMAP and Estimator Longitude Velocities for First 33 Seconds.

61

track the aircraft velocity to some degree of accuracy
even when exact initial conditions are not known.

Estimator State Variances

Latitude position variance $\hat{P}^+_{(k)}(1, 1)$, longitude
position variance $\hat{P}^+_{(k)}(4, 4)$, and bias variance $\hat{P}^+_{(k)}(7, 7)$,
are plotted for the first record of data in Figure 15. The
purpose of this chart is to observe the relative characteristics
of these variances during the first record, and not to study
the actual variance magnitudes. The values on the vertical
axis represent the variance magnitudes with the current values
for R and $\underline{Q}$. Since R and $\underline{Q}$ are subject to change, variance
magnitudes are also subject to change.

Only updated variances, $\hat{\underline{P}}^+_{(k)}(1, 1)$, $\hat{\underline{P}}^+_{(k)}(4, 4)$, and
$\hat{\underline{P}}^+_{(k)}(7, 7)$ are plotted in Figure 15; in other words, the
variance is plotted only after each measurement is taken. The
propagated variances are not shown in the figure so as to
facilitate the viewing of the overall trend in the variances.
It is apparent from Figure 15 that the bias variance begins
at $.75 \times 10^{-12}$ rad^2, or $.25 \times 10^{-12}$ rad^2 less than the initial
variance of 1×10^{-12} rad^2. This is a direct consequence of
plotting only the updated variances. The variances at time
equal to zero are plotted after the first measurement is
taken, which are, as expected, lower than the initial
variances.

Generally, the bias variance curve decreases over the
6.29 seconds interval. However, the appearance of two sharp

62
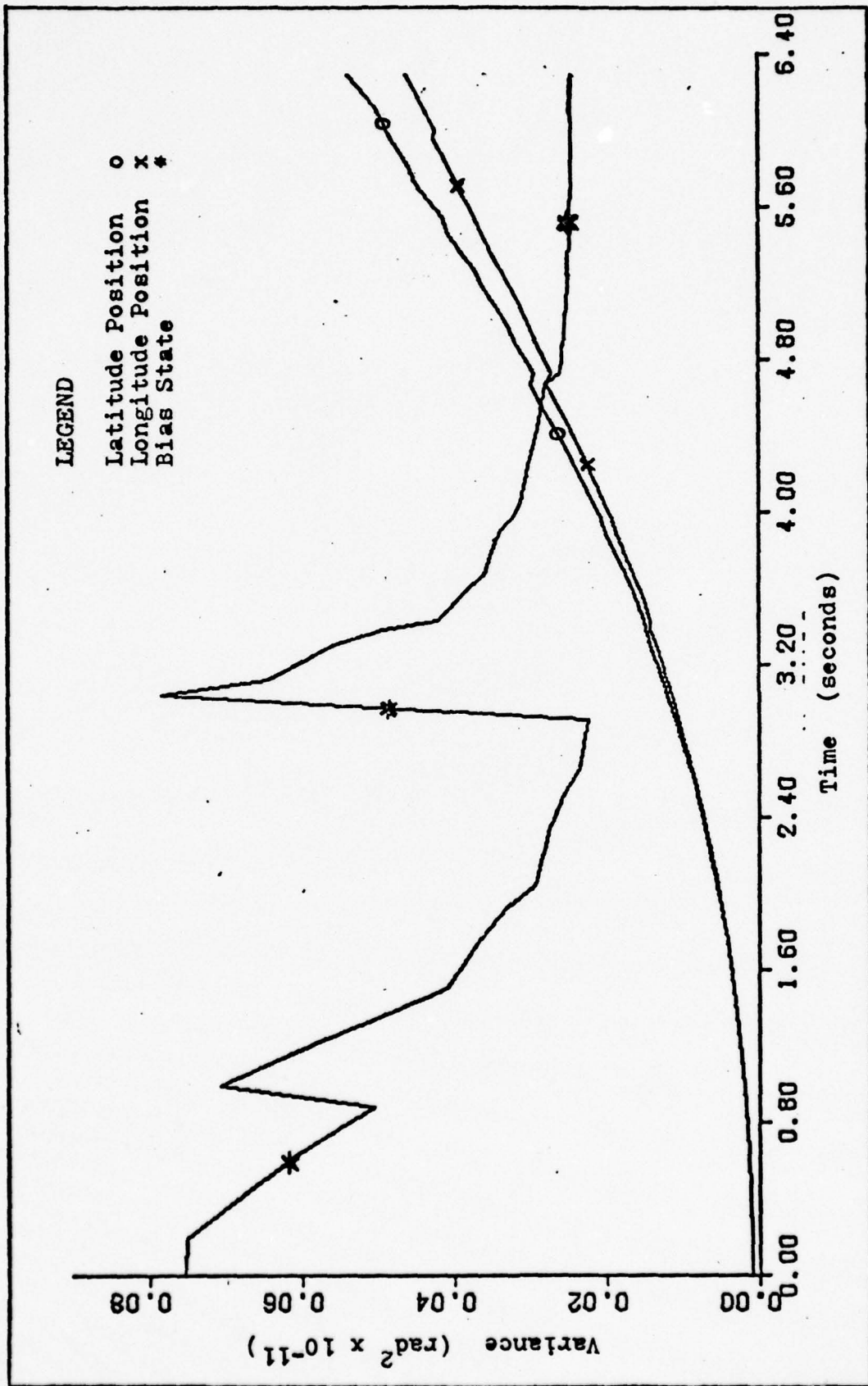
Figure 15. Estimator Variances for Latitude Position, Longitude Position and the Bias State for the First Record (6.29 Seconds)

63

peaks in the curve indicates sudden increases in bias uncertainty. The first peak occurs at $t = .99$ seconds when station 43 is called on for the first time, and the second peak occurs when channel 59 is acquired for the first time at $t = 3.12$ seconds. When a station is called on for the first time, bias for that station is completely unknown; bias uncertainty is reinitialized to $\sigma = 432$ ft^2 at each new station acquisition, causing the peaks in the bias variance curve of Figure 15.

Latitude and longitude position variances are represented by the other two curves of Figure 15. They begin at the low initial value and grow throughout the first record. To show that the position variances actually do reach an upper bound, Figure 16 carries latitude variance through the first four records of data. At $t \simeq 10$ seconds, $\hat{\underline{P}}^{+}_{-(k)}(1, 1)$ halts its ascent and settles to a value somewhat lower than the peak. At $t = 166.9$ seconds latitude, variance is equal to 105.91 ft^2 or 2.45×10^{-13} rad^2. (See Figure 16.)

The fact that station bias values are estimated with better accuracy as more measurements arrive can be a possible explanation for the variance overshoot in Figure 16. DME measurements are predicted with increasing accuracy as time goes from $t = 10$ seconds to the next station acquisition due to ever-increasing bias knowledge. With decreasing measurement uncertainty, total system variance (or uncertainty) also drops, creating the gradual decrease in the variance plot.
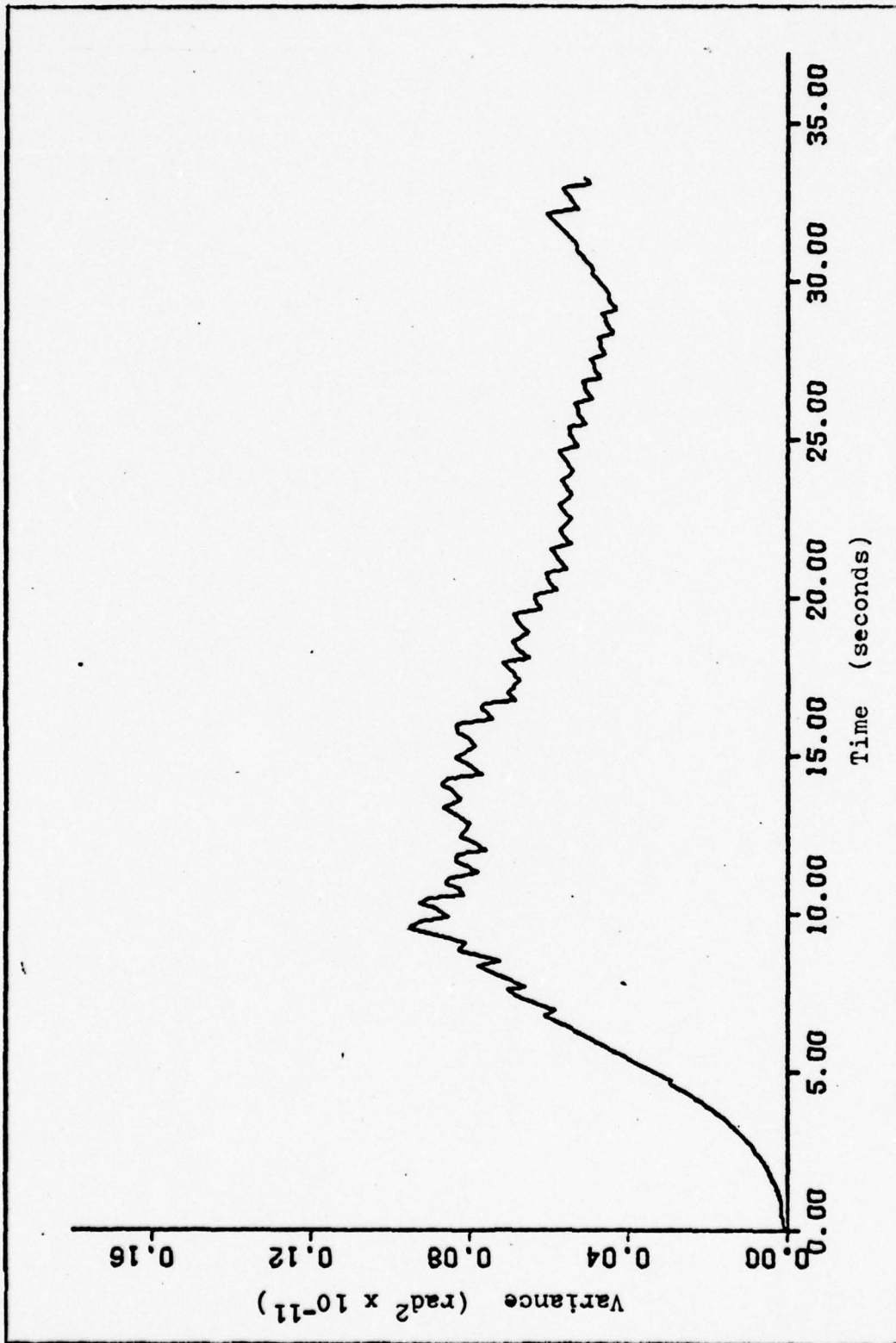
Figure 16. Latitude Position Variance $\hat{\underline{P}}_{(k)}(1, 1)$ for First 33 Seconds

DME Station Bias Results

Figure 17 shows the estimator bias values for the four stations used in the first record. Channels 57 and 37 come in at t = 0 seconds and t = .17 seconds respectively, channel 43 comes in at t = .99 seconds, and channel 59 comes in at t = 3.12 seconds. When each station is called on for the first time, the bias prediction changes the most, but the more measurements that are used, the less the bias values change. This is a direct consequence of the gradual decreasing bias variance curve of Figure 15. In other words, bias predictions must change less for lower uncertainty.

The most obvious characteristic of the bias curves in Figure 17 is the tendency to flatten out as more measurements are used. The final bias values for the first four stations during the first record can be summarized as

Channel 57 ⇒ 6.71 feet
Channel 37 ⇒ -313.16 feet
Channel 43 ⇒ -74.13 feet
Channel 59 ⇒ -257.60 feet

Of course, these values are also subject to change as the flight progresses because of changing geometry.

To illustrate that the residuals in general actually do decrease as better bias estimates are available for the prediction equation, Figures 18 and 19 show the residual and bias history of stations 37 and 59 for the first record of data. Both station biases approach an apparent steady state value, while the residuals (those corresponding to the same stations and the same time) generally decrease.

66
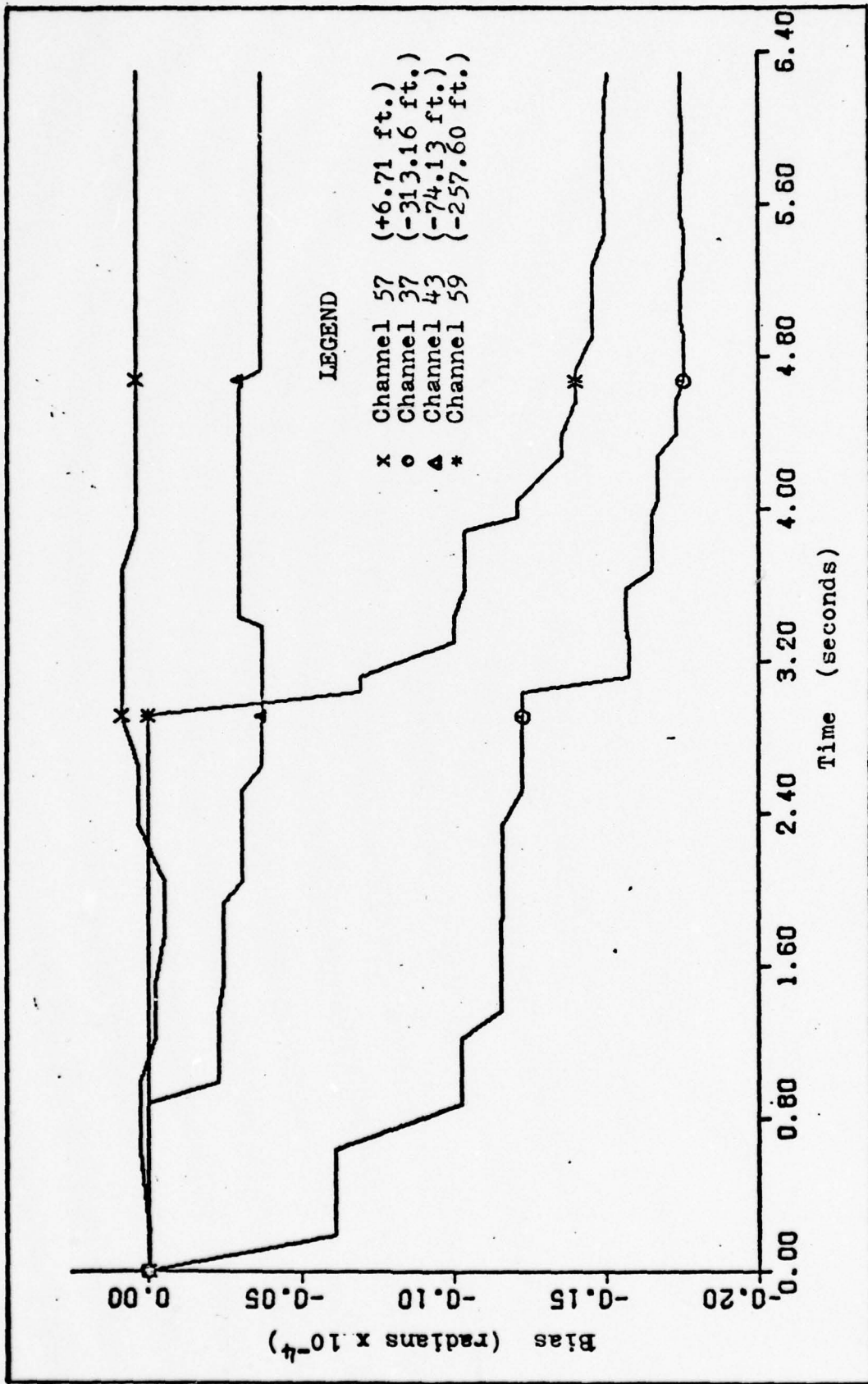
Figure 17. Four Station Bias Values for First Record Showing A Steady State Tendency
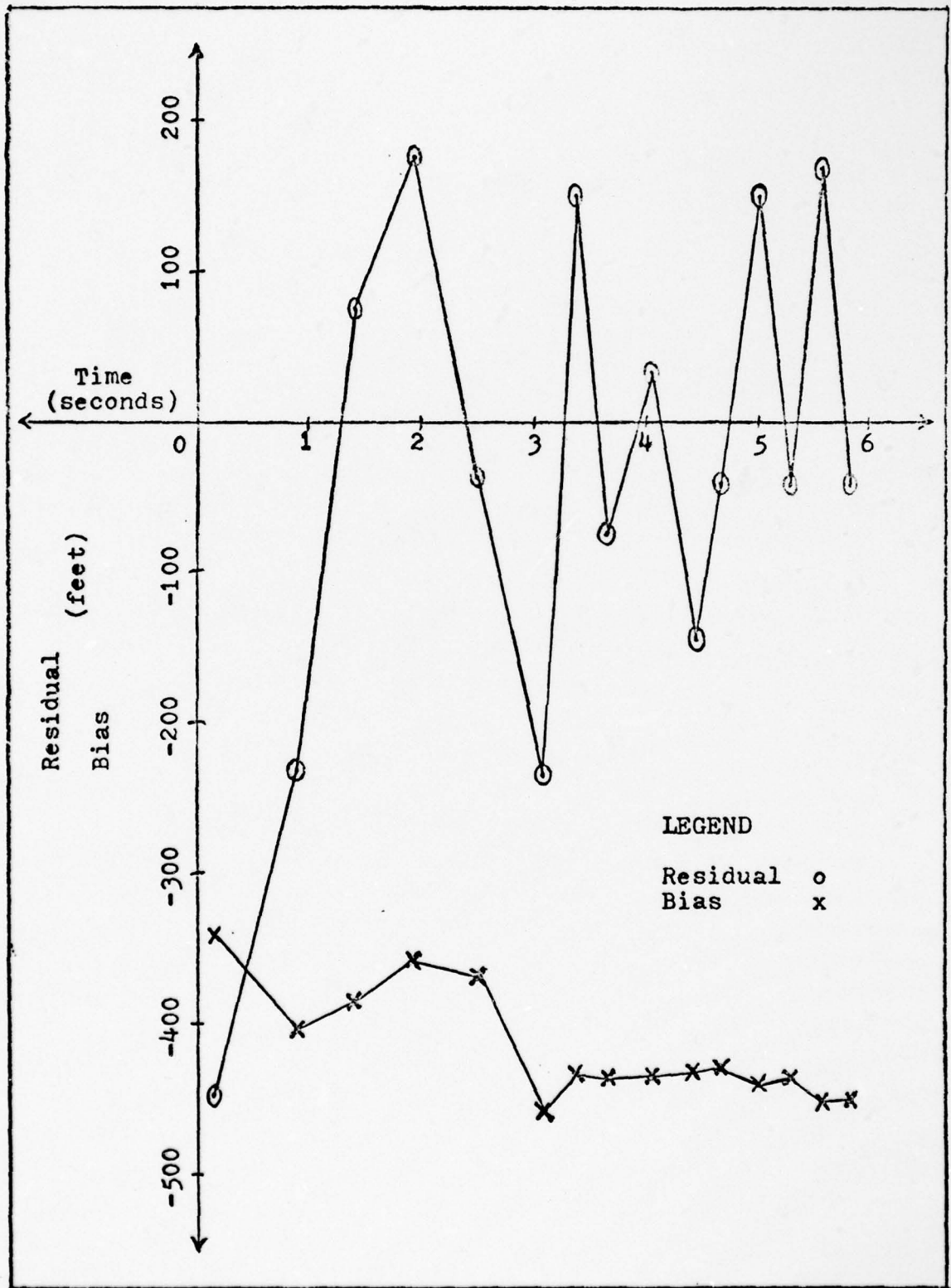
Figure 18.   Residual and Bias History for Station 37
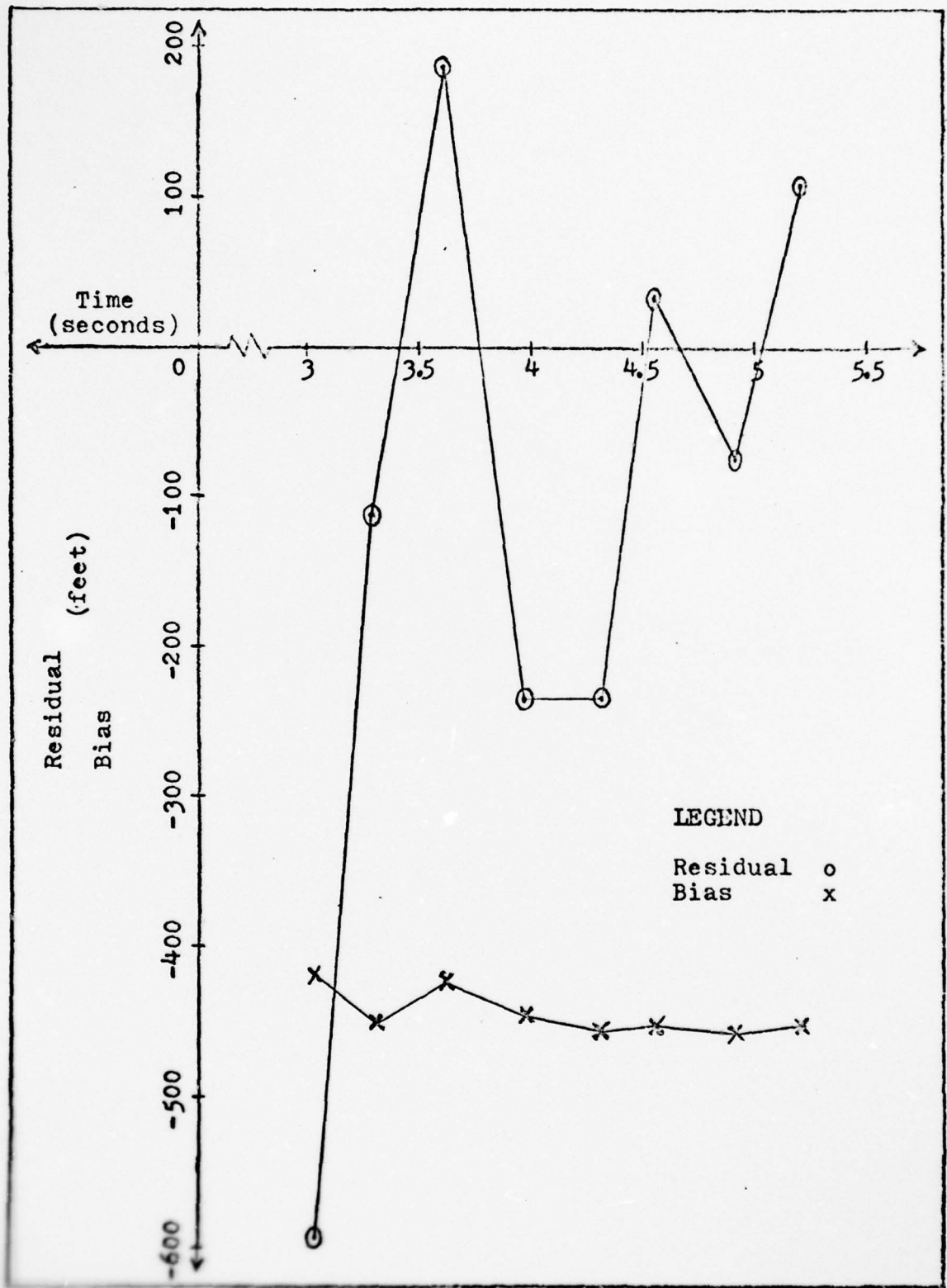
Figure 19. Residual and Bias History for Station 59

During the course of the test flight, many additional stations are acquired. Approximate bias steady state values are obtained from the estimator for all the DME stations during the first 40 minutes of the test flight. Since the FASTMAP filter does not calculate station bias estimates, the accuracy of the estimator bias estimates is not evaluated in this study. Therefore, these estimates are only presented in Table VI to show the results of the bias model. (See Chapter III.) Each approximate steady-state bias quantity in the table represents the last estimated value on or before the 40 minute mark.

Table VI. Summary of Approximate Steady State Bias for
DME Stations Used During First 40 Minutes

STATION NAME	IDENTI-FICATION	CHANNEL	APPROXIMATE STEADY STATE BIAS ESTIMATION (FEET)
Dalhart	DHT	57	14.5
Anton Chico	ACH	37	-1.7
Santa Fe	SAF	43	207.9
Texico	TXO	59	-352.0
Newman	EWM	71	-289.2
Truth or Consequences	TCS	74	-267.1
Alburquerque	ABQ	79	119.1
Holloman	HMN	85	80.3
Corona	CNX	102	164.5
Farmington	FMN	100	192.7
Roswell	ROW	108	-434.5
Cannon	CVS	104	96.0
Cimarron	CIM	111	178.8
Socorro	ONM	115	-40.2
Las Vegas	LVS	120	-65.0
Taos	TAS	123	-164.0
Zuni	ZUN	81	-331.7
Tucumcari	TCC	83	-277.7
Alamosa	ALS	86	-310.4
Colorado Springs	COS	72	-87.9
Tobe	TBE	105	-399.5
Pueblo	PUB	114	-71.8
Thurman	TXC	76	407.6
Denver	DEN	110	-91.6

V. Estimator Performance Compared to CIRIS

CIRIS Data

In Chapter IV it is shown that the designed estimator compares well to the FASTMAP filter (an accepted and usable filter). However, since FASTMAP states cannot be considered as true states, the FASTMAP filter only offers an approximate method for testing the estimator. A better method of testing is now sought to provide a more acceptable error analysis for the estimator.

Comparison to CIGTF's Completely Integrated Reference Instrumentation System (CIRIS) that recorded trajectory data (along with the FASTMAP filter) for the same test flight is the approach used in this chapter. CIRIS calculated vertical, longitude, and latitude position and velocity for the entirety of the test flight. These six states, along with a standard time (IRIG time) and 64 other words of information, are all stored for each set of calculations (one file) on a 9-track tape.

CIRIS Estimates of Error

Although a comparison to CIRIS states can be considered a more accurate method of testing the estimator than a comparison to the FASTMAP filter states, CIRIS also has associated errors. An ideal evaluation of estimator performance

would necessitate the use of the error

$$\underline{e}_E = \underline{\hat{X}}_{ESTIMATOR} - \underline{\hat{X}}_{TRUE} \tag{74}$$

However, a comparison of estimator states to CIRIS states yields results characterized by

$$\underline{d}_{EC} = \underline{\hat{X}}_{ESTIMATOR} - \underline{\hat{X}}_{CIRIS} \tag{75}$$

Therefore, CIRIS errors must be noted, which are represented by

$$\underline{e}_C = \underline{\hat{X}}_{CIRIS} - \underline{X}_{TRUE} \tag{76}$$

From Eqs (74), (75), and (76), the desired result can then be obtained as

$$\underline{e}_E = \underline{d}_{EC} + \underline{e}_C \tag{77}$$

Assuming zero-mean errors and since estimator and CIRIS errors are independent, the total error correlation can be expressed as

$$\text{TOTAL ERROR} \atop \text{CORRELATION} = E\left[\underline{e}_E\underline{e}_E^T\right] = E\left[\underline{d}_{EC}^T\underline{d}_{EC}\right] + E\left[\underline{e}_C\underline{e}_C^T\right] \tag{78}$$

CIRIS estimates of the square root of the diagonal terms of the last term in Eq (78) are located in words 35 through 40 of each file. These errors are illustrated in Table VII.

73

Table VII

CIRIS Estimates of Standard Deviation of Error

Quantity	CIRIS Estimate of Standard Deviation of Error
$\sigma_{Longitude}$	Longitude Standard Deviation
$\sigma_{Latitude}$	Latitude Standard Deviation
$\sigma_{Altitude}$	Altitude Standard Deviation
σ_{VE}	East Velocity Standard Deviation
σ_{VN}	North Velocity Standard Deviation
σ_{VV}	Vertical Velocity Standard Deviation

Table VIII shows some typical values of CIRIS errors sampled about four minutes after the initialization of the FASTMAP test. Time corresponds to the time following the FASTMAP initialization. With CIRIS errors in mind, information from the CIRIS tape can be used to evaluate estimator performance.

Matching CIRIS and Estimator States in Time

IRIG time stored on the CIRIS tape is synchronous to the IRIG time recorded on the FASTMAP filter tape. The estimator uses IRIG time from the FASTMAP filter tape, and therefore a matchup between CIRIS and estimator states is conceivable. However, both CIRIS and the FASTMAP filter have their own discrete values of IRIG time, complicating the match-up

Table VIII

Example of CIRIS Estimates of Error

Time (sec)	$\sigma_{Long.}$ (feet)	$\sigma_{Lat.}$ (feet)	σ_{VE} (ft/sec)	σ_{VN} (ft/sec)
240.78	107.4	23.2	.6900	.1407
247.86	55.9	28.3	.4584	.3102
256.14	39.5	19.7	.4380	.2310

procedure. In order to compare properly, some method is necessary to match the appropriate CIRIS states to the corresponding estimator states.

Because IRIG time is only available at different discrete values for each tape, estimator states are modified in order to be comparable to the CIRIS states that are closest in time to the estimator states. Figure 20 illustrates the fact that the estimator and CIRIS have mismatched state values. In the figure, the term "desired estimator state values" refers to the estimator states that directly correspond in time to the available CIRIS states.

To obtain the desired estimator state values, state values are propagated and updated in the manner described in Chapter III up to and including measurements (i). Next, the time at measurement (i) is subtracted from the time corresponding to the available CIRIS states. The time difference, $\Delta t'$, is employed in the estimator propagation equations to propagate the states from measurement (i) to the desired
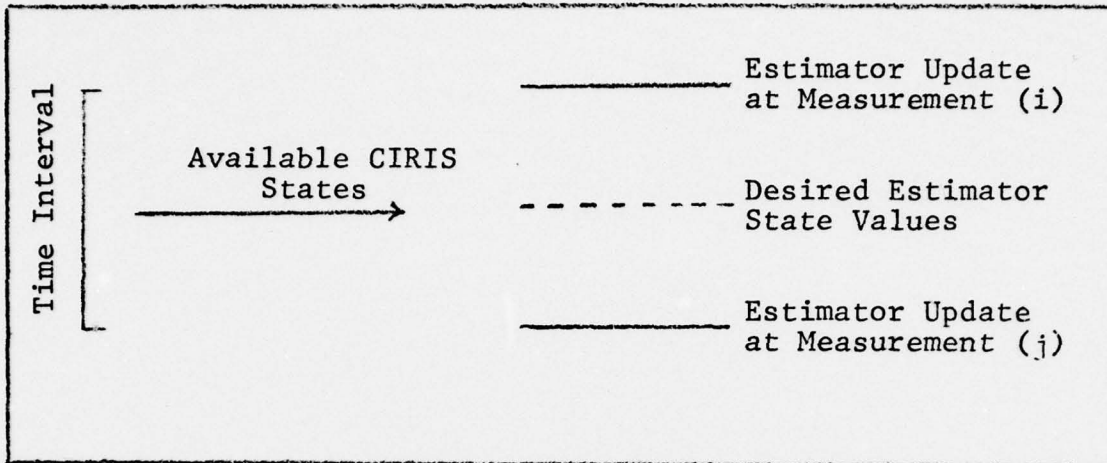
Figure 20.   CIRIS and Estimator States Mismatched in Time

estimator state values.   The two systems now have synchronous
state values that match in time and are directly comparable.
The sample time is 7 seconds and total number of sample
points are 400.   In reference to Figure 20, this procedure
can be summarized in four steps as follows:

STEP 1:   Propagate and update states to measurement (i).

STEP 2:   Obtain the time difference = $\Delta t'$ = $CIRIS_{TIME}$ - $FASTMAP_{TIME}$, where $FASTMAP_{TIME}$ corresponds to the DME measurement (i) just before the available CIRIS state.

STEP 3:   Use $\Delta t'$ in the estimator propagation equations to propagate the states to the desired time.

STEP 4:   Compare CIRIS and estimator states.

Test Results

Using the matching procedure of the previous section,
this test entails the comparison of the estimator and CIRIS

latitude, longitude, latitude velocity (V_{NORTH}) and longitude velocity (V_{EAST}). The study includes the test flight from the start of incoming DME measurements (the investigation of the FASTMAP filter) through the 180° turn and about 8 minutes past the turn, totaling 50 minutes of flight. The estimator test is extended beyond the turn to show that the estimator follows the turn.

The 180° turn provides a rigorous test for the estimator by checking its performance in such trajectory changes. Slight trajectory changes also exist in the test flight prior to the 180° turn. Figure 21 shows CIRIS latitude versus time for 18 minutes following FASTMAP initialization. A slight increase of latitude velocity (in other words, a small increase in slope) is indicated at approximately $t = 560$ seconds. A more prominent change in trajectory is noted in Figure 22, a representation of CIRIS longitude versus time. Longitude velocity changes from a westward direction (indicated by the decreasing slope) to an eastward direction at $t = 560$ seconds. Velocity estimates from the estimator should indicate these changes in trajectory.

The trajectory changes indicated above result of course from changes in velocity. Acceptable estimator performance means that estimator velocities track these CIRIS velocities. Figure 23 compares both latitude and longitude velocities for CIRIS and the estimator. The smoother upper and lower curves represent CIRIS latitude and longitude velocities

77
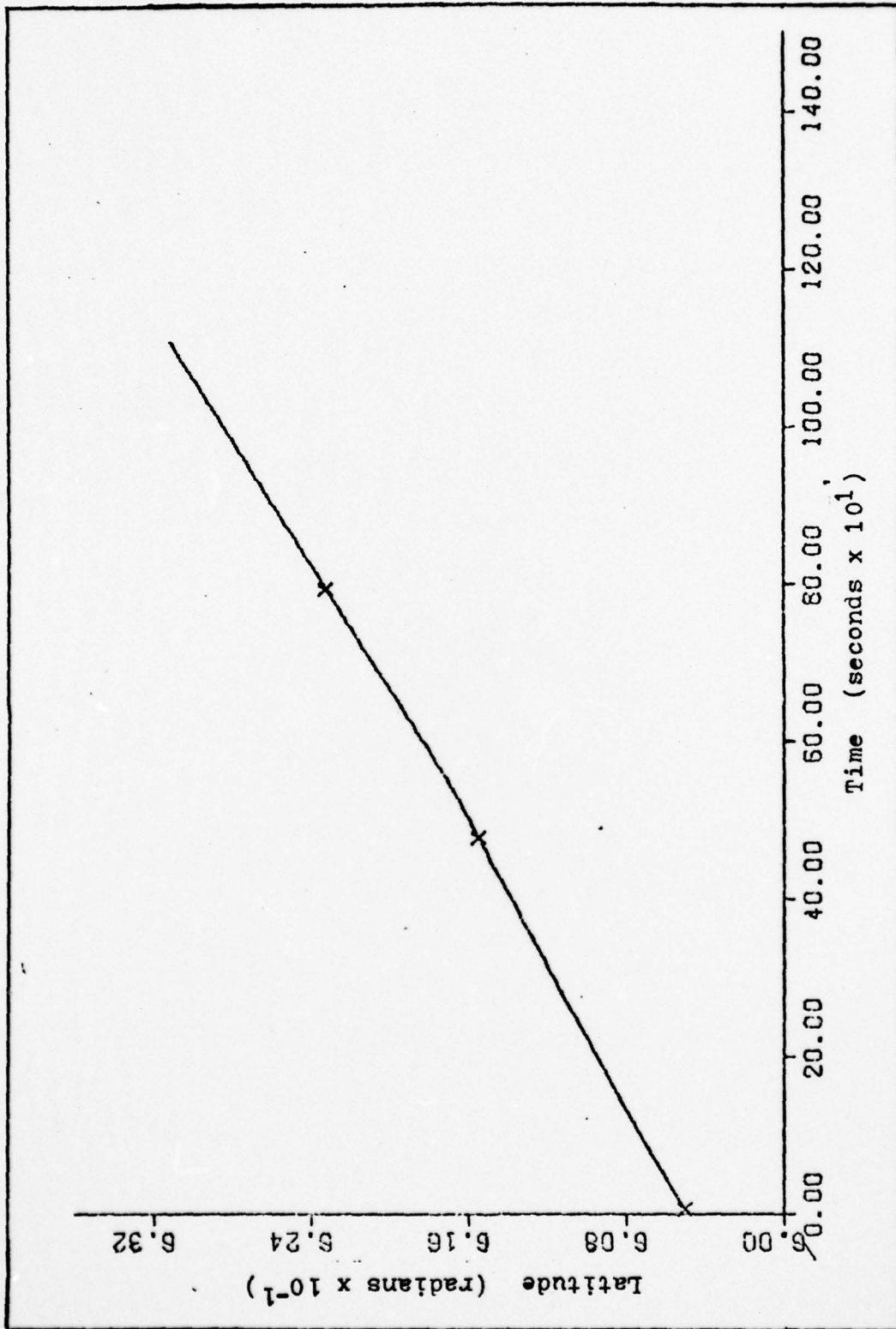
Figure 21. CIRIS Latitude versus Time for 18 Minutes of Flight

78
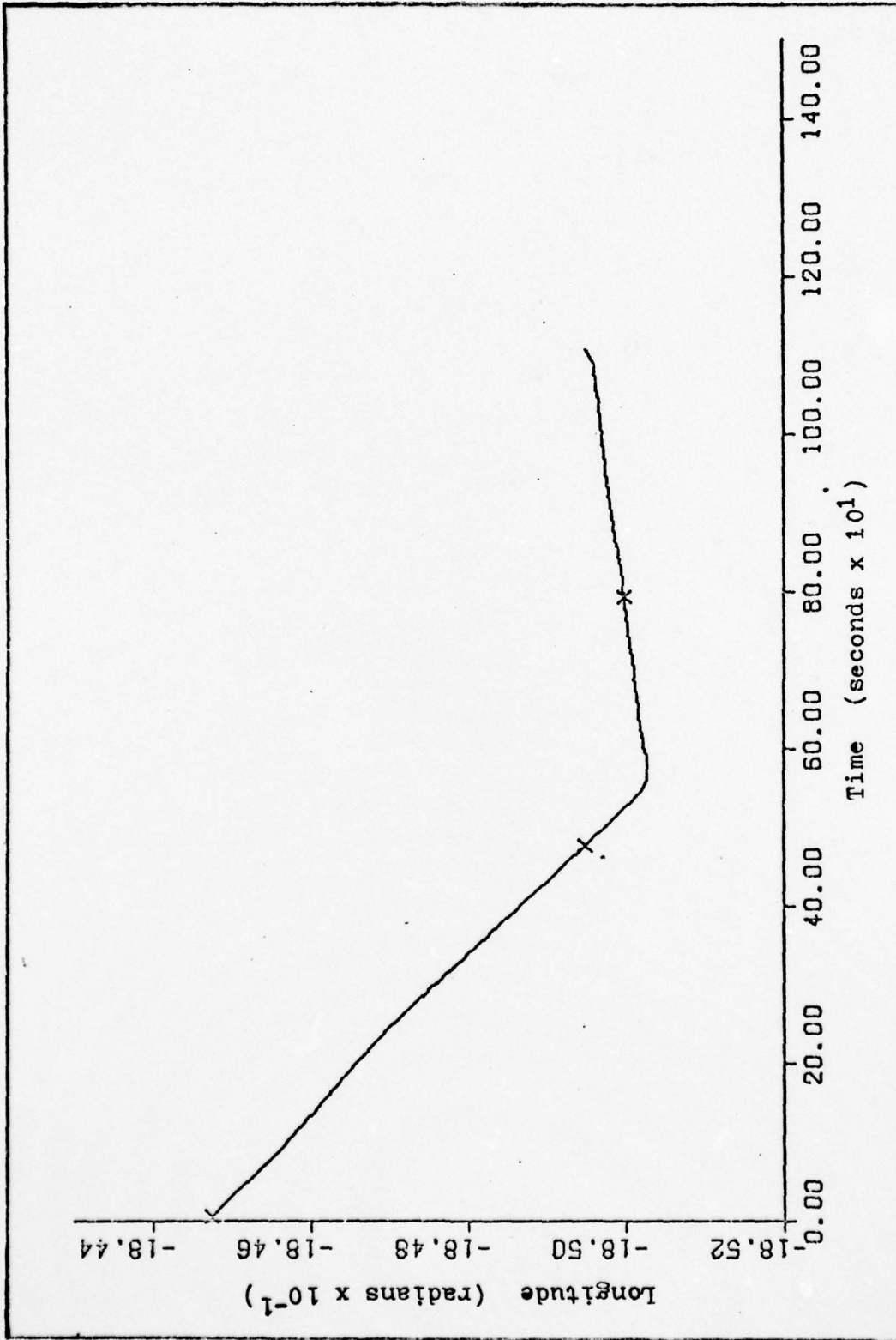
Figure 22. CIRIS Longitude versus Time for 18 Minutes of Flight

79
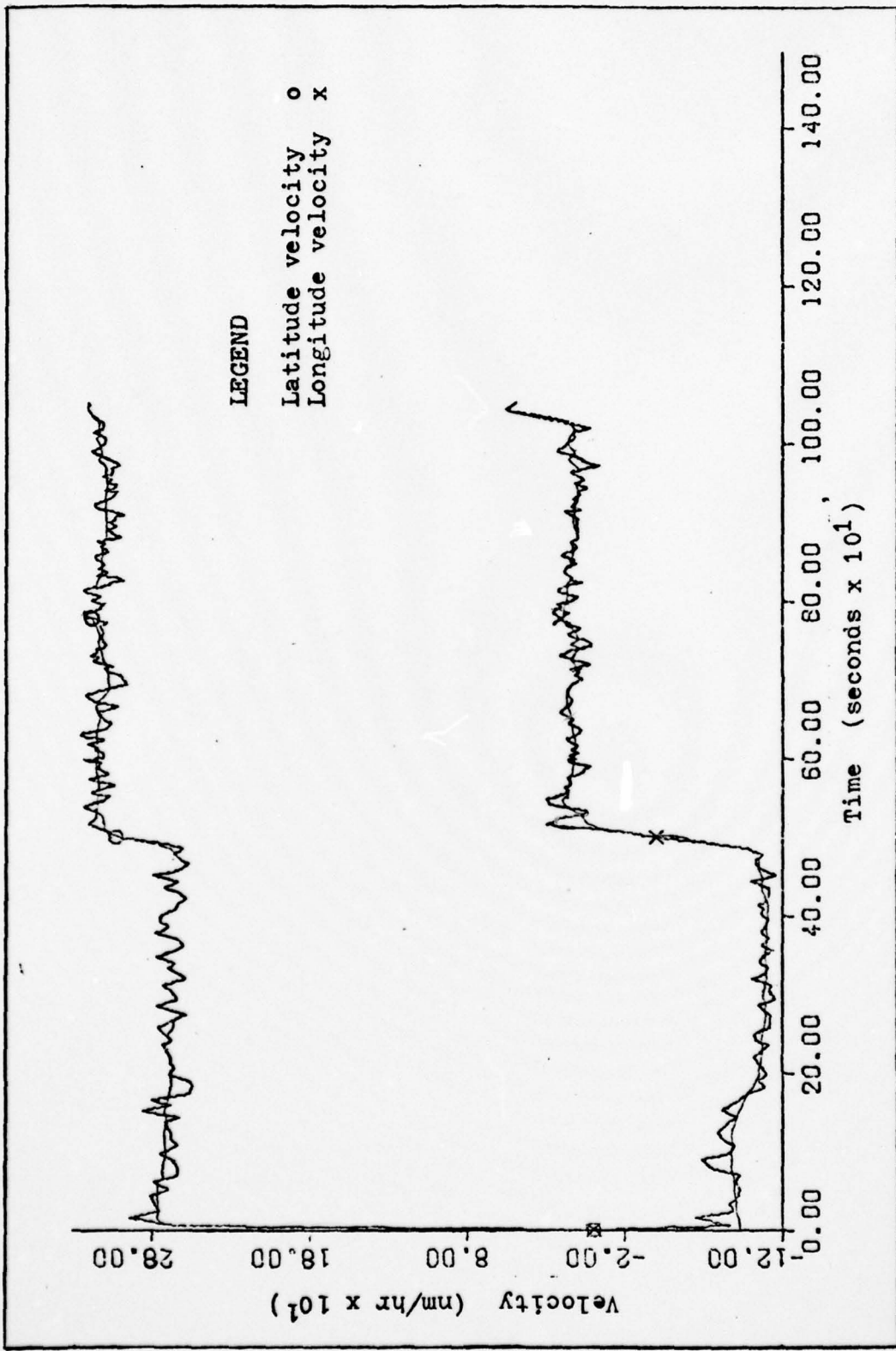
Figure 23. CIRIS and Estimator Longitude and Latitude Velocities versus Time

80

respectively, and the curves that oscillate about CIRIS velocities are the estimator's own latitude and longitude velocities. As Figure 23 shows, the estimator velocity estimates actually do track the changes in CIRIS velocity. As noted in Chapter I, high frequency errors in the reference system, such as the estimator velocity curves in Figure 23, are not as significant as unbounded error growth. On this basis, small estimator state oscillations about the smoother CIRIS states are acceptable. (Note that tuning could remove them to some degree.) The error using Eq (75) is plotted versus time for the first 50 minutes of flight in Figures 24 through 27 for positions and velocities. The sharp peaks in all the error curves represent the 180° turn. As can be expected, estimator accuracy decreases momentarily for the duration of the turn. However, these figures show that the estimates quickly recuperate from the turn. Although not attempted in this study, Q can be made to increase when a turn is indicated to put more estimator dependence on DME measurements and less on the internal model. (See recommendations.)

Figures 28 through 31 are histograms that represent the frequency distribution of the latitude and longitude position and velocity errors. Generation of these histograms is accomplished by dividing the error (Eq (75)) into 50 feet sections for position and 5 feet per second sections for
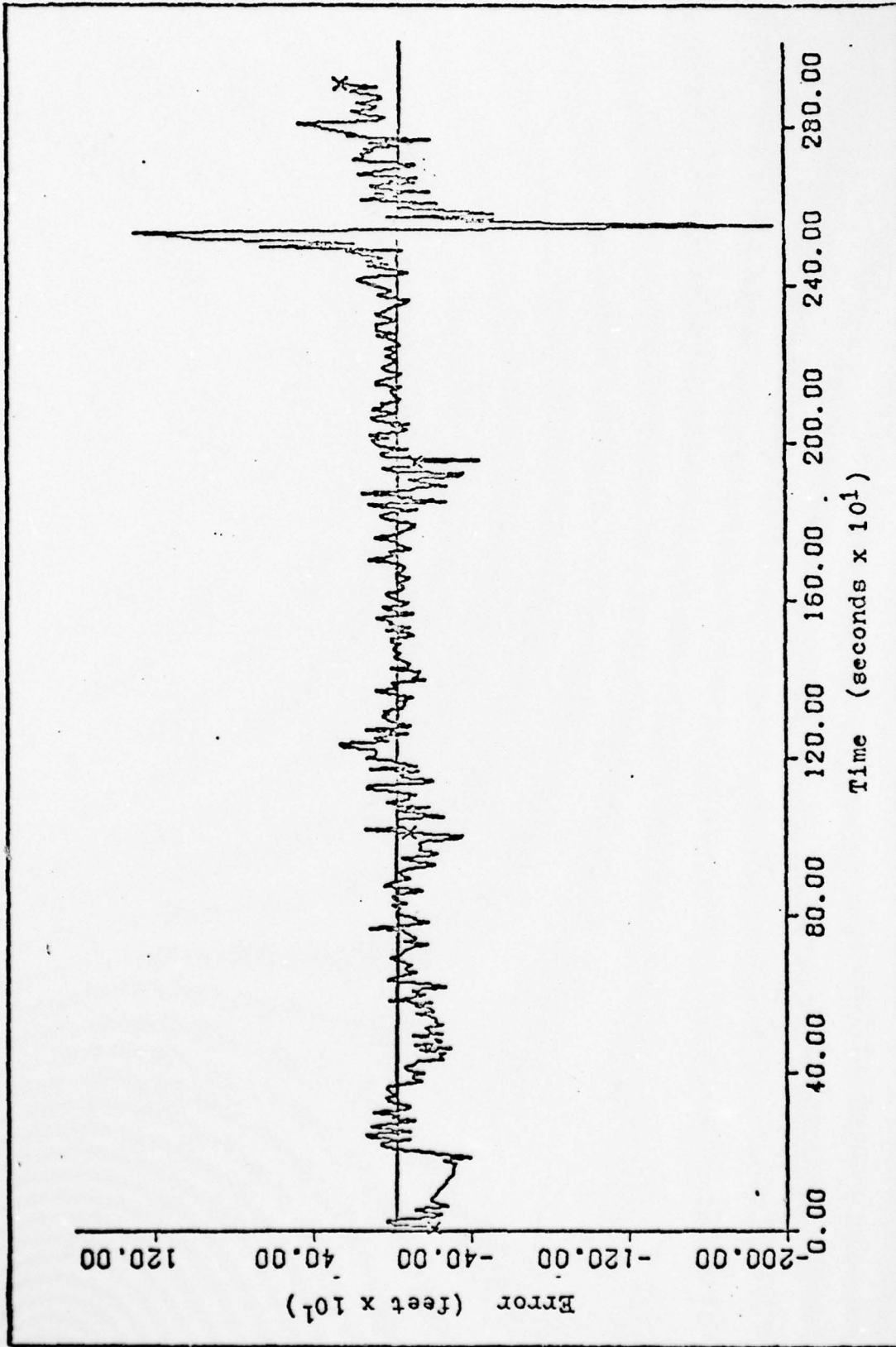
Figure 24. Latitude Position Error
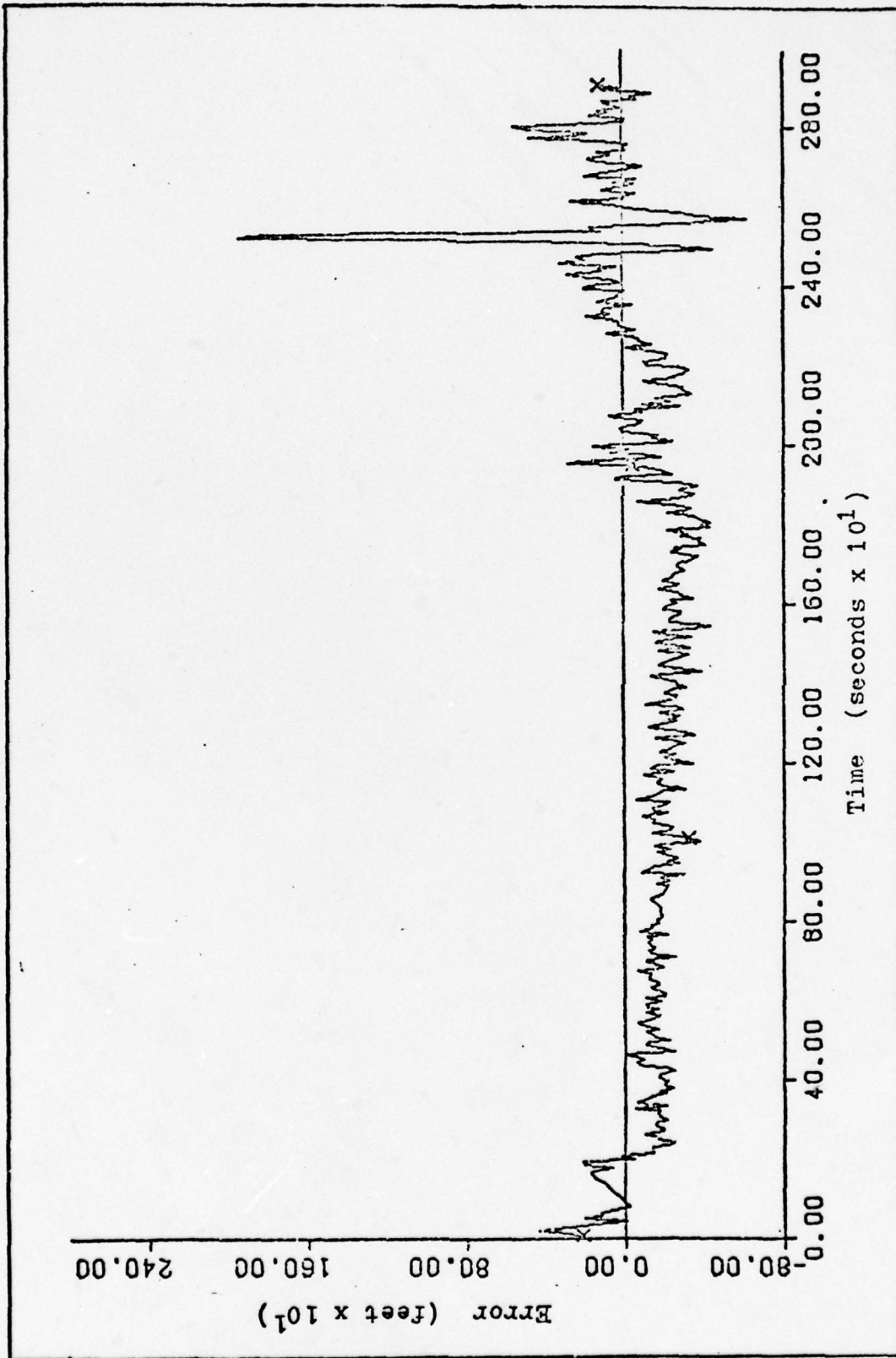
Figure 25. Longitude Position Error

83
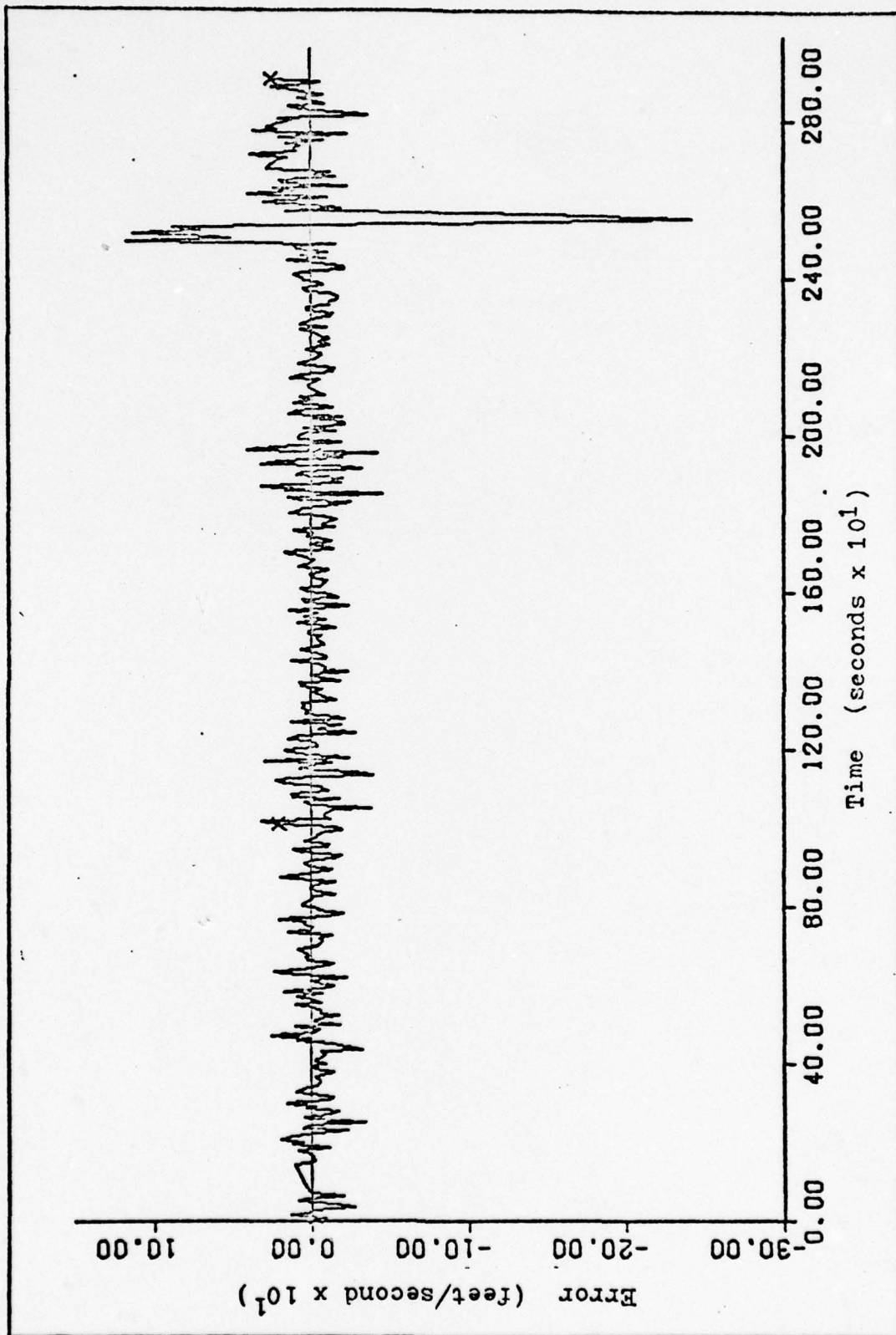
Figure 26. Latitude Velocity Error

84
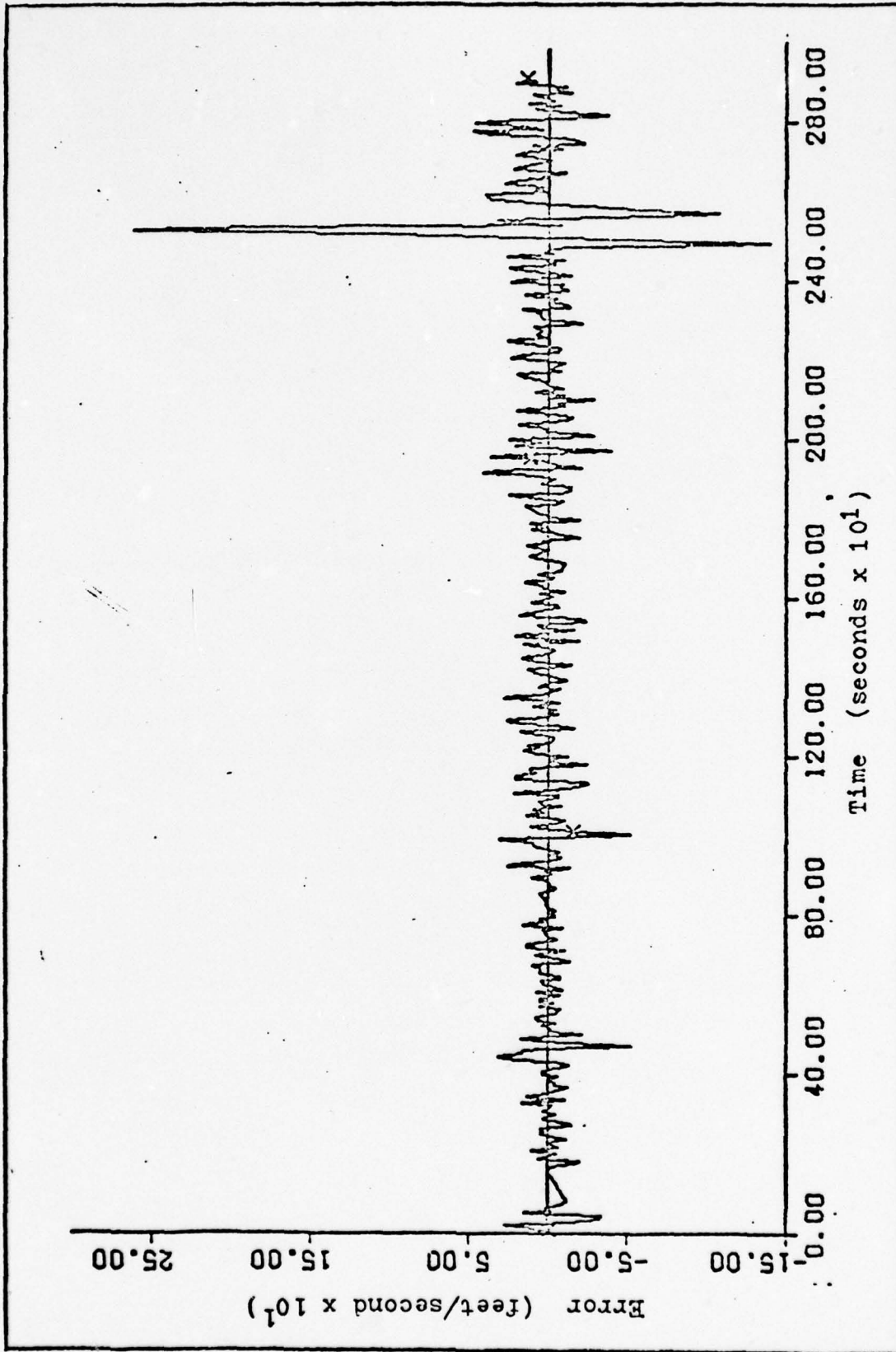
Figure 27. Longitude Velocity Error

85

CUM %	N	VALUE	
0.00	0		I
		-600	
0.00	0		I
		-550	
0.00	0		I
		-500	
0.00	0		I
		-450	
0.50	2		I X
		-400	
1.25	3		I X
		-350	
3.00	7		I X X
		-300	
6.00	12		I X X X
		-250	
10.00	16		I X X X X
		-200	
15.50	22		I X X X X X X
		-150	
26.50	44		I X X X X X X X X X X X
		-100	
42.50	64		I X X X X X X X X X X X X X X X X
		- 50	
62.00	78		I X X X X X X X X X X X X X X X X X X X X. X X X
		0	
77.75	63		I X X X X X X X X X X X X X X X X X X X
		50	
85.00	29		I X X X X X X X
		100	
89.75	19		I X X X X X
		150	
92.00	9		I X X
		200	
95.25	13		I X X X
		250	
97.00	7		I X X
		300	
98.00	4		I X
		350	
98.25	1		I
		400	
98.75	2		I X
		450	
99.25	2		I X
		500	
99.25	0		I
		550	
99.50	1		I
		600	
100.00	2		I X

Figure 28. Latitude Position Error Histogram

```
CUM %      N     VALUE

0.00       0            I
                -600
0.00       0            I
                -550
0.00       0            I
                -500
0.50       2            I X
                -450
1.50       4            I X
                -400
4.25      11            I X X X
                -350
9.50      21            I X X X X X X
                -300
20.25     43            I X X X X X X X X X X X
                -250
34.25     56            I X X X X X X X X X X X X X X X
                -200
52.50     73            I X X X X X X X X X X X X X X X X X X X X X X X
                -150
65.00     50            I X X X X X X X X X X X X X
                -100
72.25     29            I X X X X X X X X
                - 50
76.00     15            I X X X X
                  0
80.25     17            I X X X X X
                 50
83.50     13            I X X X X
                100
87.25     15            I X X X X
                150
91.00     15            I X X X X
                200
94.00     12            I X X X
                250
96.75     11            I X X X
                300
98.50      7            I X X
                350
98.50      0            I
                400
99.00      2            I X
                450
99.25      1            I
                500
99.25      0            I
                550
99.25      0            I
                600
100.00     3            I X
```

Figure 29.   Longitude Position Error Histogram

```
CUM %    N   VALUE

 0.75    3          I X
              -50
 1.25    2          I X
              -45
 1.75    2          I X
              -40
 2.25    2          I X
              -35
 3.50    5          I X
              -30
 4.75    5          I X
              -25
 8.50   15          I X X X X
              -20
15.00   26          I X X X X X X X
              -15
24.25   37          I X X X X X X X X X X X
              -10
38.75   58          I X X X X X X X X X X X X X X X X X X
              - 5
55.75   68          I X X X X X X X X X X X X X X X X X X X X X X
               0
70.00   57          I X X X X X X X X X X X X X X X X X X
               5
81.75   47          I X X X X X X X X X X X X X X X
              10
89.75   32          I X X X X X X X X X X
              15
93.25   14          I X X X X
              20
96.00   11          I X X X
              25
97.25    5          I X
              30
98.50    5          I X
              35
98.50    0          I
              40
98.75    1          I
              45
99.00    1          I
              50
100.00   4          I X
```

Figure 30. Latitude Velocity Error Histogram

88

```
 CUM %     N   VALUE

 1.75      7           I X X
                 -50
 1.75      0           I
                 -45
 1.75      0           I
                 -40
 2.00      1           I
                 -35
 2.75      3           I X
                 -30
 4.25      6           I X X
                 -25
 6.25      8           I X X
                 -20
 9.00     11           I X X X
                 -15
16.50     30           I X X X X X X X
                 -10
31.00     58           I X X X X X X X X X X X X X X X
                 - 5
48.25     69           I X X X X X X X X X X X X X X X X X X
                   0
66.50     73           I X X X X X X X X X X X X X X X X X X X
                   5
79.25     51           I X X X X X X X X X X X X X
                  10
87.25     32           I X X X X X X X X X
                  15
92.75     22           I X X X X X X
                  20
95.50     11           I X X X
                  25
96.75      5           I X
                  30
98.00      5           I X
                  35
98.25      1           I
                  40
98.75      2           I X
                  45
99.00      1           I
                  50
100.00     4           I X
```

Figure 31. Longitude Velocity Error Histogram

velocity, and noting the number of errors between each section; error sampling is one sample every seven seconds.

Figures 25 and 29 show that longitude position error is biased about 150 to 200 feet. The fact that bias errors are commonly found in EKF designs may be a possible explanation. Bias errors in EKF designs can result from assumptions of the form

$$\widehat{f(x)} \,\tilde{}\, f(\hat{x}) \tag{79}$$

for nonlinear f, such as in the calculation of the linearized measurement equation in Chapter III. Partial corrections for biases in EKF designs can be accomplished by using "Bias Correction Terms." Use of these terms partially corrects for the bias by adding higher order terms to both the state propagation and the measurement prediction equations. This procedure is reserved for a possible future study and is not attempted in this report.

Using the histograms in Figures 28 through 31, approximate values can be obtained that encompass 50 percent of all the errors for latitude, longitude, latitude velocity, and longitude velocity. The magnitudes of these values should give a rough estimate of estimator performance and feasibility for using the estimator as an INS reference system. The approximate values that contain 50 percent of the errors are obtained as

Latitude position $\Rightarrow$ $\pm$ 83 feet

Longitude position $\Rightarrow$ $\pm$ 183 feet

Latitude velocity $\Rightarrow$ $\pm$ 8.4 feet/sec

Longitude velocity $\Rightarrow$ $\pm$ 7.5 feet/sec

These approximate values exceed the accuracy goals stated in Chapter I. However, with proper tuning and with the "Bias Correction Terms," the accuracy goals might be achievable.

VI. Effects of Omitting Measurements

Omission of Bad Measurements

In designing the estimator, some method of omitting erroneous measurements should be considered. Estimator performance depends on the measurement history. If one measurement in a group of measurements is obviously different, then a possible action would be to rid the system of that measurement since keeping it might well degrade performance. On the other hand, removing a measurement is like throwing away a piece of information--information which, no mater how erroneous, might actually help the estimation process. How bad must a measurement be before no helpful information can be derived from it?

One way to define "erroneous" measurements is to include all measurements with residuals beyond an $n\sigma_{RES}$ boundary, where the residual standard deviation, σ_{RES}, is given by

$$\sigma_{RES} = \left[\underline{H}_{(k+1)} \ \underline{P}^-_{(k+1)} \ \underline{H}^T_{(k+1)} + R \right]^{\frac{1}{2}} \tag{80}$$

and n is a value on the order of 2 or 3.

Estimator values of σ_{RES} are plotted in Figure 32 for the first nine records (about 60 seconds) of measurement data.

Another way to define "erroneous" measurements in relation to this design would be to include all measurements

92
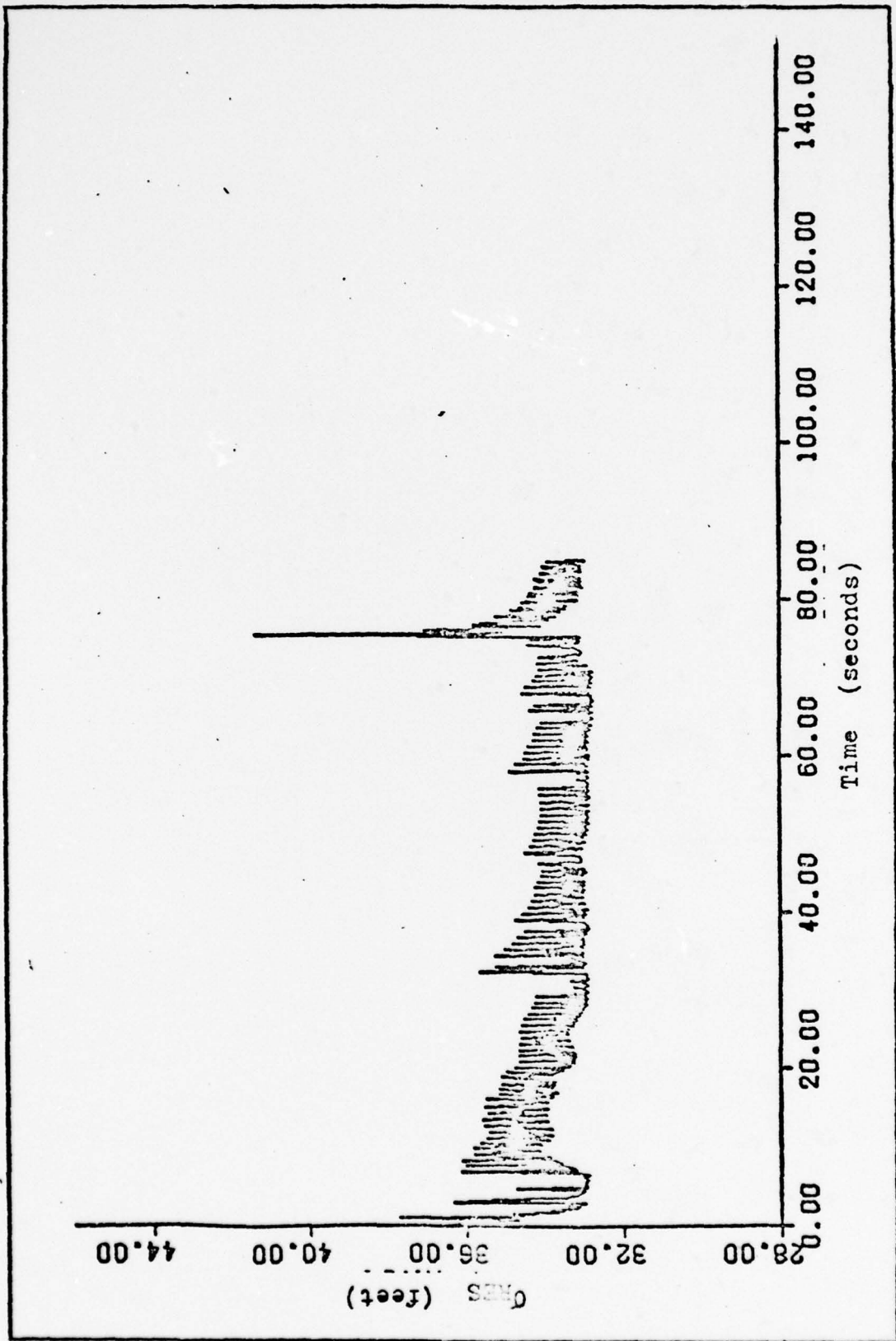
Figure 32. Time History of the Rksidual Standard Deviation

with residuals over "X" feet, with "X" selected a priori.
A concise answer to the above question would require an
appropriate value for X.   (This value could then be compared
to the time history of σ_{RES} in Figure 32.)   In order to
determine a "ball-park" value for X, a study presented below
contrasts estimator performance with four values of X.   All
measurements with residuals greater than X feet are omitted.
Estimator performance is approximated by noting the time-
averaged difference between estimator postion and the FASTMAP
filter position for each value of X.   Table IX shows four
values of X and the corresponding position differences for
both latitude and longitude.

Table IX

Four Values of X and Corresponding FASTMAP
and Estimator Position Differences

X (feet)	Latitude Difference (feet)	Longitude Difference (feet)
∞ (all measurements accepted)	66.9	98.3
600	71.6	100.8
400	255.9	452.6
300	767.1	1818.2

Table IX reveals that when all measurements with residuals
above 300 feet are omitted from the estimator equations, the
time-averaged position differences between the estimator and

the FASTMAP filter are relatively large. A plot of estimator variance for latitude position, $\hat{\underline{P}}^+_{(k+1)}(1,1)$, is shown in Figure 33. From the figure, the latitude position variance can be seen to diverge when X is set at 300 feet. As the value of X increases to 400 feet, the variance drops sharply. At X equal to 600 feet, the variance levels off close to the value for X equal to infinity (when all measurements are accepted). The difference between X equal to 600 and infinity is almost negligible in terms of estimator performance (See Table IX).

The results of this study reveal that measurements with residuals over 600 feet can effectively be dropped without losing accuracy. In reference to Table IX and Figure 33, the minimum value for X is 600 feet. A value for X to be used in the actual estimator is chosen at X equal to 2500 feet. This ensures that no bad measurements, such as wrong station coordinates and gross receiver-transmitter delays, are used in the estimator equations. On the other hand, choosing X well over the minimum (X = 600 feet) will ensure response to trajectory changes such as 180° turns. Again, Q values can be made to increase to meet trajectory changes (See Recommendations).

Now that all measurements with residuals over 2500 feet are omitted, a method for implementing this is necessary. The omission of bad measurement data is shown in the estimator flow chart, Figure 7. A measurement prediction is made from both prior measurement and state information and

95
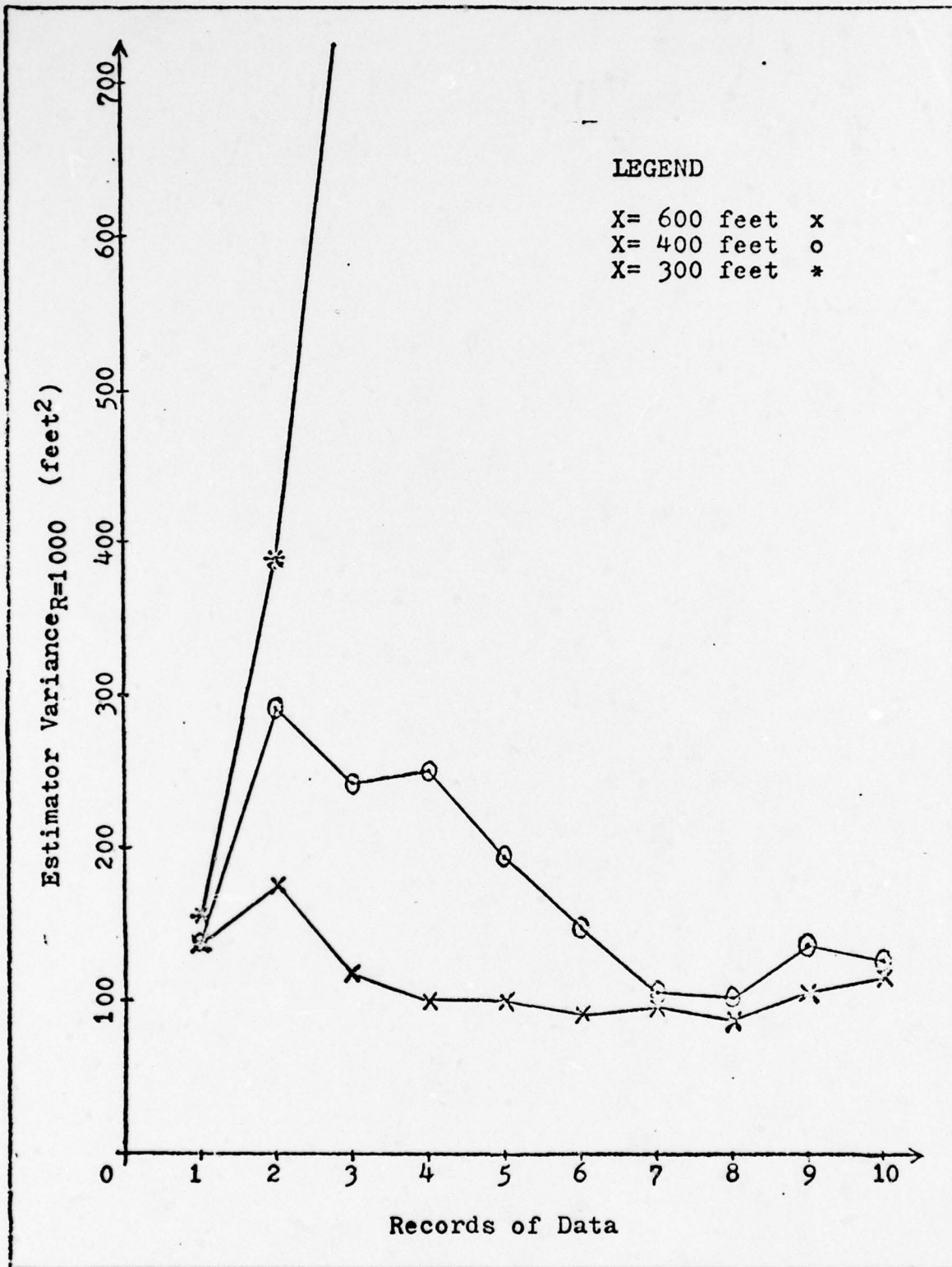
Figure 33.   Effects of Measurement Cutoffs
on Estimator Variance

96

is immediately followed by the actual measurement. If the difference between the prediction and actual measurement is greater than 2500 feet, the estimator treats that measurement as if it never existed. The estimator carries the propagation of the states across this measurement time to the next measurement. However, a sequence of residuals consistently over 2500 feet should not be omitted, since this phenomenon could well represent some trajectory change. Another future study not attempted in this report would be to monitor the residual sizes and increase Q when sequences of residuals are over a certain amount (i.e., an adaptive filter).

Effects of Increasing the Time Between Measurements

The time difference between each station acquisition for this test flight is on the order of .05 to .5 seconds. Current DME digital equipment allows station acquisition at such high rates. However, if station acquisition is only possible at a slower rate, estimator performance is expected to degrade. An additional study presented in this chapter illustrates system performance as the time between each measurement is lengthened. Performance may not be degraded to an undesirable degree when measurements are acquired at a slower rate. Perhaps there is a point where any additional measurements in a given time interval will not add a substantial amount of information to the estimation process. If there is such a point, then the plot of estimator

performance versus the time between measurements should start out flat, or in general be concave-up. In such a case, the time between measurements can be increased without significant loss of estimator performance.

Whether or not the time between measurements can be, or should be, lengthened is obtained from an investigation of the plot of estimator position error variance versus the number of measurements omitted. Figure 34 shows the relationship between the number of measurements omitted and estimator latitude variance, $\hat{\underline{P}}^{+}{}_{(k+1)}(1,1)$. Latitude variance rises almost linearly as the time between measurements increases. Since the curve is not initially flat or concave-up, then the time between measurements should not be lengthened except in necessary cases. In such cases, Figure 34 reveals how much performance degradation can be expected.
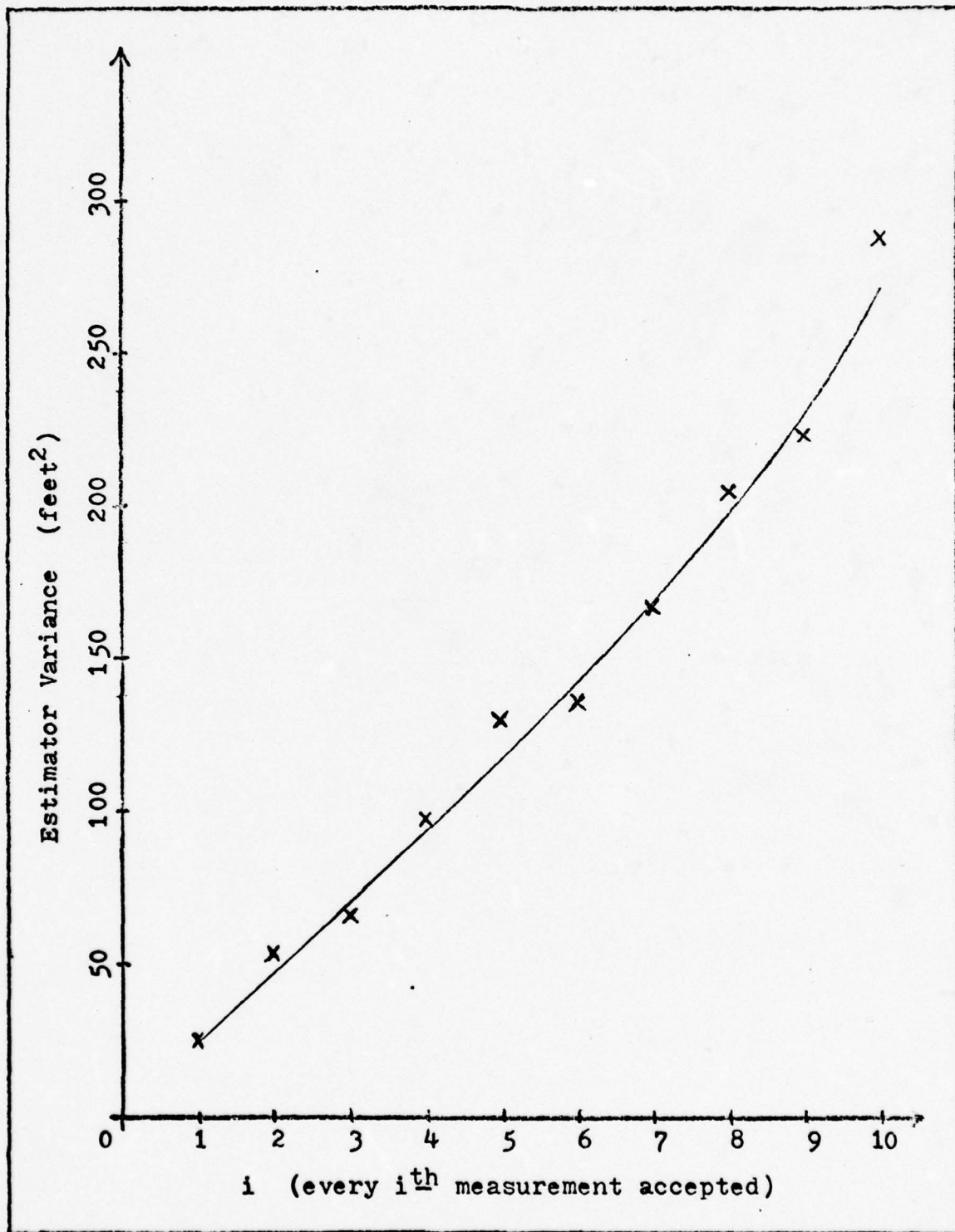
Figure 34. Relationship between the Number of Measurements Omitted and Time-Averaged Estimator Latitude Variance

99

VII. Conclusions and Recommendations

Conclusions

Based on the design and testing of the estimator, the following conclusions are drawn:

1. An extended Kalman filter using multiple DME range measurements is a feasible reference system for examining INS low frequency errors. Estimator errors in the high frequency range are greater than those of an INS, but errors in the DME-based estimator are consistent in strength and do not exhibit an unbounded growth as typical of INS errors.

2. With the Q and R used in the estimator tests, the 7-state estimator without the jerk states provides better performance than the 9-state estimator with the jerk states included.

3. For the estimator in this study, the approximate values that encompass 50 percent of all the errors for latitude, longitude, latitude velocity, and longitude velocity, as compared to CIRIS, are summarized below:

$$
\begin{aligned}
\text{Latitude position} &\implies \pm\ 83 \text{ feet} \\
\text{Longitude position} &\implies \pm\ 183 \text{ feet} \\
\text{Latitude velocity} &\implies \pm\ 8.4 \text{ feet/sec} \\
\text{Longitude velocity} &\implies \pm\ 7.5 \text{ feet/sec}
\end{aligned}
$$

Although not attempted in this study, properly tuned values of R and Q might result in lower estimator position and velocity errors.

4. The estimator is able to track changing trajectories such as a 180° turn. Errors in the estimator states do momentarily increase for such a change, but the estimator rapidly recovers following the trajectory change.

5. Measurement residuals over 600 feet (or more) can be dropped without significant loss of estimator accuracy. On the other hand, the time between measurements cannot be lengthened without loss of estimator accuracy.

6. Finally, the estimator recovers from initial conditions that are not precisely known.

Recommendations

The following recommendations are suggested for improving the performance of the multiple DME estimator and for further studies in this area:

1. Proper R and Q values for the estimator should be obtained by a covariance and/or a Monte Carlo analysis of performance.

2. An estimator using an adaptive approach should be investigated; that is, R and Q can be made functions of time, environment parameters, or current residual values. For example, the constant R used in the estimator tests can be designed to change in relation to the magnitude of the DME range measurements. Also, Q can be boosted at trajectory changes either by monitoring the residuals or by informing the estimator of commanded aircraft trajectory changes.

3. Although the 7-state estimator provides better per-
formance in this study, other approaches to designing the
estimator are suggested. The 7-state estimator is currently
modeled in the form

White
Noise → $\frac{1}{s}$ → Acceleration → $\frac{1}{s}$ → Velocity → $\frac{1}{s}$ → Position →
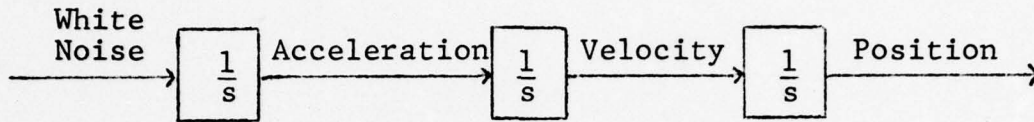
Instead of entering the white noise through a pure integrator,
investigating the use of a first-order lag is suggested as
follows:

White
Noise → $\frac{1}{s+\frac{1}{T}}$ → Acceleration → $\frac{1}{s}$ → Velocity → $\frac{1}{s}$ → Position →
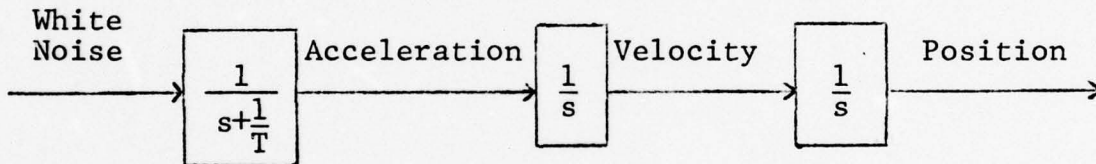
Such a form represents a reasonable model of aircraft accel-
eration in the form of an exponentially time-correlated
process.

Another possible area of study would include a combi-
nation of the 7-state and the 9-state estimators in the form

ω_1 → + ⊗ + → $\frac{1}{s+\frac{1}{T}}$ → Acceleration → $\frac{1}{s}$ → Velocity → $\frac{1}{s}$ → Position →

ω_2 → $\frac{1}{s+a}$ →
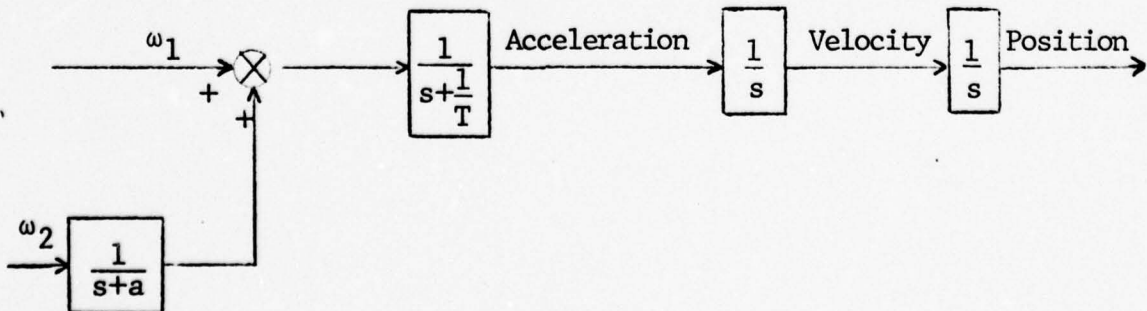
This study would search for the optimal combination of the white noise strengths for both noises ω_1 and ω_2. Parameters to vary in the preceding diagram would include R, the strengths of the white noises, ω_1 and ω_2, T, and a.

Bibliography

1. AFM 51-40. Air Navigation. Washington: Department of the Air Force and the Navy, July 1973.

2. Kaytor, Myron and Walter R. Fried. Avionics Navigation Systems. New York: Wiley, 1969.

3. Krumm, J. A., et al. Flight Testing of the Grumman FASTMAP System. Unpublished report. Holloman Air Force Base, New Mexico: Central Inertial Guidance Test Facility, May 1977.

4. -----Flight Testing of the Sierra SCORE System. Unpublished report. Holloman Air Force Base, New Mexico: Central Inertial Guidance Test Facility, May 1977.

5. Latham, R. W. "Aircraft Positioning with Multiple DME." Navigation: Journal of the Institute of Navigation, 21: 150-158 (Summer 1974).

6. Latham, R. W. and R. S. Townes. "DME Errors," Navigation: Journal of the Institute of Navigation, 22: 332-342 (Winter 1975-76).

7. Maybeck, P. S. Filter Design for a Tacon-Aided Boro-Inertial System with ILS Smoothing Capability. AFFDL-TM-74-52. Wright-Patterson Air Force Base, Ohio: Air Force Flight Dynamics Laboratory, 1974.

8. McCaskill, T., et al. "A Sequential Range Navigation Algorithm for a Medium Altitude Navigation Satellite," Navigation: Journal of the Institute of Navigation, 23: 166 (Summer 1976).

Appendix A

Local Geodetic Frame to XYZ Coordinate Transformation (Ref 8: 166)

A point on or near the earth's surface can be described by three orthogonal components, X, Y, and Z, in terms of its latitude, longitude, and height above sea-level. The equations are as follows:

$$X = \left[\frac{a}{(1-e^2 \sin^2 P_{\phi_g})^{\frac{1}{2}}} + Hgt \right] \cos P_{\phi_g} \cos P_\lambda \qquad (81)$$

$$Y = \left[\frac{a}{(1-e^2 \sin^2 P_{\phi_g})^{\frac{1}{2}}} + Hgt \right] \cos P_{\phi_g} \sin P_\lambda \qquad (82)$$

$$Z = \left[\frac{a}{(1-e^2 \sin^2 P_{\phi_g})^{\frac{1}{2}}} + Hgt - \frac{ae^2}{(1-e^2 \sin^2 P_{\phi_g})^{\frac{1}{2}}} \right] \sin P_{\phi_g}$$

$$(83)$$

where

$$
\begin{aligned}
X &= \\
Y &= \qquad \text{Cartesian coordinates of aircraft} \\
Z &= \\
a &= \qquad \text{equatorial radius of earth} \\
e &= \qquad \text{eccentricity of the earth} \\
P_{\phi_g} &= \qquad \text{aircraft latitude} \\
P_\lambda &= \qquad \text{aircraft longitude} \\
Hgt &= \qquad \text{aircraft height}
\end{aligned}
$$

Appendix B

Linearized Measurement Equation

The non-linear measurement equation

$$\varepsilon = \left[(X_u - X_s)^2 + (Y_u - Y_s)^2 + (Z_u - Z_s)^2 \right]^{\frac{1}{2}} + b_{i(k+1)} + \upsilon \qquad (84)$$

is linearized to obtain

$$\partial \varepsilon = \left[\partial \varepsilon / \partial P_{\phi_g} \Big| \quad \right] \delta P_{\phi_g} + \left[\partial \varepsilon / \partial P_{\lambda} \Big| \quad \right] \delta P_{\lambda}$$
$$\underline{\hat{X}}^-_{(k+1)} \qquad\qquad \underline{\hat{X}}^-_{(k+1)}$$

$$+ \left[\partial \varepsilon / \partial b_i \Big| \quad \right] \delta b_i \qquad (85)$$
$$\underline{\hat{X}}^-_{(k+1)}$$

and thus an $\underline{H}$ matrix becomes

$$\underline{H} = \left[\partial \varepsilon / \partial P_{\phi_g} \Big| \qquad , 0, 0, \quad \partial \varepsilon / \partial P_{\lambda} \Big| \qquad , \right.$$
$$\underline{\hat{X}}^-_{(k+1)} \qquad\qquad\qquad \underline{\hat{X}}^-_{(k+1)}$$

$$\left. 0, 0, 0, 0, \quad \partial \varepsilon \, \partial b_i \Big| \qquad \right] \qquad (53)$$
$$\underline{\hat{X}}^-_{(k+1)}$$

where

$$P_{\phi_g} = \text{aircraft latitude}$$

$$P_{\lambda} = \text{aircraft longitude}$$

$$b_{i(k+1)} = \text{measurement bias prediction}$$

$$\left. \begin{array}{l} X_u = \\ Y_u = \\ Z_u = \end{array} \right\} \begin{array}{l} \text{Cartesian coordinates of aircraft} \\ \text{using formulas in Appendix A} \end{array}$$

$$X_s = \left.\begin{matrix}\\\\\end{matrix}\right\} \text{Cartesian coordinates of the}$$

$X_s = $ ⎫ Cartesian coordinates of the
$Y_s = $ ⎬ DME stations using the formulas
$Z_s = $ ⎭ in Appendix A

$\text{Hgt} = $ aircraft altitude

Expressing equation (84) in terms of P_{ϕ_g}, P_λ, and Hgt yields

$$\varepsilon = \left[\left(\left\{ \left[\frac{a}{(1-e^2 \sin^2 P_{\phi_g})^{\frac{1}{2}}} + \text{Hgt} \right] \cos P_{\phi_g} \cos P_\lambda \right\} - X_s \right)^2 \right.$$

$$+ \left(\left\{ \left[\frac{a}{(1-e^2 \sin^2 P_{\phi_g})^{\frac{1}{2}}} + \text{Hgt} \right] \cos P_{\phi_g} \sin P_\lambda \right\} - Y_s \right)^2$$

$$+ \left(\left\{ \left[\frac{a}{(1-e^2 \sin^2 P_{\phi_g})^{\frac{1}{2}}} + \text{Hgt} - \frac{ae^2}{(1-e^2 \sin^2 P_{\phi_g})^{\frac{1}{2}}} \right] \sin P_{\phi_g} \right\} \right.$$

$$\left. \left. -Z_s \right)^2 \right]^{\frac{1}{2}} + b_{i(k+1)} + \nu \qquad (86)$$

The partial of Equation (86) with respect to latitude becomes

$$\partial \varepsilon / \partial P_{\phi_g} = \frac{1}{2} \left[(X_u - X_s)^2 + (Y_u - Y_s)^2 + (Z_u - Z_s)^2 \right]^{-\frac{1}{2}}$$

$$\times \left[2(X_u - X_s) \, \partial X_u / \partial P_{\phi_g} \bigg|_{\hat{\underline{X}}^-_{(k+1)}} + 2(Y_u - Y_s) \, \partial Y_u / \partial P_{\phi_g} \bigg|_{\hat{\underline{X}}^-_{(k+1)}} \right.$$

$$\left. + 2(Z_u - Z_s) \, \partial Z_u / \partial P_{\phi_g} \bigg|_{\hat{\underline{X}}^-_{(k+1)}} \right] \qquad (87)$$

First $\partial X_u / \partial P_{\phi_g}$ is determined:

$$\partial X_u / \partial P_{\phi_g} = \partial / \partial P_{\phi_g} \left[\left(\frac{a}{(1-e^2 \sin^2 P_{\phi_g})^{\frac{1}{2}}} + Hgt \right) \right.$$

$$\left. \cos P_{\phi_g} \cos P_{\lambda} \right] \quad (88)$$

$$\partial X_u / \partial P_{\phi_g} = - \left(\frac{a}{(1-e^2 \sin^2 P_{\phi_g})^{\frac{1}{2}}} + Hgt \right) \cos P_{\lambda} \sin P_{\phi_g}$$

$$+ ae^2 (1-e^2 \sin^2 P_{\phi_g})^{-3/2} \sin P_{\phi_g} \cos^2 P_{\phi_g} \cos P_{\lambda}$$

$$(89)$$

Similarly $\partial Y_u / \partial P_{\phi_g}$ is determined as follows:

$$\partial Y_u / \partial P_g = - \left(\frac{a}{(1-e^2 \sin^2 P_{\phi_g})^{\frac{1}{2}}} + Hgt \right) \sin P_{\lambda} \sin P_{\phi_g}$$

$$+ ae^2 (1-e^2 \sin^2 P_{\phi_g})^{-3/2} \sin P_{\phi_g} \cos^2 P_{\phi_g} \sin P_{\lambda}$$

$$(90)$$

and $\partial Z_u / \partial P_{\phi_g}$ is

$$\partial Z_u / \partial P_{\phi_g} = (1-e^2) \, ae^2 \, (1-e^2 \sin^2 P_{\phi_g})^{-3/2} \sin^2 P_{\phi_g} \cos P_{\phi_g}$$

$$+ \left[\frac{a}{(1-e^2 \sin^2 P_{\phi_g})^{\frac{1}{2}}} + Hgt - \frac{ae^2}{(1-e^2 \sin^2 P_{\phi_g})^{\frac{1}{2}}} \right] \cos P_{\phi_g}$$

$$(91)$$

108

Substituting Equations (89), (90), and (91) into Equation (87) yields an expression for $\partial \varepsilon / \partial P_{\phi_g}$. The values for $P_{\phi g}$ and P_λ are obtained from the estimator's best estimates of the states. $\partial \varepsilon / \partial P_\lambda$ is obtained in a similar manner

$$\partial \varepsilon / \partial P_\lambda = \left[\tfrac{1}{2} (X_u - X_s)^2 + (Y_u - Y_s)^2 + (Z_u - Z_s)^2 \right]^{-\frac{1}{2}}$$

$$\times \left[2(X_u - X_s) \, \partial X_u / \partial P_\lambda \Big|_{\hat{\underline{X}}^-_{(k+1)}} + 2(Y_u - Y_s) \, \partial Y_u / \partial P_\lambda \Big|_{\hat{\underline{X}}^-_{(k+1)}} \right.$$

$$\left. + 2(Z_u - Z_s) \, \partial Z_u / \partial P_\lambda \Big|_{\hat{\underline{X}}^-_{(k+1)}} \right]$$

$$\tag{92}$$

$$\partial X_u / \partial P_\lambda = -\left(\left[\frac{a}{(1 - e^2 \sin^2 P_{\phi_g})^{\frac{1}{2}}} + Hgt \right] \cos P_{\phi_g} \right) \sin P_\lambda \tag{93}$$

$$\partial Y_u / \partial P_\lambda = \left(\left[\frac{a}{(1 - e^2 \sin^2 P_{\phi_g})^{\frac{1}{2}}} + Hgt \right] \cos P_{\phi_g} \right) \cos P_\lambda \tag{94}$$

$$\partial Z_u / \partial P_\lambda = 0 \tag{95}$$

Substituting Equations (93), (94), and (95) into Equation (92) yields an expression for $\partial \varepsilon / \partial P_\lambda$. The perturbation of the nonlinear measurement equation (Equation (84)) is now in the form of a linear function - an $\underline{H}$ matrix. The units of the $\underline{H}$ matrix components are ft/radian.

109

COMPUTER PROGRAM

```
      PROGRAM MAIN(INPUT,OUTPUT,TAPE13)
      DIMENSION RI(100),CHAN(500),NAME(504),H(9),V(9),TEM1(9)
      DIMENSION ZT1(9,9),ZT2(9,9),ZT3(9,9),PR(9,9),XXX1(9),XXX2(9)
     *,XXX3(9),XXX(9)
      DIMENSION PA(9,9),XA(9),XB(9),STM(9,9),ANAME(504)
      EQUIVALENCE (ANAME,NAME)
      REAL LATT,LONGG,LATUS,LONGUS,NAUT
      I=0.
      JRI=1.
      MAX=1
      MAXX=1
  500 CONTINUE
      BUFFER IN(10,1) (NAME(1),NAME(504))
      IF(UNIT(10))3,4,4
    3 K=LENGTH(10)
      PRINT*,"K=",K
      PRINT*,"  "
      I=I+1
      IF(I.EQ.1)GO TO 500
      IF(I.EQ.2)GO TO 500
      IF(I.NE.3)GO TO 123
      AX=0.0
      AY=0.0
      E=.0181
      A=2.09257457
      DO 36 NK=1,9
      H(NK)=0.
   36 CONTINUE
      DO 34 KK=1,9
      DO 34 JJ=1,9
      PA(JJ,KK)=0.
   34 CONTINUE
      PA(1,1)=1E-14
      PA(2,2)=1E-14
      PA(3,3)=1E-15
      PA(4,4)=1E-14
      PA(5,5)=1E-14
      PA(6,6)=1E-15
      PA(7,7)=0.0
      PA(8,8)=0.0
      PA(9,9)=1E-12
      DO 35 KJ=1,9
      XA(KJ)=0.
   35 CONTINUE
      XA(1)=XA(1)+.866342425
      XA(2)=2.2659E-5
      XA(4)=XA(4)+1.848317356
      XA(5)=0.2103E-5
      DELT=0.0
```

```
      DO 76 JK=1,100
      RI(JK)=0.0
   76 CONTINUE
  123 F=100
      Q=1E-17
      SLAT=1.
      SLONG=1.
      ALS=0.
      IRI=1
      PRINT*,"     LATITUDE    LAT VEL      LONGITUDE    LONG VEL
     +LAT COV        LONG COV       STATION      BIAS        TIME DIFF"
  303 MMM=1
      KI=12*IRI-10.
      IF(JRI.EQ.1)GO TO 109
      MAXX=MAX+1
  109 CHAN(MAXX)=ANAME(KI)
      IF(JRI.EQ.1)GO TO 104
      MI=JRI-1
      DO 100 N=1,MI
      IF(CHAN(MAXX).NE.CHAN(N))GO TO 102
      MMM=N
      GO TO 104
  102 MMM=MMM+1
      IF(MMM.GT.MAX)GO TO 105
  100 CONTINUE
  105 PA(9,9)=1E-12
      MAX=MMM
  104 IF(JRI.EQ.1)GO TO 103
      IF(JRI.NE.1)GO TO 103
      DELT=ANAME(1)-YXT
  103 YB(1)=YA(1)+(XA(2)*DELT)+(XA(3)*((DELT**2)/2))+(XA(7)*((DELT**3)/
     +6))
      YB(2)=YA(2)+(XA(3)*(DELT))+(XA(7)*(DELT**2)/2)
      YB(3)=YA(3)+XA(7)*DELT
      YB(4)=YA(4)+(XA(5)*DELT)+(XA(6)*((DELT**2)/2))+(XA(8)*((DELT**3)/
     +6))
      YB(5)=YA(5)+(XA(6)*(DELT))+(XA(8)*(DELT**2)/2)
      YB(6)=YA(6)+XA(8)*DELT
      YB(7)=(1.-AX)*X1(7)
      YB(8)=(1.-AY)*X1(8)
      YB(9)=RI(MMM)
      YB1=YB(1)
      YYYYY=FO*COS(YB1)
      DO 51 JJK=1,9
      DO 51 KKJ=1,9
      STM(JJK,KKJ)=0.
   51 CONTINUE
      STM(1,1)=1.
      STM(1,2)=DELT
      STM(1,3)=(DELT**2)/2
      STM(1,7)=(DELT**3)/6
      STM(2,2)=1.
```

111

```
      STM(2,3)=DELT
      STM(2,7)=(DELT**2)/2
      STM(3,3)=1.
      STM(3,7)=DELT
      STM(4,4)=1.
      STM(4,5)=DELT
      STM(4,6)=(DELT**2)/2
      STM(4,8)=(DELT**3)/6
      STM(5,5)=1.
      STM(5,6)=DELT
      STM(5,8)=(DELT**2)/2
      STM(6,6)=1.
      STM(6,8)=DELT
      STM(7,7)=1.-AX
      STM(8,8)=1-AY
      STM(9,9)=1.
      DO 59 I=1,9
      DO 59 J=1,9
      ZT1(I,J)=0.0
 59   CONTINUE
      DO 10 K=1,9
      DO 10 J=1,9
      DO 10 I=1,9
      ZT1(J,K)=STM(J,I)*PA(I,K)+ZT1(J,K)
 10   CONTINUE
      DO 60 I=1,9
      DO 60 J=1,9
      ZT2(I,J)=0.0
 60   CONTINUE
      DO 11 K=1,9
      DO 11 J=1,9
      DO 11 I=1,9
      ZT2(J,K)=ZT1(J,I)*STM(K,I)+ZT2(J,K)
 11   CONTINUE
      ZT3(3,3)=Q*DELT**2
      ZT3(6,6)=Q*DELT**2
      DO 12 I=1,9
      DO 12 J=1,9
      PB(I,J)=ZT2(I,J)+ZT3(I,J)
 12   CONTINUE
      KI3=KI+1
      PNG=ANAME(KI3)
      XXXXY=ANAME(KI)
      CALL STATN(SLAT,CLONG,ALS,XXXXY)
      IF(SLAT.EQ.0.0)GO TO 17
 18   GO TO 19
 17   PRINT*,"NEW STATION ACQUISITION"
 19   IF(SLAT.EQ.1.0)GO TO 21
      GO TO 22
 21   PRINT*,"INITIAL LAT IS USED"
 22   KI4=KI+2
      ALT=ANAME(KI4)
```

112

```
ULAT=XB(1)
ULONG=XB(4)
X=((A/(((1-(E**2)*(SIN(ULAT)**2))**.5))+ALT)*COS(ULAT)*COS(ULONG)
Y=((A/(((1-(E**2)*(SIN(ULAT)**2))**.5))+ALT)*COS(ULAT)*SIN(ULONG)
Z=((A/((1-(E**2)*(SIN(ULAT)**2))**.5))+ALT-((A*(E**2))/((1-(E
**2)*(SIN(ULAT)**2))**.5)))*SIN(ULAT)
S=((A/((1-(E**2)*(SIN(SLAT)**2))**.5))+ALS)*COS(SLAT)*COS(SLONG)
T=((A/(((1-(E**2)*(SIN(SLAT)**2))**.5))+ALS)*COS(SLAT)*SIN(SLONG)
U=((A/((1-(E**2)*(SIN(SLAT)**2))**.5))+ALS-((A*(E**2))/((1-(E
**2)*(SIN(SLAT)**2))**.5)))*SIN(SLAT)
LATT=XB(1)
LONGG=XB(4)
TERZ1=A/((1-(E**2)*(SIN(LATT)**2))**.5)
TERMZ1=(TERZ1+ALT-(TERZ1*E**2))*COS(LATT)
TERZ2=(A/2)*(E**2-1)
TERZ3=1/(1-(E**2)*(SIN(LATT)**2))**1.5
TERZ4=(-2*E**2*SIN(LATT)*COS(LATT))
TERMZ2=(TERZ2*TERZ3*TERZ4)*SIN(LATT)
ZDELLT=TERMZ1+TERMZ2
TERX1=-A/2
TERX2=1/(1-(E**2)*(SIN(LATT)**2))**1.5
TERX3=(-2*E**2*SIN(LATT)*COS(LATT))
TERX4=COS(LATT)*COS(LONGG)
TERMY1=TERX1*TERX2*TERX3*TERX4
TERX5=TERZ1+ALT
TERX6=COS(LONGG)*SIN(LATT)
TERMY2=TERX5*TERX6
XDELLT=TERMX1-TERMX2
TERY1=-A/2
TERY2=1/(1-(E**2)*(SIN(LATT)**2))**1.5
TERY3=(-2*E**2*SIN(LATT)*COS(LATT))
TERY4=COS(LATT)*SIN(LONGG)
TERMY1=TERY1*TERY2*TERY3*TERY4
TERY5=TERZ1+ALT
TERY6=SIN(LONGG)*SIN(LATT)
TERMY2=TERY5*TERY6
YDELLT=TERMY1-TERMY2
TERE1=2*(X-S)*XDELLT
TERE2=2*(Y-T)*YDELLT
TERE3=2*(Z-U)*ZDELLT
TERMF1=TERE1+TERE2+TERE3
TERE4=(X-S)**2+(Y-T)**2+(Z-U)**2
TERMF2=.5/TERE4**.5
FDELLT=TERMF1*TERMF2
XDELLG=(-TERX5)*COS(LATT)*SIN(LONGG)
YDELLG=TERX5*COS(LATT)*COS(LONGG)
TERE5=2*(X-S)*XDELLG
TERE6=2*(Y-T)*YDELLG
TERMF3=TERE5+TERE6
FDELLG=TERMF2*TERMF3
H(1)=FDELLT
```

```
      H(4)=EDELLG
      H(9)=(H(1)**2+H(4)**2)**.5
      BIAS=XP(9)*H(9)
      P=(((X-S )**2)+((Y-T )**2)+((Z-U )**2))**.5+BIAS
      RES=((PNG)*6.076E3)-P
      RESS=RES*.001
      DO 75 I=1,9
      TEM1(I)=0.J
   75 CONTINUE
      DO 513 I=1,9
      DO 513 J=1,9
      TEM1(I)=PB(I,J)*H(J)+TEM1(I)
  513 CONTINUE
      TEM2=0.0
      DO 516 I=1,9
      TEM2=H(I)*TEM1(I)+TEM2
  516 CONTINUE
      TERMR=1/(TEM2+R)
      DO 514 III=1,9
      V(III)=TEM1(III)*TERMR
  514 CONTINUE
      DO 515 JJJ=1,9
      XA(JJJ)=XB(JJJ)+V(JJJ)*RES
  515 CONTINUE
      DO 43 IKJ=1,9
      DO 43 JKI=1,9
      XXX1(JKI)=EDELLT*PB(1,JKI)*V(IKJ)
      XXX2(JKI)=EDELLG*PB(4,JKI)*V(IKJ)
      XXX3(JKI)=PB(9,JKI)*V(IKJ)*H(9)
      XXX(IKJ)=XXX1(JKI)+XXX2(JKI)+XXX3(JKI)
      PB(IKJ,JKI)=PB(IKJ,JKI)-XXX(IKJ)
   43 CONTINUE
      PI(MYM)=XA(9)
      IRIG1=KI-1
      IRIG2=KI+11
      DELT=ANAME(IRIG2)-ANAME(IRIG1)
      IF(IPI.NE.42)GO TO 119
      YXT=ANAME(IRIG1)
  119 CONTINUE
      VELAT=XA(2)*3600)*57*60
      VELONG=XA(5)*3600*57*YYYYY
      COVLAT=PB(1,1)*4.319E14
      COVLON=PB(4,4)*(6076*YYYYY*57)**2
      BIS=XA(9)*UNIT*57.*6076
  300 FORMAT(1X,9E14.3)
      PRINT 300,XA(1),VELAT,XA(4),VELONG,COVLAT,COVLON,XXXXX,BIS,RESS
      IF(JPI.EQ.39)GO TO 191
      JPI=JPI+1
  191 CONTINUE
      IF(I.EQ.9)GO TO 4
      IF(IPI.EQ.42)GO TO 500
      IF(IPI.EQ.42.)GO TO 4
      IPI=IPI+1
      GO TO 303
    4 STOP
      END
```

114

```
      SUBROUTINE STATM(SLAT,SLONG,ALS,ANAM)
      IF(ANAM      .NE.57) GO TO 1
      SLAT=.6293135677
      SLONG=1.739733338
      ALS=3989
      GO TO 61
1     IF(ANAM      .NE.37) GO TO 2
      SLAT=.6126141393
      SLONG=1.833234149
      ALS=5000
      GO TO 61
2     IF(ANAM      .NE.43) GO TO 3
      SLAT=.6262937124
      SLONG=1.851173775
      ALS=6344
      GO TO 61
3     IF(ANAM      .NE.59) GO TO 4
      SLAT=.6020613256
      SLONG=1.794382058
      ALS=4000
      GO TO 61
4     IF(ANAM .NE.71)GO TO 5
      SLAT=.9573617849
      SLONG=1.934795332
      ALS=3900
      GO TO 61
5     IF(ANAM .NE.73)GO TO 6
      SLAT=35..61866673.141593/180
      SLONG=110.7944441*3.141593/180
      ALS=4938
      GO TO 61
6     IF(ANAM.NE.74)GO TO 7
      SLAT=33.2622220*3.141593/180
      SLONG=107.28*3.141593/180
      ALS=4860
      GO TO 61
7     IF(ANAM.NE.79)GO TO 8
      SLAT=35.3364593*3.141593/180
      SLONG=106.6158337*3.141593/180
      ALS=5352
      GO TO 61
8     IF(ANAM.NE.85)GO TO 9
      SLAT=.6735499129
      SLONG=1.35193975
      ALS=4093
      GO TO 61
9     IF(ANAM.NE.182)GO TO 10
      SLAT=.5996163344
      SLONG=1.844420632
      ALS=5500
      GO TO 61
```

115

```
   10 IF(ANAM.NE.108)GO TO 11
      SLAT=.6413791113
      SLONG=1.066671833
      ALS=5503
      GO TO 61
   11 IF(ANAM.NE.106)GO TO 12
      SLAT=.6613791394
      SLONG=1.629373108
      ALS=3609
      GO TO 61
   12 IF(ANAM.NE.104)GO TO 13
      SLAT=.6000836931
      SLONG=1.60330812
      ALS=4295
      GO TO 61
   13 IF(ANAM.NE.111)GO TO 14
      SLAT=.6358943847
      SLONG=1.630351027
      ALS=6000
      GO TO 61
   14 IF(ANAM.NE.113)GO TO 15
      SLAT=.5903258725
      SLONG=1.664361707
      ALS=4800
      GO TO 61
   15 IF(ANAM.NE.120)GO TO 16
      SLAT=.6223407730
      SLONG=1.634951339
      ALS=6856
      GO TO 61
   16 IF(ANAM.NE.123)GO TO 17
      SLAT=.6389407983
      SLONG=1.848435480
      ALS=7091
      GO TO 61
   17 IF(ANAM.NE.81.)GO TO 18
      SLAT=.6112389174
      SLONG=1.935204752
      ALS=6500
      GO TO 61
   18 IF(ANAM.NE.87.)GO TO 19
      SLAT=.6140456153
      SLONG=1.703127168
      ALS=4083
      GO TO 61
   19 IF(ANAM.NE.86.)GO TO 20
      SLAT=.6518353312
      SLONG=1.945320148
      ALS=7535
      GO TO 61
   20 IF(ANAM.NE.72.)GO TO 21
```

```
      SLAT=.6797337819
      SLONG=1.826191326
      ALS=6900
      GO TO 61
   21 IF(ANAM.NE.105)GO TO 22
      SLAT=.6502854385
      SLONG=1.808151409
      ALS=6700
      GO TO 61
   22 IF(ANAM.NE.122)GO TO 23
      SLAT=.6842351349
      SLONG=1.82102806
      ALS=7800
      GO TO 61
   23 IF(ANAM.NE.114)GO TO 24
      SLAT=.6683592925
      SLONG=1.822527945
      ALS=7500
      GO TO 61
   24 IF(ANAM.NE.75.)GO TO 25
      SLAT=.6923555242
      SLONG=1.801731591
      ALS=6000
      GO TO 61
   25 IF(ANAM.NE.110)GO TO 26
      SLAT=.6957027843
      SLONG=1.822271177
      ALS=7000
      GO TO 61
   26 IF(ANAM.NE.93)GO TO 27
      SLAT=.6191749447
      SLONG=1.901173894
      ALS=6458
      GO TO 61
   27 IF(ANAM.NE.75)GO TO 28
      SLAT=.7009925221
      SLONG=1.824785350
      ALS=6645
      GO TO 61
   28 SLAT=0.
   61 RETURN
      END
```

<u>Vita</u>

Robert <u>Nelson</u> Riggins was born on 31 March 1954 in Lynchburg, Virginia, to Robert N. and Edith C. Riggins. He graduated from Kecoughton (Hampton, Virginia) High School in 1972 and received a Bachelor of Science degree in Electrical Engineering from Virginia Polytechnic Institute and State University in 1976. He was commissioned a Second Lieutenant in the United States Air Force through the AFROTC program on June 4, 1976. Lieutenant Riggins entered the Air Force Institute of Technology Resident School of Engineering in pursuit of a Master's degree in Electrical Engineering, Guidance and Control in August 1976. Lieutenant Riggins is married.

Permanent address: 4 Crockett Drive
Hampton, Virginia

SECURITY CLASSIFICATION OF THIS PAGE (When Data Entered)

REPORT DOCUMENTATION PAGE	READ INSTRUCTIONS BEFORE COMPLETING FORM

1. REPORT NUMBER	2. GOVT ACCESSION NO.	3. RECIPIENT'S CATALOG NUMBER
AFIT/GGC/EE/78-4		

4. TITLE (and Subtitle)

A DESIGN OF A TRAJECTORY ESTIMATOR USING MULTIPLE DME RANGE MEASUREMENTS.

5. TYPE OF REPORT & PERIOD COVERED

MS Thesis

6. PERFORMING ORG. REPORT NUMBER

7. AUTHOR(s)

Robert M. Riggins

8. CONTRACT OR GRANT NUMBER(s)

9. PERFORMING ORGANIZATION NAME AND ADDRESS

Air Force Institute of Technology (AFIT-EN)
Wright-Patterson AFB, Ohio 45433

10. PROGRAM ELEMENT, PROJECT, TASK AREA & WORK UNIT NUMBERS

11. CONTROLLING OFFICE NAME AND ADDRESS

Air Force Weapons Laboratory
Kirtland AFB, New Mexico

12. REPORT DATE

Mar 78

13. NUMBER OF PAGES

118

14. MONITORING AGENCY NAME & ADDRESS(if different from Controlling Office)

15. SECURITY CLASS. (of this report)

Unclassified

15a. DECLASSIFICATION DOWNGRADING SCHEDULE

16. DISTRIBUTION STATEMENT (of this Report)

Approved for public release; distribution unlimited

17. DISTRIBUTION STATEMENT (of the abstract entered in Block 20, if different from Report)

18. SUPPLEMENTARY NOTES

Approved for public release; IAW AFR 190-17

JERRAL F. GUESS, Captain, USAF
Director of Information

19. KEY WORDS (Continue on reverse side if necessary and identify by block number)

Extended Kalman Filter
Navigation
DME Stations
INS Reference Systems

20. ABSTRACT (Continue on reverse side if necessary and identify by block number)

This report is directed toward the design of a real-time estimation algorithm, a Kalman filter, that estimates aircraft position and velocity using multiple DME range measurements. The estimator is designed and tested for feasibility as a reference system for examining Inertial Navigational System (INS) low frequency errors. Both a 9-state estimator including jerk states and a 7-state estimator without the jerk states are designed.

DD FORM 1473 EDITION OF 1 NOV 55 IS OBSOLETE

SECURITY CLASSIFICATION OF THIS PAGE (When Data Entered)

With the tuning parameters used in the estimator tests, the 7-state estimator provides better performance than the 9-state estimator. An approximate analysis of the 7-state estimator performance (by comparison to FASTMAP, a currently used and accepted filter, and CIRIS, the Completely Integrated Reference Instrumentation System,) reveals that estimator errors in the high frequency range are greater than those of an INS, but errors in the DME-based estimator are consistent in strength and do not exhibit an unbounded growth as typical of INS errors. For the estimator in this study, the approximate values that encompass 50 percent of all the errors (as compared to CIRIS) for latitude, longitude, latitude velocity, and longitude velocity were

$$
\begin{aligned}
\text{Latitude position} &= \pm 83 \text{ feet} \\
\text{Longitude position} &= \pm 183 \text{ feet} \\
\text{Latitude velocity} &= \pm 8.4 \text{ feet/second} \\
\text{Longitude velocity} &= \pm 7.5 \text{ feet/second}
\end{aligned}
$$

Improving estimator performance is suggested by proper tuning and by using an adaptive approach.